UNIVERSITY OF NAPLES FEDERICO II

POLYTECHNIC AND BASIC SCIENCES SCHOOL

Department of Chemical Sciences

Ph.D. in Chemical Sciences

Synthesis and study of nature-inspired polymers for applications in organic electronics

Fabio Mocerino

Advisors

Prof. Ugo Caruso

Prof. Alessandro Pezzella

Examiner — Prof. Michele Pavone

PhD Coordinator — Prof. Angela Lombardi

XXXVI Cycle 2020-2023

Index

Abstract

Natural polymers have attracted great interest as functional materials in the field of organic electronics for innovative technological and biomedical applications. In the panorama of biomaterials, melanins are undoubtedly among the most intriguing natural substances. The most studied and abundant class of melanins is eumelanin, a mammalian photoprotective pigment originating from the oxidative polymerization of 5,6-dihydroxy indole (DHI) and 5,6-dihydroxyindole-2 carboxylic acid (DHICA). In this context the main objectives of the present project can be summarized as follows:

a) preparation of eumelanin-inspired materials through a strategy based on a synthetic approach;
b) carry forward the process of elucidation of the structure of eumelanin through the comparison of the synthesis mechanism of melanin derivatives with that of the natural polymer starting from DHI and DHICA.
c) preparation and characterization of a eumelanin-inspired material for its potential application as an active layer for organic electronics devices with improved performance compared to natural polymer.

Regarding the results obtained, a synthetic procedure was found to functionalize the eumelanin precursor DHICA by introducing a benzothiazole synthon. Investigations of the optical properties of the acetylated derivative of the adduct, DAICA-ABtz, revealed specific chelation capabilities towards Zn^{2+} ions along with a notable increase in fluorescence intensity.

Early studies addressed the chemistry of oxidative polymerization of DHICA-ABtz focusing on the isolation of oligomeric intermediates to gain insight into the structure of the resulting polymer. The feature pattern of C–C bonds identified in the DHICA-ABtz dimers concluded that the benzothiazole system did not influence the regioselectivity of the polymerization in the early stages of the process.

Subsequent research activities focused on the potential application of the DHICA-ABtz-derived polymer as a solid active layer in electrochemical energy storage

devices, exploiting the specific ability of the eumelanin-inspired material to chelate Zn^{2+} ions as well as the intrinsic redox behaviour of eumelanin. The ionic conductivity values found by studying DHICA-ABtz-derived polymer films with different amounts of zinc were modest compared to the values of current solid polymer electrolytes. Interestingly, the electrochemical characterization of the solid melanin-inspired polymer immersed in an aqueous electrolyte containing zinc ions highlighted a remarkable specific capacity, almost two times greater than that of the DHICA eumelanin. This result is crucial for the development of an active layer for electrochemical energy storage devices, although further analyses are needed in this perspective.

1 Introduction

The expression "nature-inspired" denotes the exploitation of hints from the natural world for a wide range of purposes, including the design and preparation of active materials.

Natural materials have deep and intriguing properties that touch and intersect physics, chemistry, biology, and medicine. In particular, natural products from biological resources represent a valuable source of materials used in many applications, such as biomedicine, drug delivery, and tissue engineering [1, 2]. Recently, there has been a great interest in exploiting biological products for the fabrication of functional devices such as sensors, and optical systems in bioelectronics. The interest in biomaterials is rooted in their biocompatibility, biodegradability, and biorecognition properties. In addition to the remarkable properties listed above, a further incentive to use biological products for the development of devices has been given by the growing need to reduce electronic waste.

According to the United Nations, waste from electronic equipment is estimated to be more than 60 million tons per year [3]. This requires the adoption of sustainable processes and materials while reinterpreting the product life cycle [4]. Discarded electronic waste often includes heavy metals and/or non-degradable polymers, which can be harmful to the environment. Nowadays, most devices in everyday use are based on materials that are scare in nature or are susceptible to exhaustion, such as germanium and indium. In this scenario, biodegradable natural materials can provide an attractive solution as renewable resources that can be decomposed in the environment [5].

Natural biomaterials act as structural or active components in devices, and in some cases, as both. They can be present as a pure material or as a composite [6]. Here we will show just a few examples of the wide range of applications where natural materials are used, with a particular focusing on electronic devices.

Conducting polymers (CPs) are a broad class of materials widely used as active layers in various types of electronic devices. Their use is strictly linked to the choice of a suitable substrate.

Silk is a natural material mainly obtained from the cocoon of Bombyx mori. In the form of fabric, silk has a structure featuring woven or felted threads, which can provide a large surface area for active material loading. Sun et al. used silk fabric as a free-standing substrate for CPs such as poly (3,4-ethylenedioxythiophene):polystyrene sulfonate (PEDOT:PSS), and multiwalled carbon nanotubes (MWCNTs) with polypyrrole (PPy). These materials were coated with gel electrolyte and sandwiched with cellulose to fabricate a supercapacitor. The facile coating of this biomaterial by drop-casting with the active components of the devices has paved the way for the fabrication of smart textiles, opening up the exploration of other tissues such as cotton and linen [7].

When designing organic thin film transistors (OTFT), the dielectric layer plays a critical role in device performance as it is subject to numerous requirements, such as low leakage current and high capacitance. Keratin is the main component of hair, feathers, and nails. Since keratin waste tends to slowly degrade, animal byproducts are usually considered environmental pollutants [8]. Recent work has exploited the dielectric properties of keratin with its insolubility in organic solvents. This last feature is particularly useful in the fabrication of multilayer devices, as it does not dissolve with the addition of the solutions used for the other layers [9-11]. With this approach, Singh et al. fabricated an OTFT featuring poly(3-hexylthiophene) as the organic semiconductor, using keratin as the dielectric gate. Interestingly, the transistor of this biopolymer exhibits electrical properties such as switching voltage, carrier mobility, and threshold voltage that are superior to those obtained using SiO_2 as the dielectric layer. [12].

Natural materials, in addition to being used as a support substrate, as dielectrics to store electrical charge or, as insulators to separate electrically conductive materials, can also be used as active components within electronic devices [6, 13-15]. Nature, in fact, is also the source of fascinating materials with electrochemical and

optoelectronic properties. Many natural dyes and pigments have attracted considerable attention in scientific research thanks to their peculiar properties.

Indigo is one of the best-known dyes in the world, obtained from some plants diffused in Europe and in tropical regions. Despite its current use in various sectors, such as the conch industry, its low solubility and high melting point have severely limited the further exploitation of this material. Several works report the blue pigment as a natural semiconductor, speculating that the strength of intermolecular interactions, such as hydrogen bonds, is the basis of the good charge transport properties [16-18]. Investigations into the electrochemical properties of this material have focused interest on the development of several indigo-based electronic devices, such as field-effect transistors and organic light-emitting diodes (OLEDs) [19, 20].

Based on these examples, natural materials have noteworthy properties that have contributed to their use in electronic devices. The intrinsic biocompatibility and biodegradability, combined with the abundance with which these materials can be found, make them low-cost and environmentally friendly.

Within the panorama of materials found in nature, melanin is undoubtedly among the most interesting natural substances [21]. Investigations into the role and biological functions of melanin have broadened and increased the scientific interest in this pigment [22-29]. The ongoing process of elucidation of the structure-property-function relationships has brought to light surprising properties exhibited by this material [30-33].

Starting from this scenario, the research activity of my PhD project has been focused on the design, synthesis, and characterization of a melanin-inspired material with the aim of its potential application as an active layer in electronic devices, particularly in Electrochemical Energy Storage (EES) systems. Before going into the merits of the research activity described in chapter 3, the next chapter contains a presentation on melanin, with particular interest in the class of eumelanin.

References

1. Mandla, S., L. Davenport Huyer, and M. Radisic, *Review: Multimodal bioactive material approaches for wound healing.* APL Bioengineering, 2018. **2**(2).

2. Benwood, C., et al., *Natural Biomaterials and Their Use as Bioinks for Printing Tissues.* Bioengineering, 2021. **8**(2): p. 27.

3. Union, E. *14 October: an International E-Waste Day to shed light on "invisible" electronic waste*. 2023.

4. Irimia-Vladu, M., *"Green" electronics: biodegradable and biocompatible materials and devices for sustainable future.* Chemical Society Reviews, 2014. **43**(2): p. 588-610.

5. Irimia-Vladu, M., et al., *Green and biodegradable electronics.* Materials Today, 2012. **15**(7): p. 340-346.

6. Pradhan, S., A.K. Brooks, and V.K. Yadavalli, *Nature-derived materials for the fabrication of functional biodevices.* Materials Today Bio, 2020. **7**: p. 100065.

7. Sun, C., et al., *A freestanding polypyrrole hybrid electrode supported by conducting silk fabric coated with PEDOT:PSS and MWCNTs for high-performance supercapacitor.* Electrochimica Acta, 2019. **317**: p. 42-51.

8. Li, Q., *Progress in Microbial Degradation of Feather Waste.* Front Microbiol, 2019. **10**: p. 2717.

9. Guo, B., et al., *A sustainable resistive switching memory device based on organic keratin extracted from hair.* RSC Advances, 2019. **9**(22): p. 12436-12440.

10. Lin, Q., et al., *Human hair keratin for physically transient resistive switching memory devices.* Journal of Materials Chemistry C, 2019. **7**(11): p. 3315-3321.

11. Ko, J., et al., *Human Hair Keratin for Biocompatible Flexible and Transient Electronic Devices.* ACS Applied Materials & Interfaces, 2017. **9**(49): p. 43004-43012.

12. Singh, R., et al., *A new biodegradable gate dielectric material based on keratin protein for organic thin film transistors.* Organic Electronics, 2017. **44**: p. 198-209.

13. Bettinger, C.J. and Z. Bao, *Biomaterials-Based Organic Electronic Devices.* Polym Int, 2010. **59**(5): p. 563-567.

14. Lan, L., et al., *Sustainable Natural Bio-Origin Materials for Future Flexible Devices.* Advanced Science, 2022. **9**(15): p. 2200560.

15. Feig, V.R., H. Tran, and Z. Bao, *Biodegradable Polymeric Materials in Degradable Electronic Devices.* ACS Central Science, 2018. **4**(3): p. 337-348.

16. Głowacki, E.D., et al., *Hydrogen-Bonded Semiconducting Pigments for Air-Stable Field-Effect Transistors.* Advanced Materials, 2013. **25**(11): p. 1563-1569.

17. Irimia-Vladu, M., et al., *Indigo - A Natural Pigment for High Performance Ambipolar Organic Field Effect Transistors and Circuits.* Advanced Materials, 2012. **24**(3): p. 375-380.

18. Głowacki, E.D., et al., *A facile protection–deprotection route for obtaining indigo pigments as thin films and their applications in organic bulk heterojunctions.* Chemical Communications, 2013. **49**(54): p. 6063-6065.

19. Pitayatanakul, O., et al., *High performance ambipolar organic field-effect transistors based on indigo derivatives.* Journal of Materials Chemistry C, 2014. **2**(43): p. 9311-9317.

20. Głowacki, E.D., et al., *Epindolidiones—Versatile and Stable Hydrogen-Bonded Pigments for Organic Field-Effect Transistors and Light-Emitting Diodes.* Advanced Functional Materials, 2015. **25**(5): p. 776-787.

21. Mostert, A.B., *Melanin, the What, the Why and the How: An Introductory Review for Materials Scientists Interested in Flexible and Versatile Polymers.* Polymers (Basel), 2021. **13**(10).

22. Zucca, F.A., et al., *The Neuromelanin of Human Substantia Nigra: Physiological and Pathogenic Aspects.* Pigment Cell Research, 2004. **17**(6): p. 610-617.

23. d'Ischia, M., et al., *Melanins and melanogenesis: from pigment cells to human health and technological applications.* Pigment Cell & Melanoma Research, 2015. **28**(5): p. 520-544.

24. Hill, H.Z., *The function of melanin or six blind people examine an elephant.* BioEssays, 1992. **14**(1): p. 49-56.

25. Burkhart, C.G. and C.N. Burkhart, *The mole theory: primary function of melanocytes and melanin may be antimicrobial defense and immunomodulation (not solar protection).* International Journal of Dermatology, 2005. **44**(4): p. 340-342.

26. Różanowska, M., et al., *Free radical scavenging properties of melanin: Interaction of eu- and pheo-melanin models with reducing and oxidising radicals.* Free Radical Biology and Medicine, 1999. **26**(5): p. 518-525.

27. Dadachova, E., et al., *Ionizing Radiation Changes the Electronic Properties of Melanin and Enhances the Growth of Melanized Fungi.* Plos One, 2007. **2**(5): p. e457.

28. Galván, I. and C. Alonso-Alvarez, *The expression of melanin-based plumage is separately modulated by exogenous oxidative stress and a melanocortin.* Proceedings of the Royal Society B: Biological Sciences, 2009. **276**(1670): p. 3089-3097.

29. Hong, L. and J.D. Simon, *Insight into the Binding of Divalent Cations to Sepia Eumelanin from IR Absorption Spectroscopy.* Photochemistry and Photobiology, 2006. **82**(5): p. 1265-1269.

30. Meredith, P. and T. Sarna, *The physical and chemical properties of eumelanin.* Pigment Cell Research, 2006. **19**(6): p. 572-594.

31. Cao, W., et al., *Unraveling the Structure and Function of Melanin through Synthesis.* Journal of the American Chemical Society, 2021. **143**(7): p. 2622-2637.

32. Paulin, J.V., et al., *Melanin thin-films: a perspective on optical and electrical properties.* Journal of Materials Chemistry C, 2021. **9**(26): p. 8345-8358.

33. d'Ischia, M., et al., *Chemical and structural diversity in eumelanins: unexplored bio-optoelectronic materials.* Angew Chem Int Ed Engl, 2009. **48**(22): p. 3914-21.

2 Eumelanin

2.1 Introduction on melanin

The term Melanins (Greek μέλας, mèlas = black) [1] is used for the first time, according to Borovanksy [2] , by the Swedish chemist Berzelius in 1840 to name the large class of pigments found throughout nature, from human beings to invertebrates, plants, and fungi.

Chemically, melanin is composed of macromolecules made up predominantly of indolic units [3]. There are many different types of melanin, including eumelanin, pheomelanin, neuromelanin and allomelanin. Many animal species, including humans, have eumelanin and pheomelanin in their skin, hair, and eyes. These two classes of pigments act as photo-protectants by absorbing harmful ultraviolet and visible radiation.

It is known that eumelanin, where “Eu” is the Greek prefix meaning “good”, is constructed from 5,6-dihydroxyindole (DHI) and 5,6-dihydroxyindole-2-carboxylic acid (DHICA) and is black to brown in colour [4]. Eumelanin is the most widely studied of all melanins since it is the primary pigment found in human hair and skin and it is also the main component of squid ink and gives feathers their dark coloring [5].

Pheomelanin is a biopolymer whose oligomeric structure incorporates L-cysteine units, unlike eumelanin. Pheomelanin is also found in human skin and hair and is characterized by a color ranging from red to yellow [6, 7]. Although pheomelanin makes up approximately 25% of total melanin, its exact structure is not yet understood, as pure pheomelanin is rare to find in nature [8, 9].

Neuromelanin is a black-brown pigment whose structure is obtained from the oxidative polymerization of dopamine in the presence of cysteine [10]. Neuromelanin term refers to its similar appearance to skin melanin and its specific localization in the gray matter of the brain and within nerve cells [11]. In particular, neuromelanin

isolated from human gray matter exists in the form of granules with a diameter and shape similar to those of ~~to~~ melanin found in cuttlefish, bovine eyes, and human eyes [12]. The role of this biopolymer is unknown, although it is believed to have some implications for a variety of neurodegenerative diseases such as Parkinson's disease and Alzheimer's [13].

Unlike the first three classes of melanin, allomelanin (the prefix "allo" in Greek means “heterogeneous” or “different”) is a heterogeneous group of biopolymers that can be found in fungi, bacteria, and plants [10]. Depending on the precursor molecules, allomelanin is further divided into numerous subtypes of melanins united by the presence of hydroxylated aromatic units.

2.2 Interest in melanin

Melanin plays an essential role in the health of humans as it protects the skin from the harmful effects of UV radiation by dissipating energetic radiation into heat [14], as well as scavenging reactive oxygen/nitrogen species (ROS/RNS) resulting from exposure to radiation [15], reducing the risk of DNA damage and sunburn. Paradoxically, although melanin is a photoprotectant, the scavenged ROS/RNS modify melanin and induce signature DNA damage in cells that lead to malignant melanoma skin cancer [16, 17], although this link is very poorly understood so far. Skin cancers are among the most common cancers worldwide and are increasingly prevalent [18]. Cutaneous melanoma (CM) is characterized by the malignant transformation of melanocytes in the epidermis. Although CM shows a lower incidence than other skin cancers, it is the most aggressive and responsible for most skin cancer-related deaths [19]. According to the World Health Organization, approximately 48 000 melanoma-related deaths occur each year [20]. In CM, the photoprotective pigment melanin, which is produced by melanocytes, plays a central role in the pathology of the disease. Indeed, although skin with high melanin content is more protected from carcinogenesis than unpigmented skin [18], it is also suggested that pheomelanin might increase DNA damage in cells exposed to UV light [21], and that it might also act as a photosensitizer [22]. This aspect makes understanding the biological functionality of melanin and its role in cutaneous melanoma a health priority, particularly for equatorial countries with higher levels of solar radiation.

Additionally, melanin is also involved in numerous pigmentation disorders [23]. For example, albinism and vitiligo are caused by a genetic alteration of the melanin synthetases and melanosome-related molecules [24]. Treatments and therapies for various pigmentation disorders can be developed based on a greater understanding of the biological functions of melanin.

Melanin is a variety of complex systems characterized by a highly intriguing molecular structure that makes it an interesting model system for investigating the

role of disorder in biological systems. It is believed that disorder plays a crucial role in biological functionality as well as in the study of the structure-function relationship of biological macromolecules. The determination of melanin's precise chemical structure is limited due to the insoluble and heterogeneous character of this biopolymer [23]. Furthermore, the large-scale amorphous assembly of melanin is not accessible with standard structure determination methods [25]. These reasons make melanin an interesting novel system that can be used for the development of methods that could benefit a variety of important biosystems [26-28].

Apart from its biological importance, melanin exhibits interesting physical and chemical properties, including antioxidant activity due to its radical scavenging behaviour [29, 30], UV-vis broadband absorption with non-radiative relaxation of photo-excited electronic states [29], metal-ion chelation [31, 32], drug uptake [33, 34], thermal regulation, redox and energy transduction [35].

The in-depth comprehension of these physicochemical properties, together with the intrinsic biocompatibility of this pigment, has created novel avenues for the exploitation of various types of melanin and their precursors in cosmetic and health care domains [36].

Specifically, on a technological level, eumelanin has been the subject of in-depth studies in the field of organic electronics for the development of a wide range of devices. Possible examples include the fabrication of active layers in electrochemical energy storage devices as supercapacitors [37], extremely sensitive humidity sensors (based on the extreme sensitivity of eumelanin solid state conductivity to hydration) [38], and optoelectronic devices as organic photovoltaic [39] and solar cells [40, 41].

Although there has been a surge in interest in the application of natural and synthetic eumelanin for organic electronics and bioelectronics, the implementation of competitive eumelanin-based technology has been hampered by several issues, namely those pertaining to its insolubility in water and common organic solvents.

At the same time, one of the main goals of organic electronics research has been the development of multicomponent materials that can include different features in the hybrid system to achieve additional properties that emerge from the interaction of the components [42, 43].

Taking inspiration from these ideas, the topics of this thesis are therefore linked to the possibility of improving the solubility of this pigment and conferring additional properties to eumelanin to extend the applications of this biopolymer in the field of organic electronics.

2.3 Synthesis of eumelanin

As briefly mentioned in the first paragraph, eumelanin is the most studied pigment compared to the other classes of melanin described previously, precisely because of its abundance and its peculiar properties [44]. Due to the extreme stability and insolubility of the final product [5] as well as the high instability of the intermediates, eumelanin biosynthesis, also known as melanogenesis, is very difficult to investigate. However, intermediates have been found, mainly thanks to the innovative research of Mason and Raper [45].

The synthetic process starts from the amino acid L-tyrosine, which is oxidized by oxygen, in a reaction catalyzed by the enzyme tyrosinase to form 3,4-dihydroxyphenylalanine (DOPA) which in turn is oxidized to dopaquinone, a common precursor of eumelanin and pheomelanin. Dopaquinone is highly reactive, and in the absence of L-cysteine, undergoes the intramolecular cyclization of the amino group to produce cyclodopa, also called leucodopachrome. A redox exchange between cyclodopa and dopaquinone then gives rise to dopachrome, a red-orange intermediate [46, 47] and DOPA. Dopachrome then gradually rearranges to generate mainly 5,6-dihydroxyindole and 5,6-dihydroxyindole-2-carboxylic acid. It has been observed that while in vitro, dopachrome rearranges spontaneously, decarboxylating and producing DHI, in vivo, the rearrangement is under the control of the enzyme dopachrome-tautomerase which directs the reaction towards formation of DHICA.

Finally, eumelanin is formed after the oxidative polymerization of DHI and DHICA. The availability of dopachrome tautomerase dictates the relative amounts of DHI and DHICA produced, and therefore the ratio of these components in the final eumelanin. The reactions that occur are spontaneous and depend on various factors such as the presence of thiols, pH, the presence of ions (such as zinc and copper), and oxygen. The ratio between the two dihydroxyindoles is also affected by other environmental factors, and hence varies widely depending on the source of the eumelanin under study [48].

Over the years, various approaches have been developed to obtain enough melanin to allow its study. The isolation of eumelanin from natural sources has proven problematic due to the limited solubility of eumelanin in most common solvents. The presence of tightly bound cellular components, residual amounts of proteins, and metal cations influence the structural aggregation and physical properties of the biopolymer [49]. Current isolation strategies include extracting eumelanin from human hair, from the ink sac of cuttlefish Sepia Officinalis, and bird feathers. These approaches have proven effective in removing cellular components and proteins without altering the physicochemical properties of eumelanin [50-52].

However, a wide variety of synthetic methods and procedures have been described, involving different conditions that do not always meet the requirements of biological relevance. The structural characteristics and properties of synthetic melanin depend on the choice of starting precursors, the reaction conditions, and the post-synthetic procedures. Therefore, it can be misleading to compare pigments prepared in different conditions, even if they came from the same substrate.

Oxidative polymerization of DHI and DHICA can be carried out under a variety of conditions, including:

- Biomimetic conditions - oxidation of DHI catalyzed by the enzyme tyrosinase in aqueous buffer at neutral pH. Since this synthetic approach is very similar to the biological pathway it would appear to be the best. However, in the presence of high concentrations of enzyme [53], eumelanin synthesis proceeds rather slowly in these conditions. Furthermore, reproducibility is low due to the difficulty in measuring and controlling tyrosinase activity during this reaction [54]. Alternatively, DOPA and Tyrosine can be used as substrates for enzymatic preparations.
- The peroxidase/H_2O_2 pair at biomimetic pH provides an alternative enzyme system that is faster and with higher yields than the biomimetic conditions with enzyme tyrosinase. An analogous synthetic eumelanin, obtained oxidizing tyrosine with persulfate or peroxidase, is sold commercially [5].
- Autoxidative conditions - sometimes also in the presence of metal ions such

as copper, exploiting the high tendency of DHI and DHICA to oxidize in air under slightly alkaline conditions [55].

- Chemical oxidants such as potassium ferricyanide and sodium periodate can be used in different quantities relative to the substrate depending on their electronic nature (one- or two-electron oxidation) [56].

Because synthetic eumelanin is obtained under controlled conditions and contains known monomer units, it offers advantages for its analysis compared to the melanin isolated for extraction from natural sources, which is more complex. Synthetic eumelanin is helpful as a model system for experimenting with new approaches or theories to investigate his challenging biopolymer.

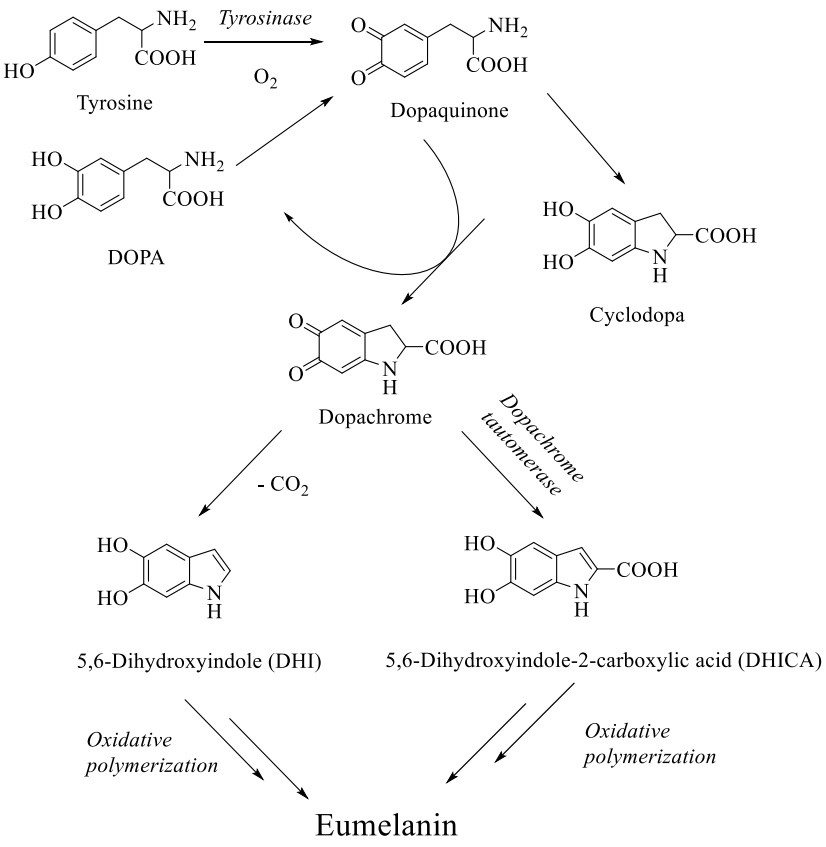

Scheme 1.1 Schematic view of the synthesis of eumelanin from tyrosine or DOPA, highlighting representative intermediates.

2.4 Structure of eumelanin

Natural eumelanin is a heterogeneous amorphous polymer consisting of DHI and DHICA units. The ratio between these two main precursors of eumelanin depends on the presence of the enzyme dopachrome tautomerase. As previously mentioned, spontaneous decarboxylation of dopachrome to DHI occurs in vitro, while in vivo, the enzyme dopachrome tautomerase promotes the formation of DHICA. The main consequence is that natural eumelanin contains over 50% DHICA [57].

The different bonding patterns through which DHI and DHICA are linked give the pigment a degree of disorder that extends to various levels [58]. Early structural models envisioned a high-molecular-weight heteropolymer system formed via random regiochemistry between different DHI and DHICA units in various oxidation states. In the mid-1990s, a different basic supramolecular architecture for eumelanin particles was proposed [59]. This model suggested that eumelanin was not a large extended heteropolymer but rather a mixture of stacked oligomeric "protomolecules" consisting of three or four planar layers of no more than five or six indole units, approximately 15–20 Å in size. Despite the high number of studies, the structure of eumelanin remains an enigma, mainly due to its amorphous character and insolubility.

Thanks to a dual approach based on the combination of the biomimetic synthesis of the oligomeric intermediates [60-62] and the pot-synthetic oxidative degradation of the polymer, which generates an array of structural marker [56], it has been possible to conclude that active positions for polymerization are 2, 3, 4, and 7 [25, 26, 32, 33]. In particular:

- DHI polymerizes by forming oligomers through C-C coupling involving the 2, 4 and 7 positions;
- DHICA polymerizes by forming oligomers through C-C coupling involving 4 and 7 positions. Position 2 is blocked for DHICA units because of carboxyl group while position 3 is mostly inactivated due to the electron-withdrawing effect of the carboxyl group at position 2 [2].

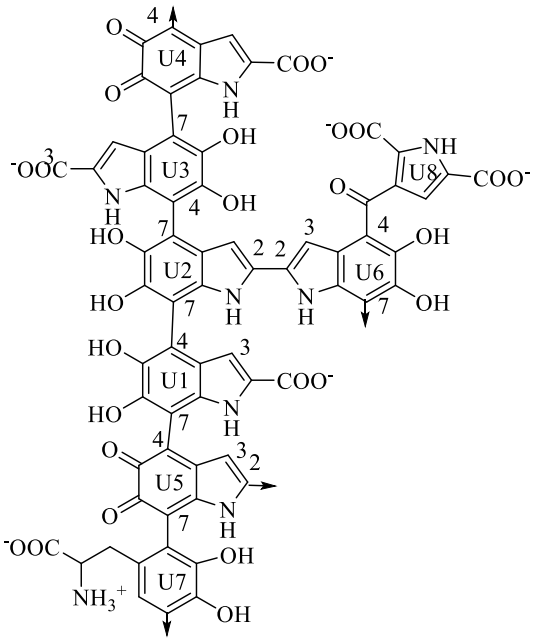

Figure 1.2 A model of the structure of eumelanin inspired by [2]. Most of the units are indolic units. Within the complex structure can be found oxidized quinone units (5,6-indolequinone, U4, and U5), unaltered L-dopa units (U7), and carboxylated pyrrole units due to partial degradation of indoles during polymerization (U8). The units are connected by a variety of bonds involving positions 4, 7, 2, and 3. The arrows indicate some possible positions for polymer growth.

While DHI oligomers can adopt a planar conformation tending towards branched oligomers, DHICA polymerizes primarily through hindered biphenyl-type bonds, resulting in the generation of a non-planar conformation tending towards a linear backbone structure that exhibits atropoisomerism in interunit bonds. Deviations from coplanarity in DHICA oligomers are supported by the negative charge of the carboxylate groups which forces twisting around the inter-ring bond [63]. The twisted backbones so formed cannot give rise to π-stacked supramolecular aggregates, in contrast to the largely planar oligomeric scaffold derived from DHI, but are only capable of establishing weak intermolecular interactions leading to rod-like assemblies [52, 64].

2.5 Eumelanin physicochemical properties

Over the past decade, eumelanin has become the focus of growing interest in materials science thanks to the unique physicochemical properties associated with the high degree of structural and supramolecular disorder discussed above.

Eumelanin shows a characteristic featureless broadband absorption throughout the UV–vis spectrum, which explains its black color [29]. This monotonic trend has been shown to arise from the superposition of the absorption profiles of oligomers of different sizes and structures and also from the coexistence of oxidized and reduced monomer units [65]. Whereas DHI eumelanin gives a typical monotonic UV-vis profile, noteworthy is the case of DHICA eumelanin, which shows an intense absorption maximum in the UV spectral region centered at 320 nm that persists at acid pH values. This feature suggests the coexistence of reduced indole units with quinonoid units during polymerization as a consequence of hindered inter-unit π-electron delocalization within oligomeric scaffolds [52, 66, 67]

Eumelanin is also able to dissipate up to 90% of the energy absorbed from solar radiation into heat [14]. This absorbed energy and its conversion to heat can contribute to the thermoregulation of pigmented organisms, which is particularly important in cold-blooded animals.

Eumelanin features functional properties in the human body, such as radical scavenging and antioxidant activity, as supported by its distinct electron paramagnetic resonance (EPR) signal [67]. Furthermore, numerous studies have shown that DHICA eumelanin has a greater homogeneity of free radical components in contrast to the wider variety of free radical species that could be generated within the delocalized DHI eumelanin system [36]. Furthermore, DHICA eumelanin exhibits more potent free radical scavenger properties than DHI eumelanin in several scavenging assays, likely due to weaker aggregation interactions, representing greater accessibility to free radicals [15]. DHICA eumelanin can also acts as a hydroxyl (OH) and nitric oxide (NO) scavenging and H donor [68].

In the 1970s, McGinnes observed for the first time the electrical properties of the eumelanin material in the hydrated state [69]. He explained this phenomenon with the amorphous organic semiconductor model, in which the absorbed water is distributed throughout the bulk of the polymer, lowering the activation energy for the hopping transport. This theory is in contrast with some different experimental evidence, such as the chemical disorder that explains the broadband UV-vis spectrum [65] and the presence of several ionizable groups in the structure of eumelanin.

Recent work has highlighted that two processes of one-electron one-proton removal can reversibly oxidize the building blocks of eumelanin, DHI and DHICA, into their ortho-quinone forms [70]. Eumelanin is hence an effective electron transfer agent in a variety of reduction-oxidation systems [71]. The redox forms of DHI and DHICA, represented in figure 1.3 coexist in eumelanin [72].

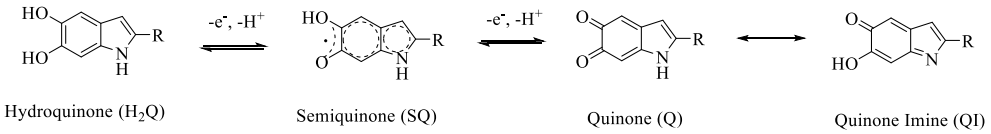

Figure 1.3 Redox forms of DHI and DHICA eumelanin building blocks: hydroquinone (H_2Q), semiquinone (SQ), Quinone (Q) and the tautomer quinone imine (QI).
R is -H in DHI and -COOH in DHICA.

In the presence of water, the comproportionation equilibrium between the quinone and catechol species controls the relative concentrations of the three redox states (figure 1.4), producing protons and free radicals (electrons) as charge carriers in the process [73]. This reaction is essential in determining the electrical properties of eumelanin that can be looked as hybrid ionic-electronic conductor [74].

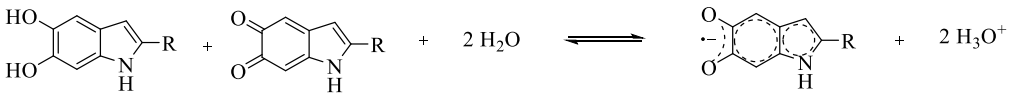

Figure 1.4 The comproportionation equilibrium reaction between hydroquinone (H_2Q) semiquinone (SQ) and quinone (Q) species in presence of water.
R is -H in DHI and -COOH in DHICA.

Other important physicochemical characteristics that make eumelanin a unique material are solid-state photoconductivity, metal, and drug binding properties [75, 76], and intrinsic biocompatibility.

2.6 Organic Electronics and Bioelectronics Applications of Eumelanin

The peculiar physicochemical properties of eumelanin as well as the intense scientific research efforts conducted so far have made these biopolymers a perfect choice for multiple and diverse applications in organic electronics [39, 77, 78].

Due to its broadband absorption across the entire UV–vis spectrum, eumelanin has been explored for use in the photovoltaic area. Mula et al. [79] have, for example, experimentally created eumelanin/porous silicon surfaces for use in solar cells. P-n eumelanin/porous silicon donor-acceptor bulk heterojunctions were formed by casting methanol-soluble fraction and methanol/water-soluble fraction of DHI eumelanin onto etched Si substrates and placing them between the top and bottom Au sputtered electrodes.

In dye-sensitized solar cells (DSSCs) based on TiO_2 nanocomposite electrodes, Lee et al. have employed eumelanin from pure squid ink as a dye [80], demonstrating the potential of eumelanin to sensitize TiO_2 nanotubes. Despite these intriguing results, the exploitation of eumelanin in photovoltaic area is still in its infancy due to several difficulties, the main one being the uncertainty surrounding the energetic levels of its HOMO and LUMO.

In a more recent paper, Migliaccio et al. have reported the integration of the commercial poly(3,4-ethylenedioxythiophene):poly(4-styrenesulfonate) (PEDOT: PSS) with eumelanin [81]. Eumelanin/PEDOT:PSS films have showed good conductivity, high transparency, and better water resistance than PEDOT:PSS film, suggesting their application as anodes for indium tin oxide (ITO)-free organic light emitting diodes (OLEDs [82]). The voltage-efficiency and luminance-efficiency curves of eumelanin/PEDOT:PSS anodes have been compared with those of an ITO electrode and an ITO-free electrode PEDOT:PSS. Eumelanin/PEDOT:PSS anodes have OLED efficiency close to that of ITO-free anodes. Comparing eumelanin/PEDOT: PSS anodes with ITO and ITO-free anodes, the authors have reported lower turn-on voltage for those containing biopolymer. This outcome not

only demonstrated that the presence of eumelanin in PEDOT: PSS enhances its hole injection properties, but also laid the foundation for the potential of eumelanin in OLEDs technology.

The employment of eumelanin as an active component in energy storage devices has been made possible by the combined effects of the redox activity and metal ion binding capabilities of the building blocks of DHI and DHICA. Both natural and synthetic eumelanin thin films have been explored as anodes and cathodes for sodium-ion [83] and magnesium-ion batteries [84] respectively. Furthermore, Xu et al. have developed light-assisted eumelanin-based supercapacitors [85] that couple the solar energy conversion and energy storage properties of eumelanin, where the electrodes made from this biopolymer have been obtained by drop casting on activated carbon paper.

The hydration-dependent electrical response of this pigment, which is described in the previous paragraph, has inspired the development of biosensors [38, 86] and eumelanin-based organic electrochemical transistors (OECTs) [78]. Recently, an OECT device has been fabricated for studying the electrical response of eumelanin in a biomimetic aqueous suspension state, exploring the possible development of a biosensor aimed at evaluating the biopolymer concentration and redox state in its environment [87]. The work in this study has brought to light the high sensitivity of the device response to eumelanin, which provides new insight into the redox properties of the polymer and guides the rational design and implementation of bioinspired devices with tailored electrical behaviour.

Additionally, in 2018 Mosert et al. demonstrated a novel eumelanin-based all-solid-state OECT that is capable of efficiently transducing proton-to-electron currents, representing a significant advance in the field of bioelectronics [78].

Thanks to its intrinsic biocompatibility combined with unique physicochemical and electrical properties, many research and technological efforts have directed the exploration of eumelanin applications in biocompatible batteries [83] and memory devices [88].

Furthermore, remaining in the field of bioelectronics, it has been possible to create eumelanin-based 3D architectures of potential interest for tissue engineering

applications. A valuable example is the fabrication of eumelanin-coated polylactic acid (PLA) microfibers that have been tested as scaffolds to control and direct the growth and maturation of SH-SY5Y neuroblastoma cells [89].

Ultimately, eumelanin is also a promising choice for biotechnological and biomedical applications such as drug delivery [90, 91], melanoma detection [92], liver protection from alcohol-induced stress [91], and many others [93, 94].

2.7 Thin film fabrication

The process of miniaturization of electronic and bioelectronic devices in common daily use is largely based on the manufacture of thin films of functional materials.
For this reason, an absolute prerequisite to the full realization of eumelanin active layers within organic electronic devices is the production of smooth, continuous, uniform, and reproducible thin films.
A turning point in film fabrication was the study conducted by Bothma and de Boor in 2008 [101], who used a eumelanin solution produced by alkaline treatment to fabricate high-quality synthetic eumelanin thin films.
Following this, many other publications have described the fabrication of eumelanin films using drop casting or spin coating. These methods typically require alkaline treatment of eumelanin samples [95, 96] or very aggressive synthetic procedures such as the oxidation of L-DOPA in dimethyl sulfoxide (DMSO) promoted by benzoyl peroxide over days [97-99]. Good biocompatibility of eumelanin films by spin-casting from DMSO [100] or an aqueous alkaline solution has been reported by Bettinger and Bruggeman.
Numerous research groups have focused on solution processing for the fabrication of eumelanin thin films [97, 101-107] during which alternative fabrication techniques such as spray-coating [108], electrospray deposition [109, 110], matrix-assisted pulsed laser deposition [110, 111], thermal evaporation [112] have also been explored throughout the past twenty years. Furthermore, alkaline suspensions of eumelanin aggregates [98, 113, 114] have also been employed for the self-assembly of eumelanin films on Au and graphite surfaces via electrochemical methods.
Despite the good results obtained, promising developments have been made, starting with a different approach based on the polymerization of eumelanin precursors on substrates. Regarding this strategy, Subianto and Will have electrochemically oxidized a DOPA solution on an ITO glass electrode [115] to produce free-standing eumelanin films. Cyclic voltammetry and constant potential methods [98] have been employed for the electrochemical polymerization of DHI on ITO. Furthermore,

dopamine has been used as a precursor to obtain polydopamine, which is a eumelanin-like film. This allows for the coating of a wide range of substrates by simple immersion in dopamine solution [116, 117]. It should be noted that in these works the alkaline medium [117, 118] has produced the thickest films.

To obtain a thin film of eumelanin featuring high quality and deep chemical control, the Ammonia Induced Solid State Polymerization (AISPP) protocol was first introduced by Pezzella et al. [101]. It is mainly based on a two-step approach:

1. Spin coating deposition of a thin film of the monomer precursor, DHI, that is completely soluble in common organic solvents.
2. Exposing the DHI thin film to air-equilibrated ammonia gas vapours to promote solid-state oxidative polymerization.

Furthermore, by fabricating the film on quartz substrates, the polymerization process can be easily followed by UV-vis spectroscopy through the disappearance of the characteristic absorption maximum of DHI simultaneously with the increase in absorbance in the visible spectral region, which leads to the typical broadband absorption of eumelanin. The authors have reported extremely smooth, homogeneous, and stable eumelanin films using the AISSP methodology. Films observed with the atomic force microscope (AFM) have revealed the existence of columnar structures a few nanometers high. Pezzella et al. have recently conducted morphological studies on eumelanin films made with AISSP methodology. starting from DHI solutions with concentrations varying from 25 mg ml^{-1} to 200 mg ml^{-1}. From these investigations, it has been underlined that the oxidized DHI films spontaneously form wrinkles only in films with a thickness greater than 250 nm under ambient conditions [106], while the thinner films are smooth, showing columnar structures. These results have led to the hypothesis that the self-wrinkling of AISSP-DHI is caused by inhomogeneous oxidation processes of the thick film, in which the outer and inner layers would undergo faster and slower oxidation rates, respectively.

References

1. Riley, P.A., J. Borovanský, and I. Wiley, *Melanins and melanosomes : biosynthesis, biogenesis, physiological, and pathological functions*. 2011, Weinheim John Wiley distributor: Chichester : Wiley-VCH.

2. Solano, F., *Melanins: Skin Pigments and Much More—Types, Structural Models, Biological Functions, and Formation Routes.* New Journal of Science, 2014. **2014**: p. 498276.

3. Swan, G.A., *Structure, chemistry, and biosynthesis of the melanins.* Fortschr Chem Org Naturst, 1974. **31**(0): p. 521-82.

4. Prota, G., *Melanins and melanogenesis*. 2012: Academic Press.

5. Kollias, N., et al., *New trends in photobiology: Photoprotection by melanin.* Journal of Photochemistry and Photobiology B-biology, 1991. **9**: p. 135-160.

6. Hearing, V.J., *Biochemical control of melanogenesis and melanosomal organization.* J Investig Dermatol Symp Proc, 1999. **4**(1): p. 24-8.

7. Nordlund, J.J. *The pigmentary system : physiology and pathophysiology*. 1998.

8. Simon, J.D. and D.N. Peles, *The red and the black.* Acc Chem Res, 2010. **43**(11): p. 1452-60.

9. Solano, F., *Photoprotection versus photodamage: updating an old but still unsolved controversy about melanin.* Polymer International, 2016. **65**(11): p. 1276-1287.

10. Cao, W., et al., *Unraveling the Structure and Function of Melanin through Synthesis.* J Am Chem Soc, 2021. **143**(7): p. 2622-2637.

11. Smythies, J., *On the Function of Neuromelanin.* Proceedings: Biological Sciences, 1996. **263**(1369): p. 487-489.

12. Bush, W.D., et al., *The surface oxidation potential of human neuromelanin reveals a spherical architecture with a pheomelanin core and a eumelanin surface.* Proc Natl Acad Sci U S A, 2006. **103**(40): p. 14785-9.

13. Badillo-Ramírez, I., J.M. Saniger, and S. Rivas-Arancibia, *5-S-cysteinyl-dopamine, a neurotoxic endogenous metabolite of dopamine: Implications for Parkinson's disease.* Neurochem Int, 2019. **129**: p. 104514.

14. Pezzella, A. and J. Wünsche, *Eumelanin: An Old Natural Pigment and a New Material for Organic Electronics – Chemical, Physical, and Structural Properties in Relation to Potential Applications*, in *Organic Electronics*. 2013. p. 113-137.

15. Jiang, S., et al., *Regulation of DHICA-mediated antioxidation by dopachrome tautomerase: Implication for skin photoprotection against UVA radiation.* Free Radical Biology and Medicine, 2010. **48**(9): p. 1144-1151.

16. Nofsinger, J.B., S.E. Forest, and J.D. Simon, *Explanation for the Disparity among Absorption and Action Spectra of Eumelanin.* The Journal of Physical Chemistry B, 1999. **103**(51): p. 11428-11432.

17. Menon, I.A. and H.F. Haberman, *Mechanisms of action of melanins.* British Journal of Dermatology, 1977. **97**(1): p. 109-112.

18. Lin, J.Y. and D.E. Fisher, *Melanocyte biology and skin pigmentation.* Nature, 2007. **445**(7130): p. 843-50.

19. Cabaço, L.C., et al., *The Dark Side of Melanin Secretion in Cutaneous Melanoma Aggressiveness.* Front Oncol, 2022. **12**: p. 887366.

20. McMichael, A.J., et al. *Solar Ultraviolet Radiation: Global burden of disease from solar ultraviolet radiation*. 2006.

21. Scott, M.C., et al., *Human melanocortin 1 receptor variants, receptor function and melanocyte response to UV radiation.* Journal of Cell Science, 2002. **115**(11): p. 2349-2355.

22. Kennedy, C., et al., *Melanocortin 1 receptor (MC1R) gene variants are associated with an increased risk for cutaneous melanoma which is largely independent of skin type and hair color.* J Invest Dermatol, 2001. **117**(2): p. 294-300.

23. Prota, G., *Progress in the chemistry of melanins and related metabolites.* Med Res Rev, 1988. **8**(4): p. 525-56.

24. Koike, S. and K. Yamasaki, *Melanogenesis Connection with Innate Immunity and Toll-Like Receptors.* Int J Mol Sci, 2020. **21**(24).

25. *Melanins: Functions, Biotechnological Production, and Applications*. 2023: Springer Cham.

26. Xie, H., et al., *Functional anthology of intrinsic disorder. 3. Ligands, post-translational modifications, and diseases associated with intrinsically disordered proteins.* J Proteome Res, 2007. **6**(5): p. 1917-32.

27. Shimizu, K., et al., *Predicting mostly disordered proteins by using structure-unknown protein data.* BMC Bioinformatics, 2007. **8**: p. 78.

28. Loettgers, A., *Getting Abstract Mathematical Models in Touch with Nature.* Science in Context, 2007. **20**(1): p. 97-124.

29. Meredith, P. and T. Sarna, *The physical and chemical properties of eumelanin.* Pigment Cell Research, 2006. **19**(6): p. 572-594.

30. Meredith, P., et al., *Towards structure–property–function relationships for eumelanin.* Soft Matter, 2006. **2**(1): p. 37-44.

31. Samokhvalov, A., Y. Liu, and J.D. Simon, *Characterization of the Fe(III)-binding Site in Sepia Eumelanin by Resonance Raman Confocal Microspectroscopy.* Photochemistry and Photobiology, 2004. **80**(1): p. 84-88.

32. Hong, L., Y. Liu, and J.D. Simon, *Binding of Metal Ions to Melanin and Their Effects on the Aerobic Reactivity.* Photochemistry and Photobiology, 2004. **80**(3): p. 477-481.

33. Bridelli, M.G., A. Ciati, and P.R. Crippa, *Binding of chemicals to melanins re-examined: adsorption of some drugs to the surface of melanin particles.* Biophys Chem, 2006. **119**(2): p. 137-45.

34. Larsson, B.S., *Interaction between chemicals and melanin.* Pigment Cell Res, 1993. **6**(3): p. 127-33.

35. Berg, S.Z. and J. Berg, *Melanin: a unifying theory of disease as exemplified by Parkinson's, Alzheimer's, and Lewy body dementia.* Front Immunol, 2023. **14**: p. 1228530.

36. Panzella, L., et al., *The Late Stages of Melanogenesis: Exploring the Chemical Facets and the Application Opportunities.* Int J Mol Sci, 2018. **19**(6).

37. Kumar, P., et al., *Melanin-based flexible supercapacitors.* Journal of Materials Chemistry C, 2016. **4**(40): p. 9516-9525.

38. Wu, T.-F. and J.-D. Hong, *Synthesis of water-soluble dopamine–melanin for ultrasensitive and ultrafast humidity sensor.* Sensors and Actuators B: Chemical, 2016. **224**: p. 178-184.

39. Vahidzadeh, E., A.P. Kalra, and K. Shankar, *Melanin-based electronics: From proton conductors to photovoltaics and beyond.* Biosensors and Bioelectronics, 2018. **122**: p. 127-139.

40. Meredith, P., et al., *Broadband Photon-harvesting Biomolecules for Photovoltaics*, in *Artificial Photosynthesis*. 2005. p. 35-65.

41. Panzella, L., et al., *The First 5,6-Dihydroxyindole Tetramer by Oxidation of 5,5‘,6,6‘-Tetrahydroxy- 2,4‘-biindolyl and an Unexpected Issue of Positional Reactivity en Route to Eumelanin-Related Polymers.* Organic Letters, 2007. **9**(7): p. 1411-1414.

42. Kalachyova, Y., et al., *Reversible switching of PEDOT:PSS conductivity in the dielectric–conductive range through the redistribution of light-governing polymers.* RSC Advances, 2018. **8**(20): p. 11198-11206.

43. Wakayama, Y., et al., *Photochromism for optically functionalized organic field-effect transistors: a comprehensive review.* Journal of Materials Chemistry C, 2020. **8**(32): p. 10956-10974.

44. d'Ischia, M., et al., *Melanin Biopolymers: Tailoring Chemical Complexity for Materials Design.* Angew Chem Int Ed Engl, 2020. **59**(28): p. 11196-11205.

45. Raper, H.S., *The aerobic oxidases.* Physiological Reviews, 1928. **8**(2): p. 245-282.

46. Raper, H.S., *The Tyrosinase-tyrosine Reaction: Production from Tyrosine of 5: 6-Dihydroxyindole and 5: 6-Dihydroxyindole-2-carboxylic Acid-the Precursors of Melanin.* Biochem J, 1927. **21**(1): p. 89-96.

47. Mason, H.S., *The chemistry of melanin; mechanism of the oxidation of dihydroxyphenylalanine by tyrosinase.* J Biol Chem, 1948. **172**(1): p. 83-99.

48. Pezzella, A., et al., *An integrated approach to the structure of Sepia melanin. Evidence for a high proportion of degraded 5,6-dihydroxyindole-2-carboxylic acid units in the pigment backbone.* Tetrahedron, 1997. **53**(24): p. 8281-8286.

49. Liu, Y. and J.D. Simon, *Isolation and Biophysical Studies of Natural Eumelanins: Applications of Imaging Technologies and Ultrafast Spectroscopy.* Pigment Cell Research, 2003. **16**(6): p. 606-618.

50. d'Ischia, M., et al., *Melanins and melanogenesis: methods, standards, protocols.* Pigment Cell & Melanoma Research, 2013. **26**(5): p. 616-633.

51. Nicolaus, R.A., *Melanins*. 1968, Hermann Paris: Paris.

52. d'Ischia, M., et al., *Melanins and melanogenesis: from pigment cells to human health and technological applications.* Pigment Cell Melanoma Res, 2015. **28**(5): p. 520-44.

53. d'Ischia, M., et al., *New intermediates in the oxidative polymerisation of 5,6-dihydroxyindole to melanin promoted by the peroxidase/H2O2 system.* Tetrahedron, 1990. **46**(16): p. 5789-5796.

54. Prota, G., *Melanins and melanogenesis*. 1992, Academic Press Inc: San Diego.

55. Micillo, R., et al., *Unexpected impact of esterification on the antioxidant activity and (photo)stability of a eumelanin from 5,6-dihydroxyindole-2-carboxylic acid.* Pigment Cell Melanoma Res, 2018. **31**(4): p. 475-483.

56. d'Ischia, M., et al., *Melanins and melanogenesis: methods, standards, protocols.* Pigment Cell Melanoma Res, 2013. **26**(5): p. 616-33.

57. Ito, S., *Reexamination of the structure of eumelanin.* Biochimica et Biophysica Acta (BBA) - General Subjects, 1986. **883**(1): p. 155-161.

58. d'Ischia, M., et al., *Melanin Biopolymers: Tailoring Chemical Complexity for Materials Design.* Angewandte Chemie International Edition, 2020. **59**(28): p. 11196-11205.

59. Cheng, J., S.C. Moss, and M. Eisner, *X-ray characterization of melanins--II.* Pigment Cell Res, 1994. **7**(4): p. 263-73.

60. d'Ischia, M., et al., *5,6-Dihydroxyindoles and Indole-5,6-diones.* Advances in Heterocyclic Chemistry, 2005. **89**: p. 1-63.

61. d'Ischia, M., A. Napolitano, and A. Pezzella, *5,6-Dihydroxyindole Chemistry: Unexplored Opportunities Beyond Eumelanin.* European Journal of Organic Chemistry, 2011. **2011**(28): p. 5501-5516.

62. Panzella, L., et al., *The first 5,6-dihydroxyindole tetramer by oxidation of 5,5',6,6'-tetrahydroxy- 2,4'-biindolyl and an unexpected issue of positional reactivity en route to eumelanin-related polymers.* Org Lett, 2007. **9**(7): p. 1411-4.

63. Pezzella, A., D. Vogna, and G. Prota, *Atropoisomeric melanin intermediates by oxidation of the melanogenic precursor 5,6-dihydroxyindole-2-carboxylic acid under biomimetic conditions.* Tetrahedron, 2002. **58**: p. 3681-3687.

64. Pezzella, A., D. Vogna, and G. Prota, *Synthesis of optically active tetrameric melanin intermediates by oxidation of the melanogenic precursor 5,6-dihydroxyindole-2-carboxylic acid under biomimetic conditions.* Tetrahedron-asymmetry, 2003. **14**: p. 1133-1140.

65. Tran, M.L., B.J. Powell, and P. Meredith, *Chemical and structural disorder in eumelanins: a possible explanation for broadband absorbance.* Biophys J, 2006. **90**(3): p. 743-52.

66. Pezzella, A., et al., *Short-Lived Quinonoid Species from 5,6-Dihydroxyindole Dimers en Route to Eumelanin Polymers: Integrated Chemical, Pulse Radiolytic, and Quantum Mechanical Investigation.* Journal of the American Chemical Society, 2006. **128**(48): p. 15490-15498.

67. Panzella, L., et al., *Atypical Structural and π-Electron Features of a Melanin Polymer That Lead to Superior Free-Radical-Scavenging Properties.* Angewandte Chemie International Edition, 2013. **52**(48): p. 12684-12687.

68. Jiang, S., et al., *Regulation of DHICA-mediated antioxidation by dopachrome tautomerase: implication for skin photoprotection against UVA radiation.* Free Radic Biol Med, 2010. **48**(9): p. 1144-51.

69. McGinness, J., P. Corry, and P. Proctor, *Amorphous semiconductor switching in melanins.* Science, 1974. **183**(4127): p. 853-5.

70. Gan, E.V., H.F. Haberman, and I.A. Menon, *Electron transfer properties of melanin.* Arch Biochem Biophys, 1976. **173**(2): p. 666-72.

71. Figge, F., *Melanin A Natural Reversible Oxidation-Reduction System and Indicator.* Experimental Biology and Medicine, 1939. **41**: p. 127-127.

72. Di Mauro, E., et al., *Natural melanin pigments and their interfaces with metal ions and oxides: emerging concepts and technologies.* MRS Communications, 2017. **7**(2): p. 141-151.

73. Mostert, A.B., et al., *Role of semiconductivity and ion transport in the electrical conduction of melanin.* Proc Natl Acad Sci U S A, 2012. **109**(23): p. 8943-7.

74. Sheliakina, M., A.B. Mostert, and P. Meredith, *Decoupling Ionic and Electronic Currents in Melanin.* Advanced Functional Materials, 2018. **28**(46): p. 1805514.

75. Fan, Q., et al., *Transferring Biomarker into Molecular Probe: Melanin Nanoparticle as a Naturally Active Platform for Multimodality Imaging.* Journal of the American Chemical Society, 2014. **136**(43): p. 15185-15194.

76. Araújo, M., et al., *Bioactivity, mechanical properties and drug delivery ability of bioactive glass-ceramic scaffolds coated with a natural-derived polymer.* Materials Science and Engineering: C, 2017. **77**: p. 342-351.

77. Kautz, R., et al., *Cephalopod-Derived Biopolymers for Ionic and Protonic Transistors.* Adv Mater, 2018. **30**(19): p. e1704917.

78. Sheliakina, M., A.B. Mostert, and P. Meredith, *An all-solid-state biocompatible ion-to-electron transducer for bioelectronics.* Materials Horizons, 2018. **5**(2): p. 256-263.

79. Mula, G., et al., *Photovoltaic properties of PSi impregnated with eumelanin.* Nanoscale Res Lett, 2012. **7**(1): p. 377.

80. Lee, J.-W., et al., *Dye-sensitized solar cells using purified squid ink nanoparticles coated on TiO_2 nanotubes/nanoparticles.* Journal of the Ceramic Society of Japan, 2013. **121**(1409): p. 123-127.

81. Migliaccio, L., et al., *Eumelanin–PEDOT:PSS Complementing En Route to Mammalian-Pigment-Based Electrodes: Design and Fabrication of an ITO-Free Organic Light-Emitting Device.* Advanced Electronic Materials, 2017. **3**(5): p. 1600342.

82. Migliaccio, L., et al., *Impact of Eumelanin–PEDOT Blending: Increased PEDOT Crystalline Order and Packing–Conductivity Relationship in Ternary PEDOT:PSS:Eumelanin Thin Films.* Advanced Electronic Materials, 2019. **5**(3): p. 1800585.

83. Kim, Y.J., et al., *Biologically derived melanin electrodes in aqueous sodium-ion energy storage devices.* Proc Natl Acad Sci U S A, 2013. **110**(52): p. 20912-7.

84. Kim, Y.J., et al., *Catechol-mediated reversible binding of multivalent cations in eumelanin half-cells.* Adv Mater, 2014. **26**(38): p. 6572-9.

85. Xu, R., et al., *Melanin: A Greener Route To Enhance Energy Storage under Solar Light.* ACS Omega, 2019. **4**(7): p. 12244-12251.

86. Wu, T.-F., B.-H. Wee, and J.-D. Hong, *An Ultrasensitive and Fast Moisture Sensor Based on Self-Assembled Dopamine–Melanin Thin Films.* Advanced Materials Interfaces, 2015. **2**(15): p. 1500203.

87. Tarabella, G., et al., *Irreversible evolution of eumelanin redox states detected by an organic electrochemical transistor: en route to bioelectronics and biosensing.* Journal of Materials Chemistry B, 2013. **1**(31): p. 3843-3849.

88. Ambrico, M., et al., *Hysteresis-type current–voltage characteristics in Au/eumelanin/ITO/glass structure: Towards melanin based memory devices.* Organic Electronics, 2010. **11**(11): p. 1809-1814.

89. Fasolino, I., et al., *Eumelanin Coated PLA Electrospun Micro Fibers as Bioinspired Cradle for SH-SY5Y Neuroblastoma Cells Growth and Maturation.* ACS Appl Mater Interfaces, 2017. **9**(46): p. 40070-40076.

90. Fan, Q., et al., *Transferring biomarker into molecular probe: melanin nanoparticle as a naturally active platform for multimodality imaging.* J Am Chem Soc, 2014. **136**(43): p. 15185-94.

91. Araujo, M., et al., *Bioactivity, mechanical properties and drug delivery ability of bioactive glass-ceramic scaffolds coated with a natural-derived polymer.* Mater Sci Eng C Mater Biol Appl, 2017. **77**: p. 342-351.

92. Jimbow, K., et al., *Characterization of melanogenesis and morphogenesis of melanosomes by physicochemical properties of melanin and melanosomes in malignant melanoma.* Cancer Res, 1984. **44**(3): p. 1128-34.

93. Solano, F., *Melanin and Melanin-Related Polymers as Materials with Biomedical and Biotechnological Applications-Cuttlefish Ink and Mussel Foot Proteins as Inspired Biomolecules.* Int J Mol Sci, 2017. **18**(7).

94. Galeb, H.A., et al., *Melanins as Sustainable Resources for Advanced Biotechnological Applications.* Global Challenges, 2021. **5**(2): p. 2000102.

95. Ambrico, M., et al., *Melanin layer on silicon: an attractive structure for a possible exploitation in bio-polymer based metal-insulator-silicon devices.* Adv Mater, 2011. **23**(29): p. 3332-6.

96. Sangaletti, L., et al., *Polymerization effects and localized electronic states in condensed-phase eumelanin.* Physical Review B, 2009. **80**(17): p. 174203.

97. Dezidério, S.N., et al., *Thin films of synthetic melanin.* Journal of Non-Crystalline Solids, 2004. **338-340**: p. 634-638.

98. Kim, I.G., et al., *Electrochemical growth of synthetic melanin thin films by constant potential methods.* Electrochimica Acta, 2011. **56**(7): p. 2954-2959.

99. Lynge, M.E., et al., *Polydopamine--a nature-inspired polymer coating for biomedical science.* Nanoscale, 2011. **3**(12): p. 4916-28.

100. Bettinger, C.J., et al., *Biocompatibility of biodegradable semiconducting melanin films for nerve tissue engineering.* Biomaterials, 2009. **30**(17): p. 3050-7.

101. Pezzella, A., et al., *Stem cell-compatible eumelanin biointerface fabricated by chemically controlled solid state polymerization.* Materials Horizons, 2015. **2**(2): p. 212-220.

102. da Silva, M.I.N., et al., *Synthetic melanin thin films: Structural and electrical properties.* Journal of Applied Physics, 2004. **96**(10): p. 5803-5807.

103. Bronze-Uhle, E.S., et al., *Synthesis and characterization of melanin in DMSO.* Journal of Molecular Structure, 2013. **1047**: p. 102-108.

104. Bettinger, C.J., et al., *Biocompatibility of biodegradable semiconducting melanin films for nerve tissue engineering.* Biomaterials, 2009. **30**(17): p. 3050-3057.

105. Wünsche, J., et al., *Eumelanin thin films: solution-processing, growth, and charge transport properties.* Journal of Materials Chemistry B, 2013. **1**(31): p. 3836-3842.

106. Oscurato, S.L., et al., *Spontaneous wrinkle emergence in nascent eumelanin thin films.* Soft Matter, 2019. **15**(45): p. 9261-9270.

107. Bothma, J.P., et al., *Device-Quality Electrically Conducting Melanin Thin Films.* Advanced Materials, 2008. **20**(18): p. 3539-3542.

108. Abbas, M., et al., *Structural, electrical, electronic and optical properties of melanin films.* Eur Phys J E Soft Matter, 2009. **28**(3): p. 285-91.

109. Abbas, M., et al., *Control of Structural, Electronic, and Optical Properties of Eumelanin Films by Electrospray Deposition.* The Journal of Physical Chemistry B, 2011. **115**(38): p. 11199-11207.

110. Bloisi, F., et al., *Matrix assisted pulsed laser deposition of melanin thin films.* Journal of Applied Physics, 2011. **110**(2).

111. Bloisi, F., et al., *Effect of substrate temperature on MAPLE deposition of synthetic eumelanin films.* Applied Physics A, 2011. **105**(3): p. 619-627.

112. De Marchi, F., et al., *Self-assembly of 5,6-dihydroxyindole-2-carboxylic acid: polymorphism of a eumelanin building block on Au(111).* Nanoscale, 2019. **11**(12): p. 5422-5428.

113. Orive, A.G., et al., *Electrochemical preparation of metal–melanin functionalized graphite surfaces.* Electrochimica Acta, 2009. **54**(5): p. 1589-1596.

114. Díaz, P., et al., *Electrochemical Self-Assembly of Melanin Films on Gold.* Langmuir, 2005. **21**(13): p. 5924-5930.

115. Subianto, S., G. Will, and P. Meredith, *Electrochemical synthesis of melanin free-standing films.* Polymer, 2005. **46**(25): p. 11505-11509.

116. Lee, H., et al., *Mussel-inspired surface chemistry for multifunctional coatings.* Science, 2007. **318**(5849): p. 426-30.

117. Bernsmann, F., et al., *Protein adsorption on dopamine-melanin films: role of electrostatic interactions inferred from zeta-potential measurements versus chemisorption.* J Colloid Interface Sci, 2010. **344**(1): p. 54-60.

118. Müller, M. and B. Kessler, *Deposition from dopamine solutions at Ge substrates: an in situ ATR-FTIR study.* Langmuir, 2011. **27**(20): p. 12499-505.

3 Design, synthesis, and characterization of a novel eumelanin derivative for applications in energy storage systems

3.1 Introduction

Electrochemical energy storage (EES) devices are considered key future technologies, as their need is expected to increase in the next few years to store excess renewable energy associated with environmental conditions and distribute it back to the grid when it's needed [1-3]. Thanks to their energy efficiency, EES devices are becoming increasingly important in our everyday lives because they are applied to larger devices like electric vehicles and small devices such as laptops and cell phones [4].

Batteries are one of the most popular EES devices, and they are widely used throughout the world. Through redox reactions on the negative and positive electrodes, both of the insertion/intercalation and conversion type, the batteries guarantee a stable operating potential with a high specific charge storage capacity [5]. The main disadvantages of batteries are their inherently low power capacity (< 1 kW/kg) and short device cycle life [6-8].

For energy storage applications needing high specific power, supercapacitors are more appealing, with values usually > 10 kW/kg [9]. They provide high cyclic stability, but the low energy storage capacity (< 10 Wh/kg) is a severe constraint of

these supercapacitive systems [9]. An illustrative schematization of the performance of energy storage devices is summarized in the Ragone plot in figure 3.1.

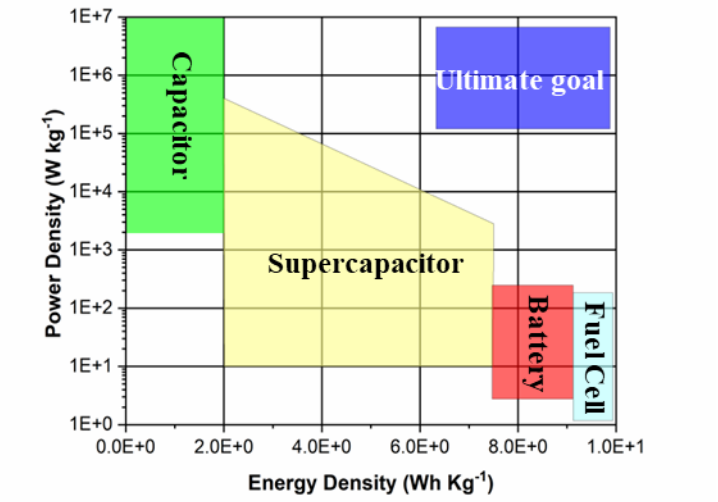

Figure 3.1 Ragone plots of energy storage devices inspired by [10].

The development of energy storage systems is focused on improving the performance of devices to simultaneously achieve high specific energy and high specific power.

One of the most recent aspects on which scientific and technological research is focusing its efforts concerns the use of safe, low-cost, and environmental-friendly materials [11]. In this context, organic compounds have been pervasive in the fabrication of modern energy storage devices, representing an attractive alternative to their traditional inorganic counterparts.

Organic materials are widely used as electrodes and electrolytes in the design of energy storage devices thanks to their unique properties. For the last few decades, different kinds of carbon-based materials such as graphene [12], carbon nanotube [13], and carbon cloth [14] have been used in various forms, such as powder, fiber, and foils, as organic electrodes. At the same time, redox active organic materials like small molecules, such as quinones [15], and conducting polymers including, PEDOT, polyaniline, polypyrrole, and polyindole, have been broadly studied as active components for EES devices [16].

There has been a growing focus on the utilisation of electrolytes in electrochemical energy storage devices [9]. Electrolytes can support charge transportation thanks to their peculiar ionic mobility, but at the same time, their chemical nature usually does not allow electron flow [17, 18]. One of the main applications of electrolytes is in electrochemical cells, where the first used electrolytes were liquid. They can be divided in aqueous or organic electrolytes, depending on the nature of the solvent in which the medium containing ions is dissolved. Propylene carbonate, ethylene carbonate, acetonitrile (ACN), and tetrahydrofuran (THF) are generally used as organic solvents [19]. Liquid electrolytes have been widely used in electrochemical energy storage devices thanks to their high ionic conductivity (10^{-2} – 10^{-1} S cm^{-1} for aqueous electrolytes and 10^{-3} – 10^{-2} S cm^{-1} for organic electrolytes) [20]. However, the organic redox electrode materials should be ideally insoluble in the electrolyte media [21]. Furthermore, the safety concerns associated with electrolytes, particularly the flammability and volatility of some organic solvents [22], combined with practical complications, including reduced flexibility, and packaging issues [23, 24] have represented serious limitations to their use. In recent years, the key role of this component in EES devices has been demonstrated by the development of innovative forms of electrolytes, including ionic liquid-based and polymer-based electrolytes [25, 26]. Solvent-free polymer electrolytes (PEs) have the potential to overcome the limitations associated with liquid electrolytes [27, 28]. A polymer electrolyte is made up of salt dissolved in a polymer matrix with a high molecular weight [29].

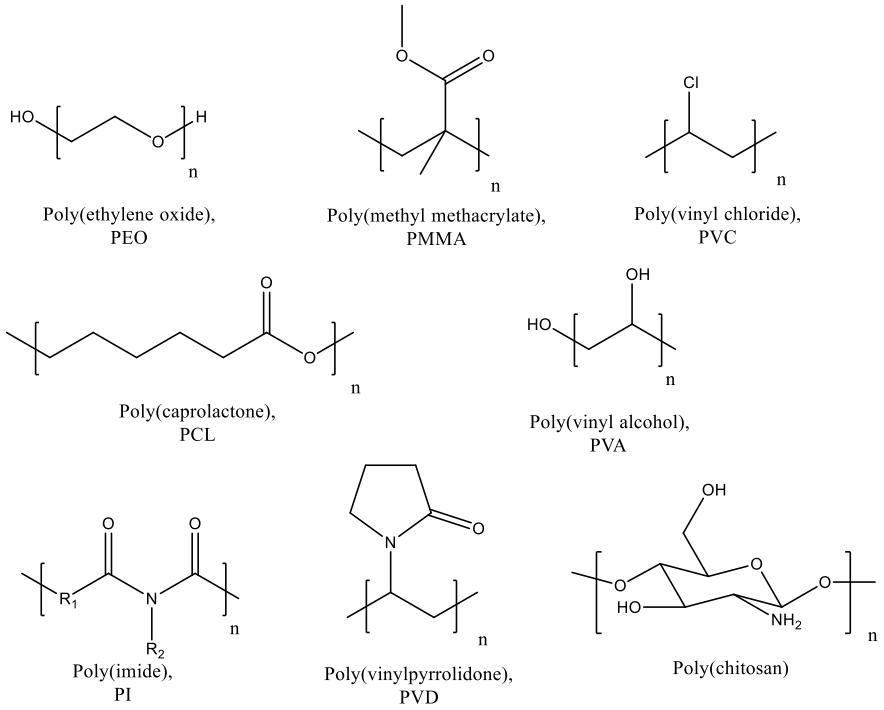

Figure 3.2 Chemical structures of common polymer electrolytes

The first ion conducting polymer was poly(ethyleneoxide) (PEO) dissolved with alkali metal salts, used for the first time in the 1970's [30]. This system was employed for the fabrication of the first all-solid-state battery, based on PEO-lithium salt electrolyte [31].

For the realization of electrochemical energy storage devices, the polymer electrolyte material should have the following properties [32-34]:

- Discrete ionic conductivity ($\sigma > 10^{-4}$ S cm^{-1}) at room temperature to achieve a level of performance close to that of liquid electrolyte-based devices.
- Ionic transference number close to 1. This is not strictly required, but the polymer electrolyte should preferably be a single-ion (cation) conducting system.
- Electrochemical and thermal stabilities. Polymer electrolytes should have a wide window of electrochemical stability around 3-4 V. To allow the device

to operate over a wider temperature range, they should also be thermally stable.

- Compatibility with the electrode materials. To avoid unwanted chemical reactions at the electrode/electrolyte interfaces, polymer electrolytes should possess high chemical stability.

Although significant progress has been made in improving the performance of polymer electrolytes, several issues still exist that largely hinder the development of PE-based EES devices. The main limitations are related to their intrinsic low ionic conductivity, lower than that of their liquid counterpart, poor contact at the electrode-electrolyte interface, and narrow electrochemical window potential, resulting in poor cycling performance [35, 36]. The literature has offered several approaches that can be employed to improve the shortcomings of the polymer electrolyte discussed above [37]. Blending, consisting of chemically or physically mixing two or more polymers, represents a way to reduce the degree of crystallinity of a host polymer matrix by increasing the amorphicity of the entire system, resulting in increased ion mobility and improved ion conduction [29, 38, 39]. For instance, the electrolyte obtained by combining poly(ethyleneoxide) and poly(epichlorohydrin), (EO-co-EPI), has shown encouraging levels of ionic conductivity compared to those observed with the two polymers alone [40].

The modifications made to the polymer electrolyte can also be chemical, exploiting one of the main advantages of organic electronics. Organic compounds allow for a level of chemical modification not achievable with inorganic counterparts. As chemists gain better control over the synthesis of organic species, various components can be modified to optimize their performance or integrated with biological systems to make the final products biocompatible, greatly expanding the fields of application of organic materials.

Among the emerging strategies for EES devices, considerable attention has been paid to the design of electrolyte systems that can support ionic mobility and at the same time allow electron flow. Specifically, this approach involves redox-active electrolyte

to improve the capacitance of electrode materials through redox reactions at the electrolyte-electrode interfaces [9, 41-44].

Redox active species, such as halide ions [45, 46], and phenylamide [47], quinones [48-60] have been reported in the literature to be capable of undergoing fast redox reactions on the surfaces of some carbon or metal oxide-based electrode materials.

At the same time, the growing interest in the production of biocompatible [61-63], biodegradable, and bioinspired [64] devices is encouraging the use of biological materials as active components in electronic devices [65, 66], thanks to the combination of their origin with properties suitable for the world of electronics. Among the various natural materials most widely used in electrochemical energy storage devices, eumelanin, and eumelanin-based materials have increasingly emerged as valuable choices in recent years. The biocompatibility and biodegradability properties of eumelanin associated with its redox activity have enabled the development of Na^+ and Mg^{2+} batteries [51, 67] and supercapacitors [68-73] for biomedical and green electronics applications.

In the next paragraphs will be discussed the chemical integration of DHICA eumelanin precursor as a redox active biological material with the syntone 2-amino-6-methylbenzothiazole (ABtz) [74]. The reported capability of ABtz to act as a metal chelating moiety [74-77] makes it a perfect candidate for eumelanin modification to explore its possible use as a redox-active polymer electrolyte in EES devices.

3.2 Synthesis of the acetylated DHICA derivative

The first step in the route towards a novel eumelanin derivative began with the choice of the most suitable starting indole monomer to introduce chemical modifications. In this perspective, the carboxyl group of DHICA offered an excellent anchoring site for the grafting of the benzothiazole system. The optical properties of ABtz, combined with its ability to chelate many metal ions, have attracted our interest [76, 78-81]. Direct conjugation of the two bicyclic indole-benzothiazole systems via an amide bond was expected to influence the chromophore of the final product, leading to a eumelanin derivative with optical features different from those of the biopolymer. Furthermore, the choice of the 2-amino-benzothiazole derivative was expected to be a good option for the stability of the final amide under physiological conditions, as well as favouring good solubility in organic solvents. For all these reasons, an optimized procedure for the preparation of DHICA amide was investigated (scheme 3.2.1) [82].

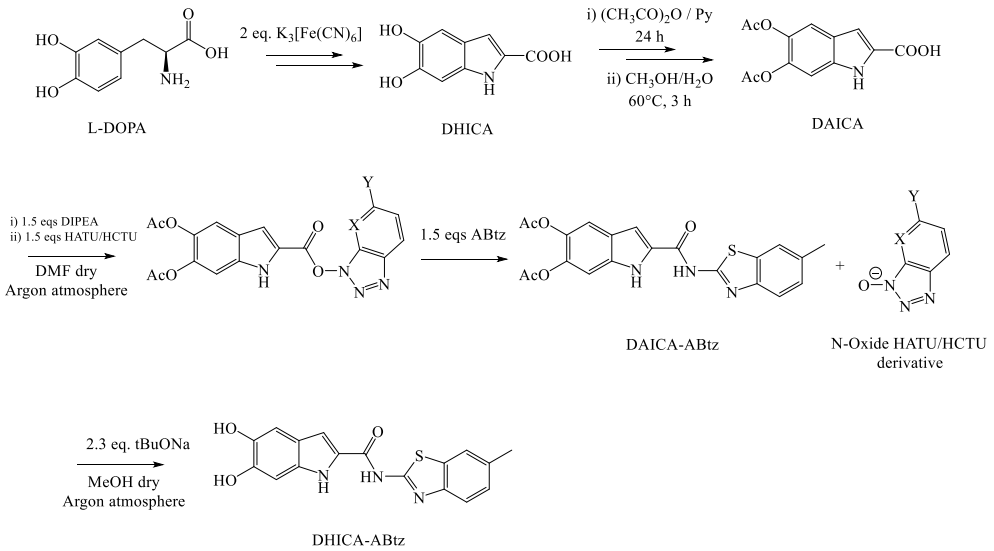

Scheme 3.2.1 Synthetic procedure for DHICA-ABtz. DHICA from DOPA.
Shown is also preparation of DHICA from DOPA.

First, the eumelanin precursor was synthesized through a one-pot reaction involving the oxidation of DOPA using potassium ferricyanide as an oxidizing agent [83]. The hydroxyl groups of DHICA were protected due to their sensitivity to oxidation and because they were expected to compete with the amine during the amidation reaction. For this purpose, the eumelanin precursor was acetylated using anhydride acetic/pyridine treatment overnight. To hydrolyze the unwanted anhydride generated in the carboxyl group, the acetylation crude was treated with 1:1 v/v methanol/water solution under reflux for 3 hours, obtaining the acetylated derivative, 5,6-diacetoxyindole-2-carboxylic acid (DAICA).

At this point, the designed synthesis involved the use of an activating agent to convert the OH of the carboxyl group of DAICA into a good leaving group before treatment with the amine. For this purpose, two of the most efficient coupling reagents used in peptide synthesis were explored, i.e. 1-[Bis(dimethylamino)methylene]-1H-1,2,3-triazolo[4,5-b] pyridinium 3-oxid hexafluorophosphate (HATU) and O-(1H-6-Chlorobenzotriazole-1-yl)-1,1,3,3-tetramethyluronium hexafluorophosphate (HCTU) [84-86], represented in figure 3.2.1.

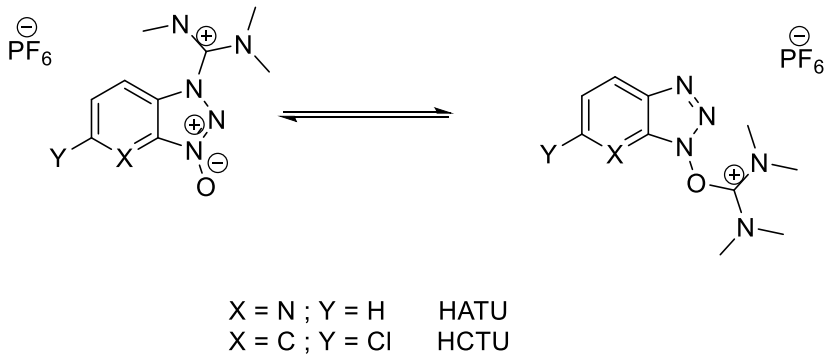

Figure 3.2.1 Structure of the coupling agents investigated.

The amidation reaction was carried out by simultaneously adding 1.5 equivalents of coupling agent and 1.5 equivalents of N,N-diisopropylethylamine (DIPEA) to a solution of DAICA in dry DMF. The reaction was carried out under argon atmosphere.

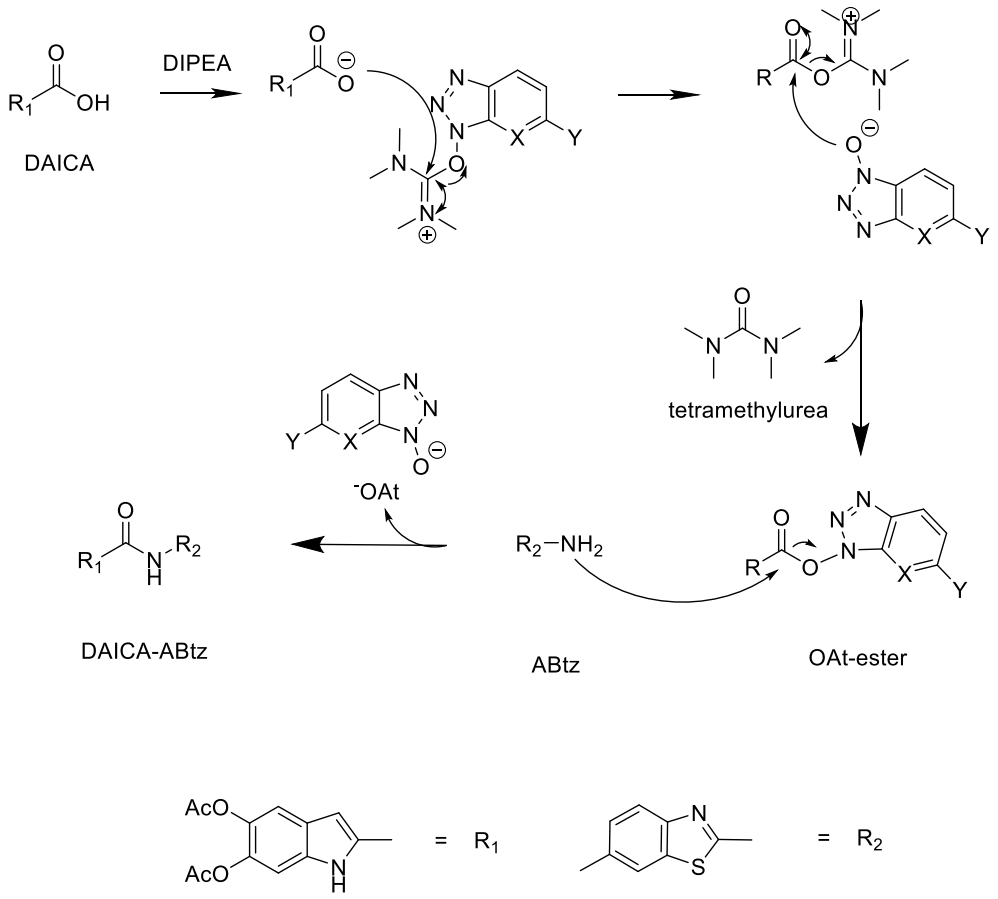

Scheme 3.2.2 Synthetic route of the coupling reaction.

In the first step of the amidation route (scheme 3.2.2), the reaction between the carboxylate anion (formed by deprotonation of the hindered organic base) and the coupling reagent led to the formation of the active ester of 1-hydroxy-7-azabenzotriazole (HOAt), abbreviated in the scheme 3.2.2 as OAt-ester.

One of the advantages of using these modern coupling reagents is the stability of the activated ester. In particular, the use of HATU promoted the nucleophilic attack of the amine thanks to the formation of a possible 7-membered cyclic transition state containing a hydrogen bond with the pyridine nitrogen (figure 3.2.2) [87].

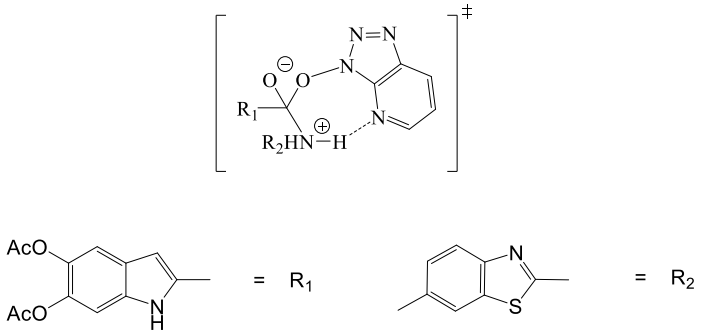

Figure 3.2.2 Possible 7-membered cyclic transition state formed during the nucleophilic attack of the amine.

The formation of this cyclic species reflects high coupling efficiency and high reaction rates.

The progress of the reaction was followed by thin-layer chromatography (TCL). After 30 minutes of reaction, the chromatographic analysis indicated the complete consumption of DAICA and the presence of an intense fluorescent spot, absent in the starting mixture, attributable to the formation of the OAt-ester. Subsequently, 1.5 equivalents of ABtz dissolved in dry DMF were added to the reaction mixture. Although after 1 hour the presence of a new spot was already observed in the TCL analysis, the reaction mixture was kept under stirring for up to 24 hours. Indeed, only after one day, the chromatographic analysis highlighted a complete consumption of the OAt-ester with the presence of the spot observed previously. By simply adding water to the reaction mixture, the formation of a yellowish precipitate was observed. The final product was taken up with ethyl acetate using a 5% v/v acetic acid solution to remove excess amine and water to eliminate excess coupling reagent and reaction byproducts.

The reaction promoted by HATU allowed to obtain a pure product with an isolation yield of 69%, compared to just over 50% with HCTU at the same reaction times.

Structural confirmation of the desired product, indicated in the reaction schemes 3.2.1 and 3.2.2 as DAICA-ABtz, occurred by 1D and 2D NMR and MALDI-TOF mass analysis. The ^{1}H-NMR spectrum of the amide (figure 3.2.3) showed a noteworthy signal at 11.25 ppm, absent in the DAICA spectrum attributable to the amide NH,

and no NH_2 signal compared to that present in the ABtz spectrum at 6.76 ppm (figure 3.2.4). Finally, the MALDI-TOF mass spectrum revealed the presence of signals at m/z 446 and 462, attributable to the $[M+Na]^+$, $[M+ K]^+$ ions of DAICA-ABtz respectively.

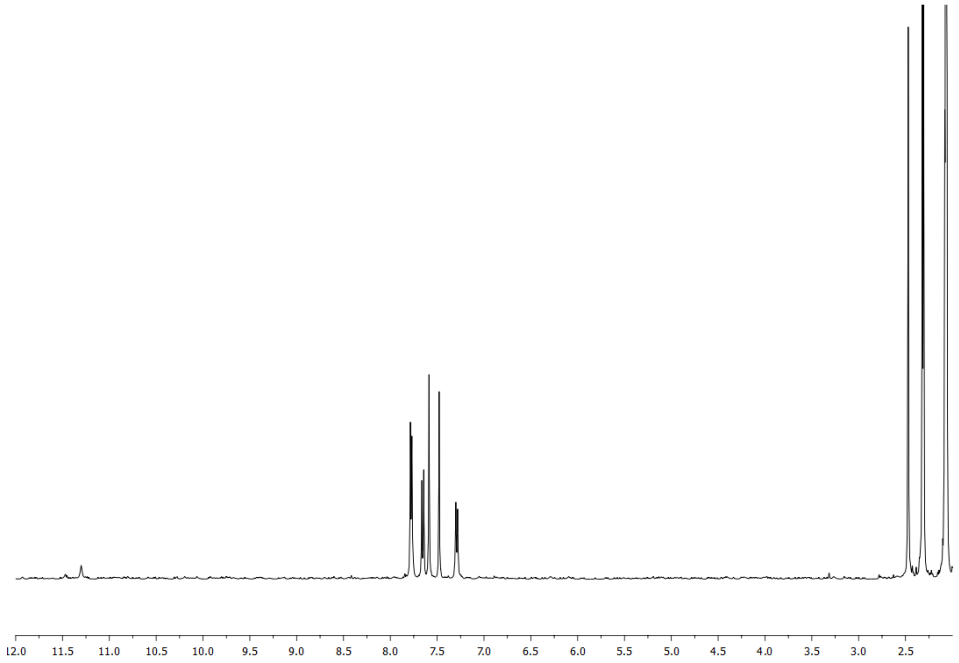

Figure 3.2.3 ^{1}H-NMR spectrum of DAICA-ABtz in acetone-d_6.

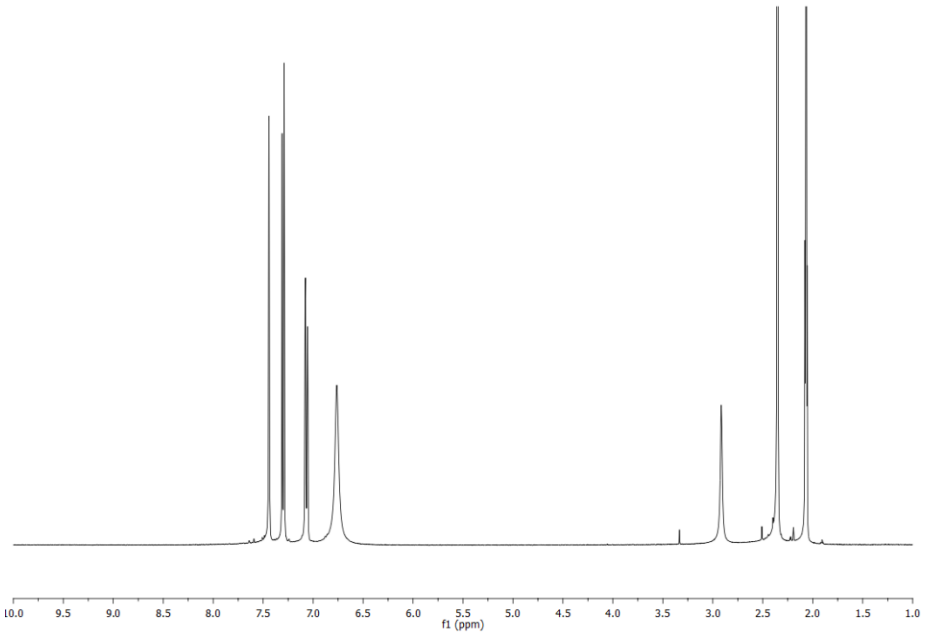

Figure 3.2.4 ^{1}H-NMR spectrum of ABtz in acetone-d_6.

3.3 Optical characterization of acetylated DHICA-ABtz with zinc

The first investigation of the optical properties of the DAICA derivative was carried out by UV-vis spectroscopy, recording the spectra of the amide in common organic solvents. In methanol, a solvent in which DAICA-ABtz showed notable solubility, the absorption profile showed two main bands at 218 nm and 327 nm, with a small shoulder in the region around 250 nm.

Subsequently, the optical behaviour of the amide was evaluated in presence of different metal ions such as Na^{+}, Mg^{2+}, Ca^{2+}, Cr^{2+}, Mn^{2+}, Fe^{3+}, Fe^{2+}, Ni^{2+}, Cu^{2+}, Ag^{+}, and Zn^{2+}.

Ni^{2+}, Fe^{3+}, and Fe^{2+} had little effect when added to amide, producing no variation in the original absorption spectrum but a slight red shift was observed for the three ions. No changes in the absorption profiles were observed for all metal ions investigated, except for the zinc ion, which produced marked changes in the UV-vis spectrum of the amide (figure 3.3.1).

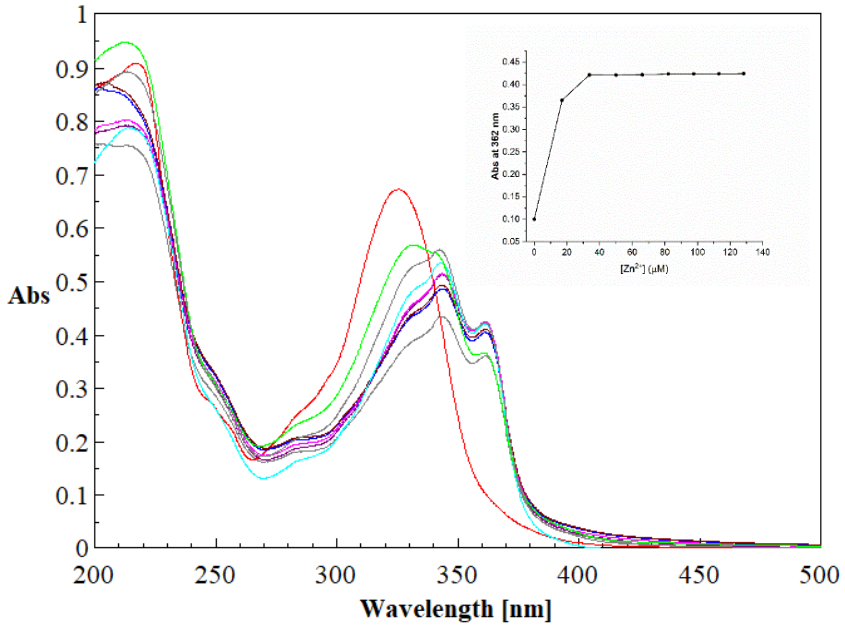

Figure 3.3.1 Absorption intensity changes of DAICA-ABtz (68.5 µM) upon addition of Zn^{2+} (0 - 2.0 equivalents: 0 (red) – 0.25 (mint) – 0.5 (ash grey) – 0.75 (cyan) - 1.0 (fuchsia) – 1.25 (purple) – 1.5 (brown) – 1.75 (blue) – 2.0 (anthracite grey)). Inset: variation of absorption at 362 nm as a function of Zn^{2+} concentration.

As the $Zn^{2+:}$ DAICA-ABtz ratio increased, the band at 218 nm remained unchanged, the peak at 327 nm decreased in intensity, while at the same time, two new bands at 344 nm and 362 nm increased in intensity reaching a plateau to 1.25 equivalents cation. The peculiar optical behaviour of the amide in the presence of zinc suggested the ability of DAICA-ABtz to chelate Zn^{2+} ions and therefore the formation of a complex.

To obtain information on the portion of the molecule involved in coordination, the impact of the zinc ion on the absorption profiles of two aliphatic amides containing the DAICA-ABtz precursors (figure 3.3.2) was studied.

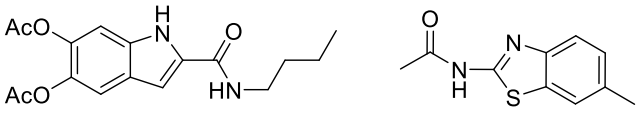

DAICA butylamide ABtz acetamide

Figure 3.3.2 Structures of two amides containing the acid (left) and amino (right) precursors of DAICA-ABtz, respectively.

In particular, the UV-vis spectra in the presence of zinc ions in methanol showed no alterations of the spectra of the two amides, demonstrating the central contribution of both bicyclic structures in the interaction of DAICA-ABtz with the metal cation, supporting a synergistic action of indole and benzothiazole, as well as potentially of the amide group.

Subsequently, further spectrophotometric investigations were carried out to obtain information on the binding stoichiometry between DAICA-ABtz and zinc ions using the method of continuous variation, also called Job's method [88, 89]. From the analysis of the graph obtained (figure 3.3.3) it emerged that the maximum absorbance occurred when the mole fraction of metal ion was 0.33, which suggested that the 1:2 ratio was the possible binding stoichiometry of amide with Zn^{2+}.

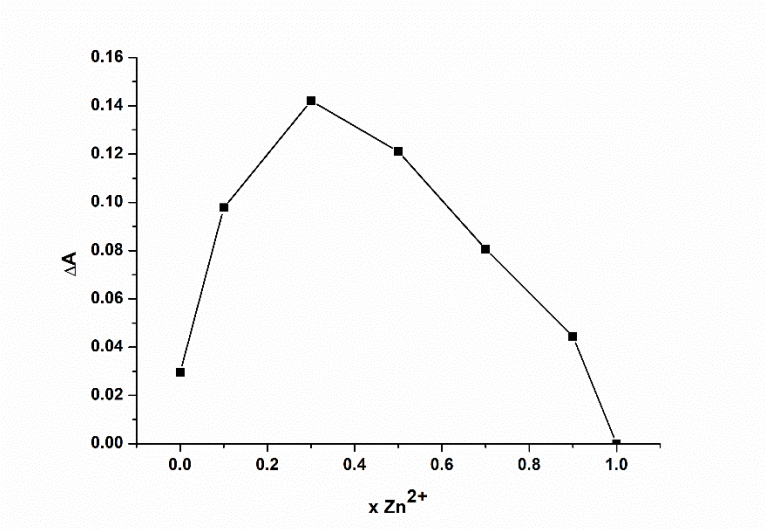

Figure 3.3.3 Job's plot for the binding stoichiometry of DAICA-ABtz with Zn^{2+} was obtained by plotting ΔA vs. x Zn^{2+} where ΔA is the change of absorbance of the absorption spectrum at 362 nm during titration with zinc and x Zn^{2+} is the mole fraction of the zinc ions.

By applying the Benesi-Hildebrand method [90], it was also possible to spectrophotometrically obtain the association constant (Ka) of the complex between

DAICA-ABtz and Zn^{2+}. The obtained value of log Ka = 4.88 highlighted the reasonable stability of the complex.

The second part of the amide investigations concerned fluorescence properties. Exciting at the wavelength corresponding to the absorption maximum observed in the UV-vis profile, DAICA-ABtz showed emission peak at 417 nm in methanol. The fluorescence titrations up to 2 equivalents carried out for all the metal ions investigated in the first part showed no changes in the fluorescence spectra, while after the addition of different amounts of Zn^{2+}, the profile of the spectra did not change, but a noteworthy increase in the emission intensity was observed. Fluorescence titration of DAICA-ABtz with metal ions exhibited an 8-fold increase in emission intensity compared to free amide (figure 3.3.4), reaching a plateau at 0.75 equivalents of zinc ions (figure 3.3.5).

Figure 3.3.4 DAICA-ABtz solution (68.5 μM) (left) and after the addition of 0.75 equivalents of Zn^{2+} ions (right) under a UV lamp at 365 nm.

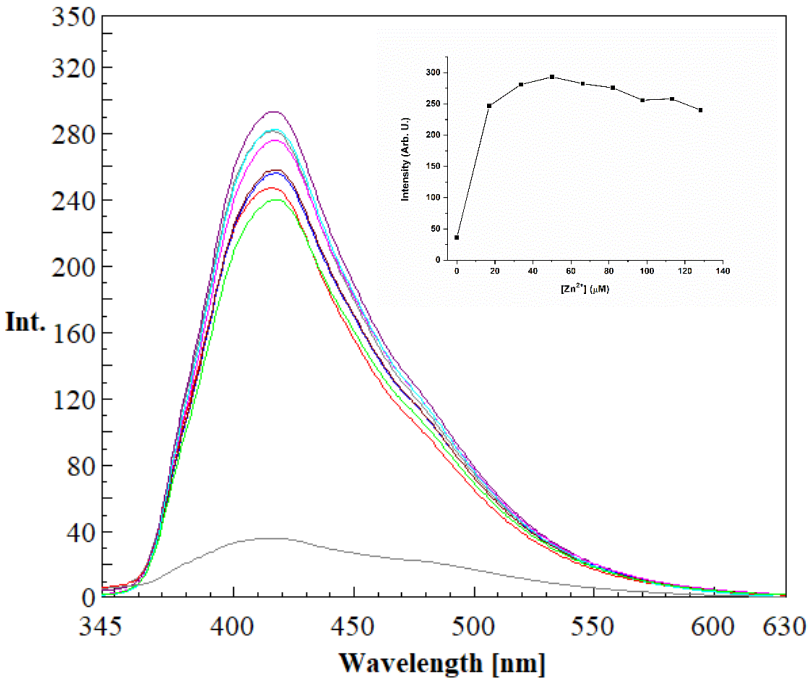

Figure 3.3.5 Emission intensity changes of DAICA-ABtz (68.5 μM) upon addition of Zn^{2+} ions (0 - 2.0 equivalents: 0 (anthracite grey) – 0.25 (violet) – 0.5 (cyan) – 0.75 (purple) - 1.0 (ash grey) – 1.25 (burgundy) – 1.5 (blue) – 1.75 (red) – 2.0 (green)). Inset: variation of emission intensity at 417 nm as a function of Zn^{2+} concentration. λ_{ex} = 325 nm.

Motivated by these results, the increase in fluorescence intensity of DAICA-ABtz in the presence of Zn^{2+} was investigated to determinate the quantum yield (QY), which led to a greater than 4-fold increase in QY compared to free amide (0.035 and 0.12 for DAICA-ABtz and DAICA-ABtz + Zn^{2+}, respectively).

A possible explanation for the increase in the fluorescence intensity of DAICA-ABtz in the presence of zinc could be sought in the chelation enhanced fluorescent (CHEF) effect [91-94]. Generally, ligands showing this effect have separate conjugated units in their semirigid structure and would be integrated into a rigid coplanar conjugation system after metal coordination [95]. Furthermore, the role of the metal ion in fluorescent zinc(II) complexes is to freeze the conformations associated with nonradiative relaxation processes [96]. When zinc is coordinated with the DAICA-ABtz, the free torsional motions between the two aromatic moieties, which provide

the main channels for nonradiative excited-state depopulation of the amide, can be blocked upon complex formation, resulting in increased conjugation in the amide which could facilitate the ligand-centered charge transfer (LCT) processes, producing an enhancement of fluorescence intensity [97].

3.4 Optical characterization of DHICA-ABtz with zinc

Before studying the oxidative chemistry of the novel DHICA amide and its interaction with zinc ions, a procedure for the deprotection of the catechol group was developed (scheme 3.2.1) [82].

A solution of sodium tert-butoxide (t-BuONa), previously dissolved in anhydrous methanol, was added to a solution of DAICA-ABtz in the same solvent. The reaction was carried out under argon atmosphere to avoid unwanted autoxidation of the amide in the alkaline environment. After 7 minutes, TLC analysis of the reaction mixture revealed the disappearance of the acetylated amide spot and the presence of only one spot with a retention factor (Rf) lower than the first. The reaction mixture was acidified and rapidly dried under vacuo. The solid was then taken up with ethyl acetate and it was treated with water. Finally, the organic phase was dried under vacuo, obtaining a yellow powder. Confirmation of the deacetylated product was obtained by ^{1}H-NMR spectroscopy, which revealed the disappearance of the signals of the acetyl groups at 2.26 ppm, and by MALDI-TOF mass analysis, which showed the presence of signals at m/z 362 and 378, attributable to the $[M + Na]^{+}$, $[M+ K]^{+}$ ions of DHICA-ABtz, respectively.

Subsequent studies aimed to investigate the optical properties of deacetylated amide in the presence of zinc ions. Starting from the UV-Vis spectrum of DHICA-ABtz in methanol, exposure to metal ions revealed a marked change in the absorption profile, resulting in a red shift of the absorption maximum of approximately 25 nm. As the Zn^{2+}: DHICA-ABtz ratio increases, the peak at 351 nm decreases in intensity, while at the same time, a new band at 401 nm increases in intensity, reaching a plateau at 1.00 zinc ions equivalent. The change in the amide absorption profile suggested the formation of a complex between the DHICA derivative and the metal ion even after the deprotection of the catechol group.

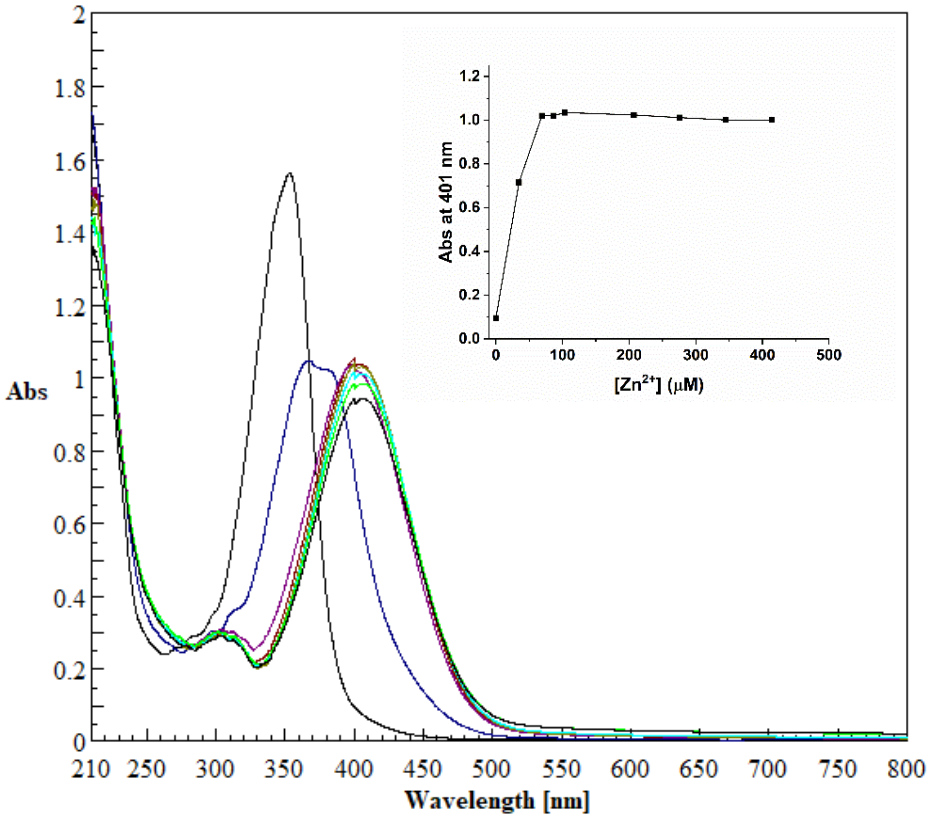

Figure 3.4.1 Absorption intensity changes of DHICA-ABtz (68.5 μM) (black line) and after addition of Zn^{2+} ions in methanol. (0 – 6.0 eqs.). Inset: variation of absorption at 401 nm as a function of Zn^{2+} concentration.

By applying the method of continuous variation in a similar way to what was done for DAICA-ABtz, it was possible to obtain the Job's plot, whose interpretation revealed a 1:1 stoichiometry as the binding mode of DHICA-ABtz with zinc ions.

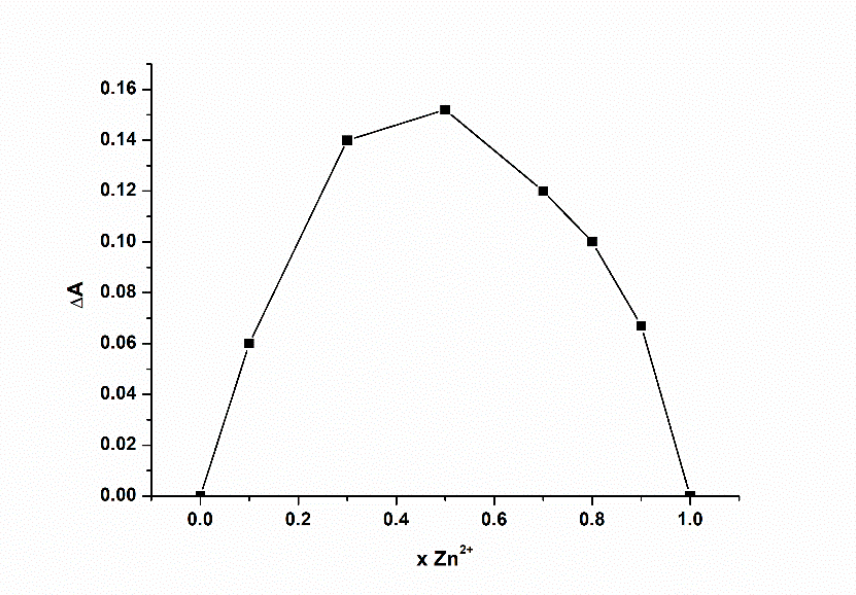

Figure 3.4.2 Job's plot for the binding stoichiometry of DHICA-ABtz with Zn^{2+} was obtained by plotting ΔA vs. x Zn^{2+} where ΔA is the change of absorbance of the absorption spectrum at 401 nm during titration with zinc and x Zn^{2+} is the mole fraction of the zinc ions.

3.5 Preparation of DHICA-ABtz dimers

Having developed a facile procedure for the deprotection of the catechol group, the first experiments on the oxidative chemistry of DHICA-ABtz were carried out.
In this regard, understanding the oxidative polymerization mechanism of the DHICA derivative was of fundamental interest to obtain information on the structure of the final polymer as well as for a comparison with the mechanism of synthesis of eumelanin starting from DHI and DHICA. To achieve this goal, it was necessary to find a specific procedure that would allow the isolation of a sufficient amount of oligomeric intermediates for chemical investigation. It was therefore decided to start from the conditions of autoxidation catalyzed by metal ions (such as Co^{2+} and Cu^{2+}) which led to the obtaining of a mixture of oligomers, with the 4,4'-DHICA dimer as the majority product [98].
On this basis, a procedure for the isolation of DHICA-ABtz oligomers was obtained. In detail, a solution of DHICA-ABtz in methanol was added to an equal volume of 50 mM phosphate buffer at pH 7.5, in which an equivalent of copper (II) acetate had previously been dissolved. The final amide concentration was 3 mM. After 30 minutes, the reaction was stopped by adding sodium dithionite ($Na_2S_2O_4$) and acidified to avoid further oxidation of the product during processing. The mixture was extracted, and the organic layer was acetylated with acetic anhydride/pyridine treatment to avoid oxidation in the air and facilitate composition analysis by LC-MS analysis (ESI^+). The analysis of the oxidation mixture confirmed the presence, besides the starting monomer eluted at tR = 5.1 minutes (pseudomolecular ion peaks at m/z 446 and 462), of two other peaks with pseudomolecular ion signals at m/z 867 and 883 at tR = 7.4 minutes and tR = 16.5 minutes, likely for dimeric species (figure 3.5.1).

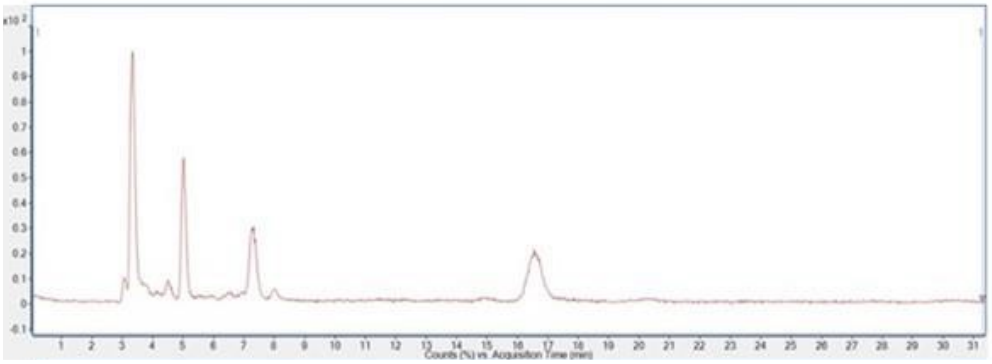

Figure 3.5.1 Total ion current (TIC) chromatogram of the acetylated reaction mixture of DHICA-ABtz.

Subsequently, further polymerization experiments of DHICA-ABtz were conducted by increasing the reaction time up to 60 and 120 minutes under the same conditions. HPLC analysis of the mixture after one hour showed a higher concentration of the dimers and a similar amount of DHICA-ABtz compared to the previous experiment. HPLC analysis of the mixture oxidized for 120 minutes showed only the monomer signal, with a significant reduction in the concentration of the latter compared to previous experiments. In this case, the longer duration of the oxidative treatment likely overpolymerized the DHICA-ABtz, possibly consuming more oxidizable oligomeric species than the monomer.

Once one hour was identified as the optimal reaction time for the amount of desired products formed, the dimers were accumulated in repeated reactions with progressive scale-up and isolated by preparative TLC. The two dimers, whose structure is shown in figure 3.5.2, were completely characterized by 1D (figure 3.5.3 and figure 3.5.4) and 2D NMR analyses.

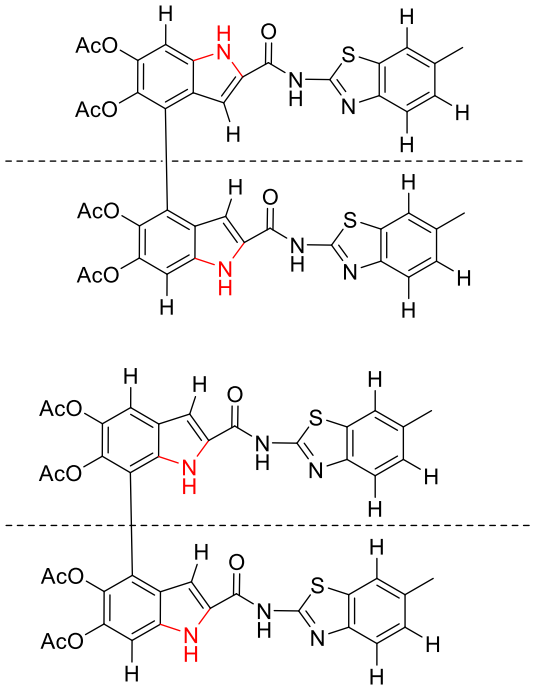

Figure 3.5.2 Structures of isolated DHICA-ABtz acetylated dimers: 4,4'-DHICA-ABtz (up) and 4,7'- DHICA-ABtz (down).

The regiochemistry of DHICA-ABtz oligomers involving positions 4 and 7 of the indole system is similar that found in DHICA eumelanin and its derivatives [99-101]. The introduction of a bulky bicyclic aromatic system via an amide bond appeared not to influence the polymerization pattern in the early stages of polymerization.

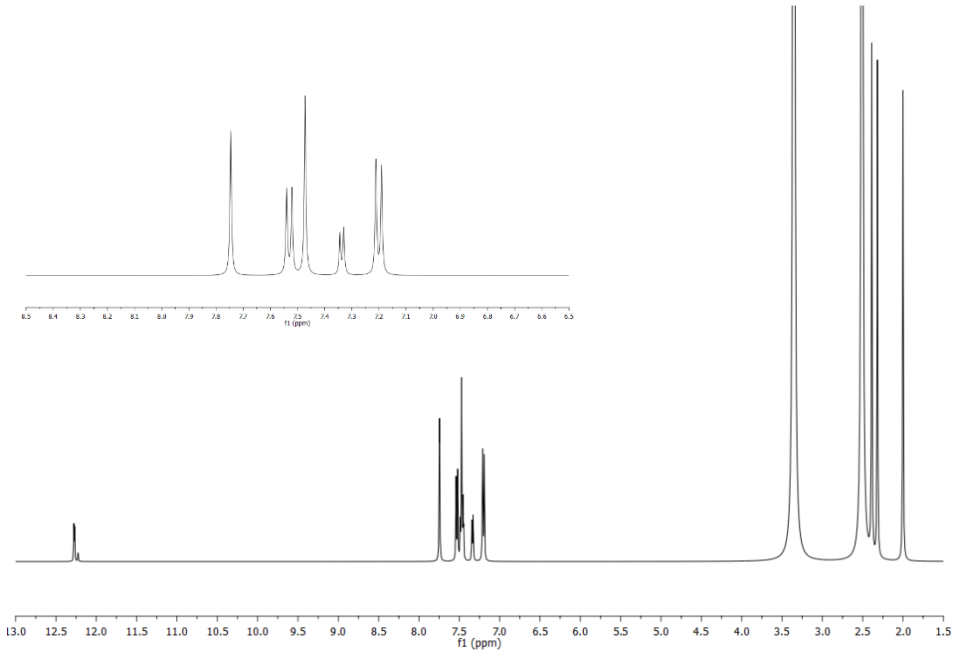

Figure 3.5.3 ^{1}H-NMR spectrum of acetylated 4,4'-DHICA-ABtz in DMSO-d_6.
Inset: zoom of the spectrum in the region between 6.5 and 8.5 ppm.

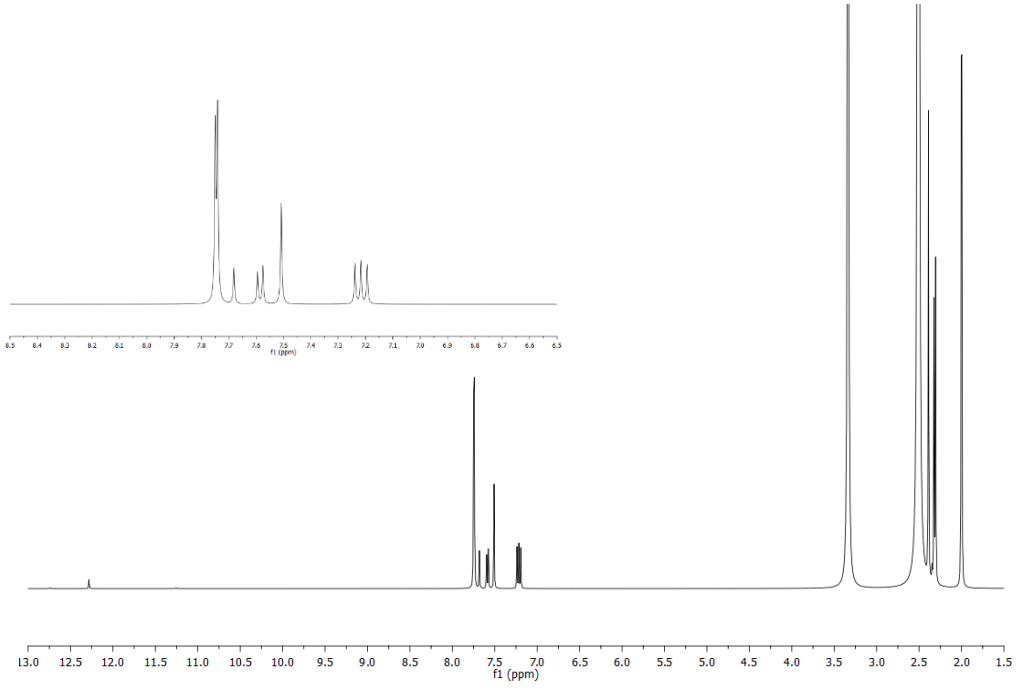

Figure 3.5.4 ^{1}H-NMR spectrum of acetylated 4,7'-DHICA-ABtz in DMSO-d_6.
Inset: zoom of the spectrum in the region between 6.5 and 8.5 ppm.

3.6 Preparation and characterization of the DHICA-ABtz-derived polymer in presence of zinc

3.6.1 Physicochemical and optical characterization

Subsequent studies were directed toward the synthesis of the DHICA-ABtz-derived polymer. The progress of the oxidative polymerization reaction was monitored by UV-Vis spectroscopy, following the variation of the absorption maximum of the starting monomer.

A first polymerization experiment of DHICA-ABtz was carried out under autoxidative conditions in carbonate buffer at pH 9.0, a value at which a significant fraction of the monomer is present in the more oxidizable ionized form [102]. For comparison purposes, DHICA eumelanin was prepared under the same conditions. Regarding the polymerization of DHICA, after 24 hours, the UV-vis profiles of the reaction mixture showed a notable broadening in the absorption maximum centred at 320 nm and an increase in absorption throughout the UV-Vis spectral range (figure 3.6.1) as a superimposition effect of the absorption of the oligomers into different redox forms, formed during the polymerization process [103]. Noteworthy, a broad band in the region between 550-575 nm, was visible in the absorption profile after 2 hours of reaction, likely attributable to the maximum absorption of the oxidized oligomeric species [104, 105].

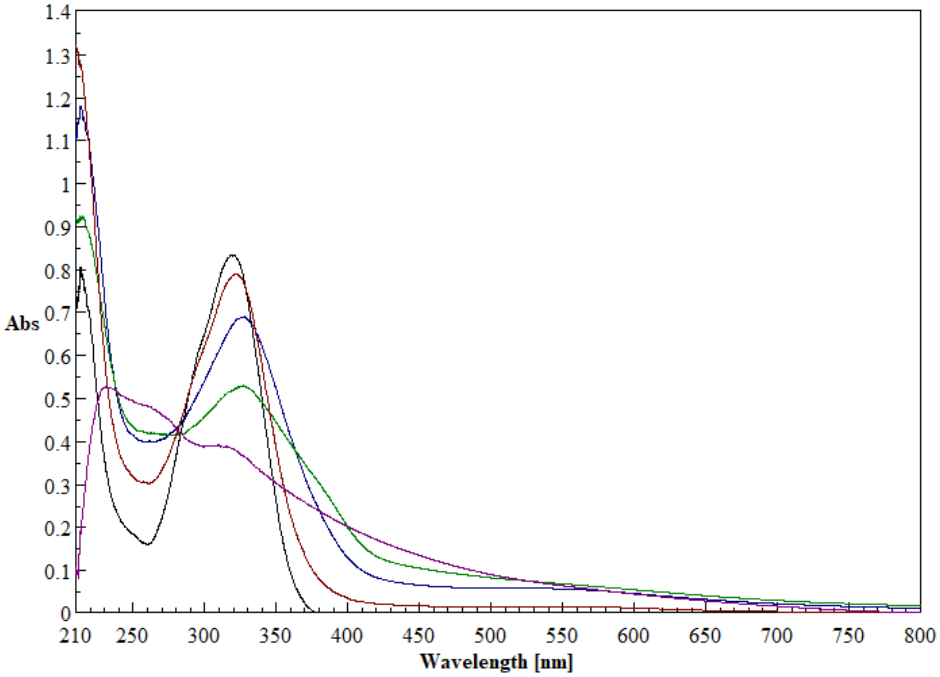

Figure 3.6.1 UV–Vis profiles of the autoxidation of DHICA (1mM) in carbonate buffer at pH 9 over 24 hours. t0 (black), 1h (red), 2h (blue), 5h (green) and 24 hours (violet).

For DHICA-ABtz, the UV-vis spectra of the reaction mixture recorded during polymerization showed a broadening of the absorption maximum at 355 nm with a blue shift of approximately 25 nm, probably due to a decrease in the fraction of indole units ionized during polymerization (figure 3.6.2).

The absence of peaks in the visible spectral region could be explained by the greater energetic instability of the quinonoid form of DHICA-ABtz compared to that of the melanin precursor, with consequent difficulty in formation.

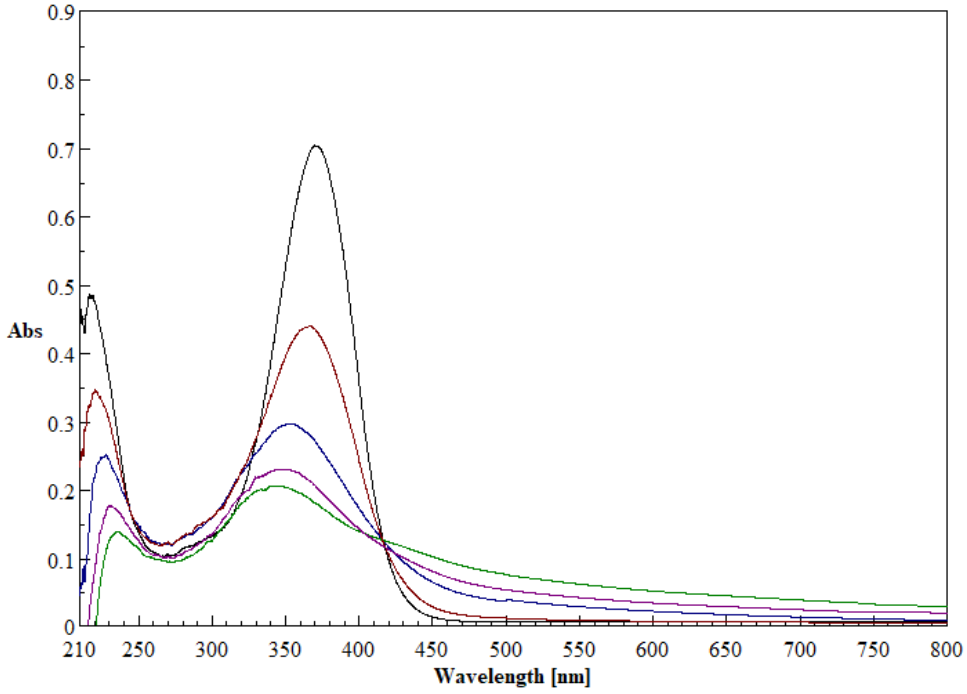

Figure 3.6.2 UV–Vis profiles of the autoxidation of DHICA-ABtz (1mM) in carbonate buffer at pH 9 over 24 hours. t0 (black), 1h (red), 2h (blue), 5h (violet) and 24 hours (green).

At the end of 24 hours, both reaction mixtures were acidified, centrifuged, and freeze-dried, obtaining the two powders shown in figure 3.6.3.

Figure 3.6.3 DHICA eumelanin (left) and DHICA-ABtz-derived polymer (right) powders.

The materials obtained by autoxidation of DHICA and DHICA-ABtz were dissolved in methanol (figure 3.6.4), and a UV-Vis analysis was carried out (figure 3.6.5) at a concentration that allowed the complete solubilization of both the solids. Of note, the presence of a broad peak around 345 nm was observed for the DHICA-ABtz-derived polymer in contrast to a DHICA eumelanin absorption profile characterized by increased absorption in the visible spectral region and a broad absorption maximum around 320 nm. The peculiar optical profile of the dark red pigment could be explained by recalling the energetic instability of the oxidized forms of the DHICA-ABtz oligomers responsible for the delocalization of the inter-unit π electron delocalization [106] due to the presence of the benzothiazole system, coherently with the lack of quinonoid species observed during spectrophotometric analysis.

Figure 3.6.4 DHICA eumelanin (left) DHICA-ABtz-derived polymer (right) solutions at 0.050 mg / mL in methanol.

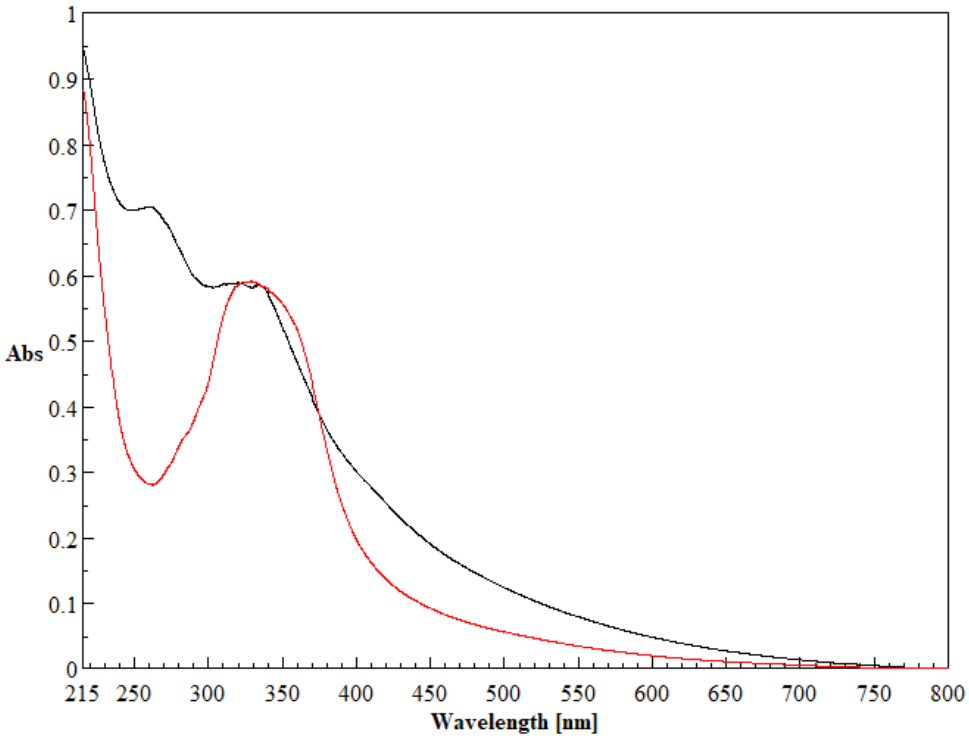

Figure 3.6.5 DHICA eumelanin (black line) and DHICA-ABtz-derived polymer (red line) UV-vis spectra in methanol (0.025 mg /mL).

Titrations of the two polymers with different amounts of zinc ions (figures 3.6.6 and 3.6.7) highlighted that the interaction between the DHICA-ABtz monomer units with the metal ion once polymerization occurred, in contrast to the lack of changes observed in the absorption profile of DHICA eumelanin.

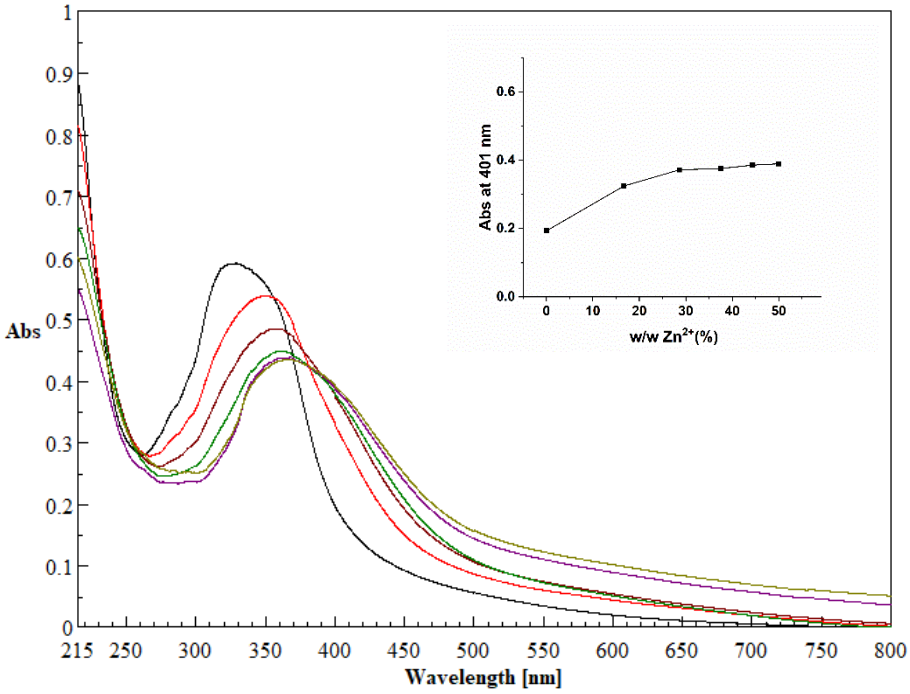

Figure 3.6.6 Absorption intensity changes of 0.025 mg of DHICA-ABtz-derived polymer in 2 mL of methanol (black line) and after addition of Zn^{2+} ions (0 – 50.0 % w/w): 16.7 % (red), 28.6 % (brown), 37.5 % (green), 44.4 % (purple), 50.0 % (dark yellow).
Inset: variation of absorption at 401 nm as a function of Zn^{2+} concentration.

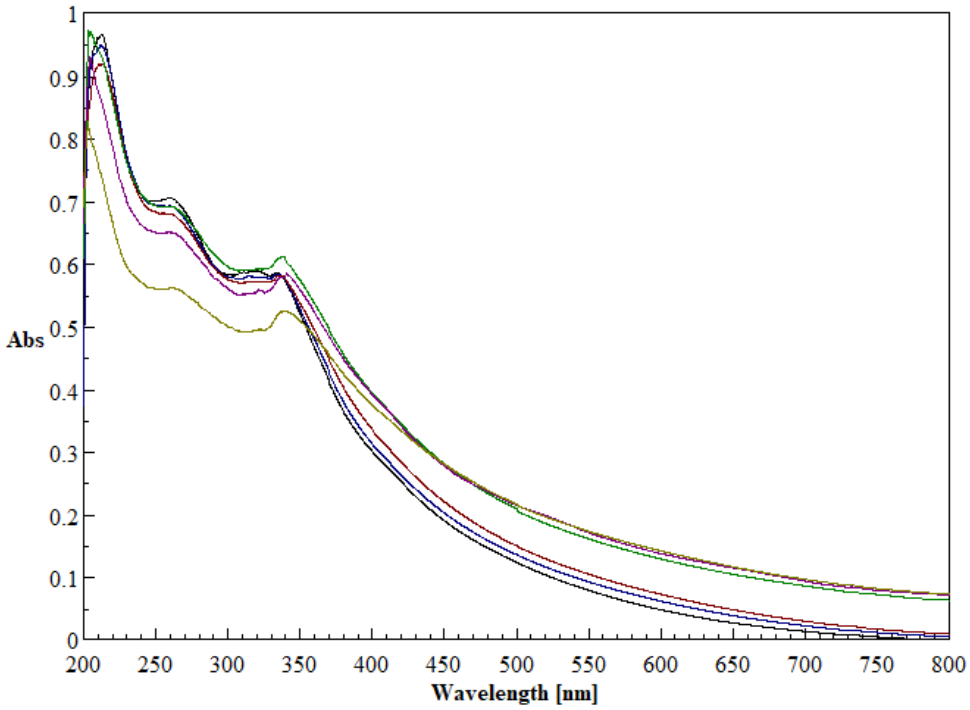

Figure 3.6.7 Absorption intensity changes of DHICA eumelanin (0.025 mg/mL) (black line) and after addition of Zn^{2+} ions (0 – 50% w/w): 16.7 % (red), 28.6 % (brown), 37.5 % (green), 44.4 % (purple), 50.0 % (dark yellow).

Additional oxidative polymerization conditions were explored for DHICA-ABtz using potassium ferricyanide. In this case, the oxidative polymerization of the amide at a concentration of 1mM was carried out in 0.05 M phosphate buffer at pH 7.4. UV-Vis spectra of the reaction mixture showed a notable reduction in maximum absorption without any appreciable change in absorption profiles at different reaction times compared to what was observed for autoxidative conditions (figure 3.6.8).

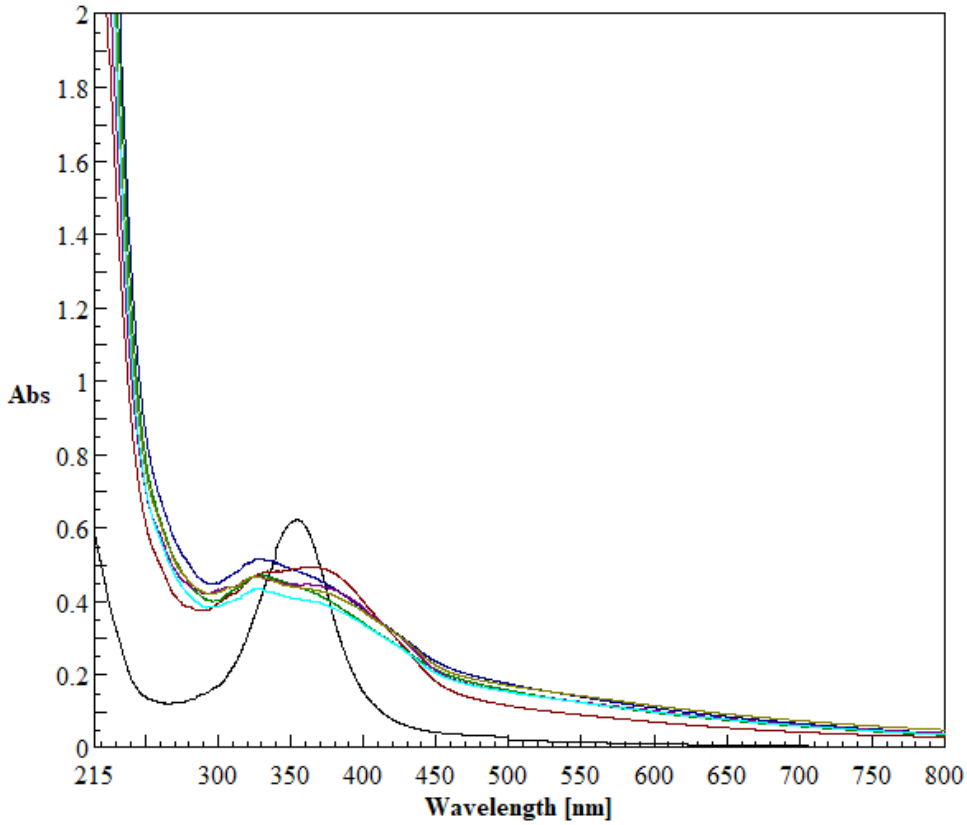

Figure 3.6.8 UV–Vis profiles of the oxidation of DHICA-ABtz (1mM) with $K_3[Fe(CN)_6]$ in phosphate buffer at pH 7.4 over 24 hours: t0 (black) – 5' (dark red) – 15' (purple) – 30' (dark yellow) – 90' (sky blue) – 4h (blue).

The solid obtained by autoxidation of DHICA-ABtz was acetylated by acetic anhydride/pyridine treatment and analyzed by HPLC. Chromatographic analysis of the acetylated DHICA-ABtz-derived polymer (figure 3.6.9) provided evidence of the presence of a variety of species eluted at higher retention times than those of acetylated 4,4'-DHICA-ABtz and 4,7'-DHICA ABtz dimers, probably attributable to oligomers higher than the dimers, as confirmed by the MALDI-TOF mass analysis of the powder shown in figure 3.6.10.

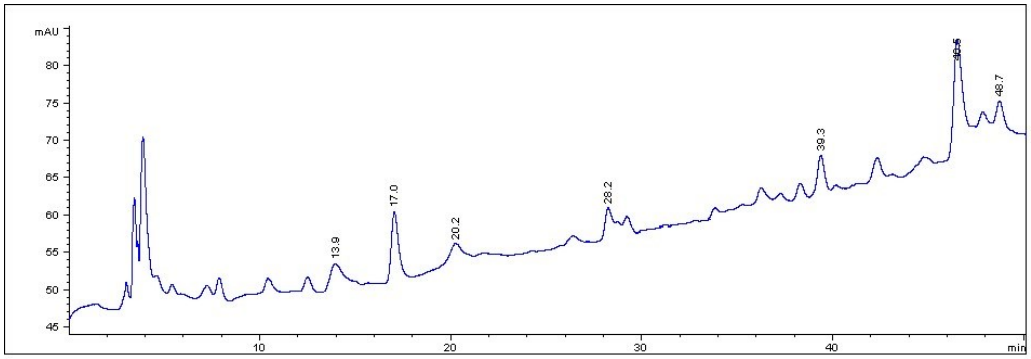

Figure 3.6.9 HPLC profile of the DHICA-ABtz-derived polymer 0.025 mg / mL in methanol. Detection wavelength at 300 nm.

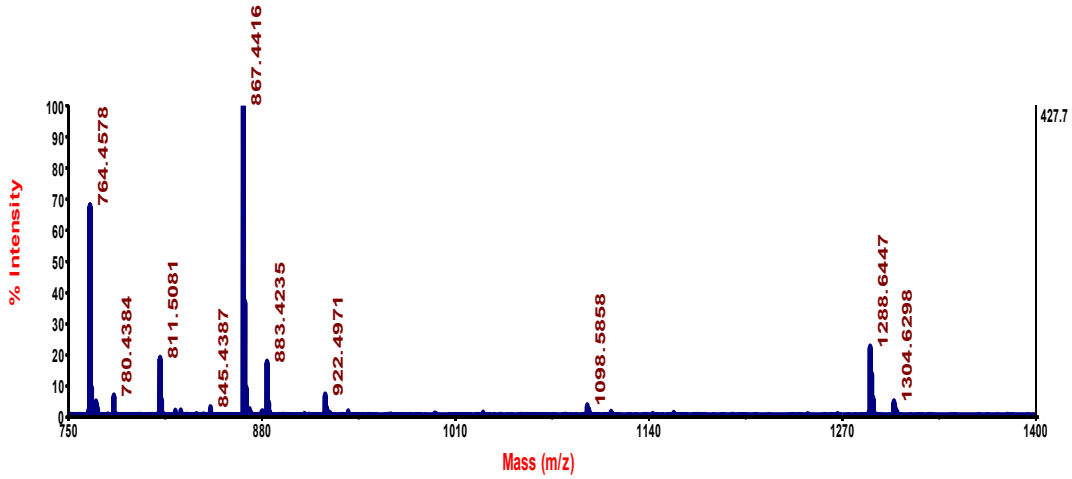

Figure 3.6.10 Segment of MALDI-TOF mass spectrum (m/ z: 750-1400 Da) of the DHICA-ABtz-derived polymer revealed the presence of signals at m/z 867 and 883 attributable to the ions $[M + Na]^+$, $[M+ K]^+$ of dimers of DHICA-ABtz and m/z 1288 and 1304 attributable to the ions $[M + Na]^+$, $[M+ K]^+$ of trimers of DHICA-ABtz.

3.6.2 Structural and thermal characterization

The first part of the studies carried out on the DHICA-ABtz-derived polymer highlighted the rationale for the functionalization of the eumelanin precursor, revealing chelating properties not dependent on the catechol moiety. The next part of the investigations focused on characterization of the eumelanin derivative for its potential application as a Zn ion-conducting solid electrolyte with redox activity.

For this purpose, films were prepared by solution casting and spin coating techniques using DHICA-ABtz-derived polymer as the host polymer and zinc acetate dihydrate ($Zn(CH_3COO)_2 * 2H_2O$) as the dopant salt. For the preparation of solid electrolytes, molar ratios of 0.1:1.0, 0.5:1.0, 1.0:1.0, and 2.0:1.0 ($Zn(CH_3COO)_2 * 2H_2O$: DHICA-ABtz) were chosen, denoting them as pDHICA-ABtz/Zn-0.1, pDHICA-ABtz/Zn-0.5, pDHICA-ABtz/Zn-1.0, and pDHICA-ABtz/Zn-2.0, respectively. In the second part, the effects of different zinc contents in the host polymer were studied to establish the optimal composition for the development of an electrolyte system.

The films prepared with the solution casting method were obtained by adding the desired amount of zinc salt to a solution of DHICA-ABtz monomer in methanol until completely dissolved. The solutions obtained were poured onto glass plates and dried at 50 °C for 4 hours to completely evaporate the solvent. The samples were subjected to the ammonia-induced solid-state polymerization (AISSP) methodology [107, 108] to obtain the desired host polymer matrix. The exposure lasted approximately 16 hours.

Finally, the films were characterized by X-ray diffraction (XRD), and their thermal stability was evaluated by thermogravimetric analysis (TGA).

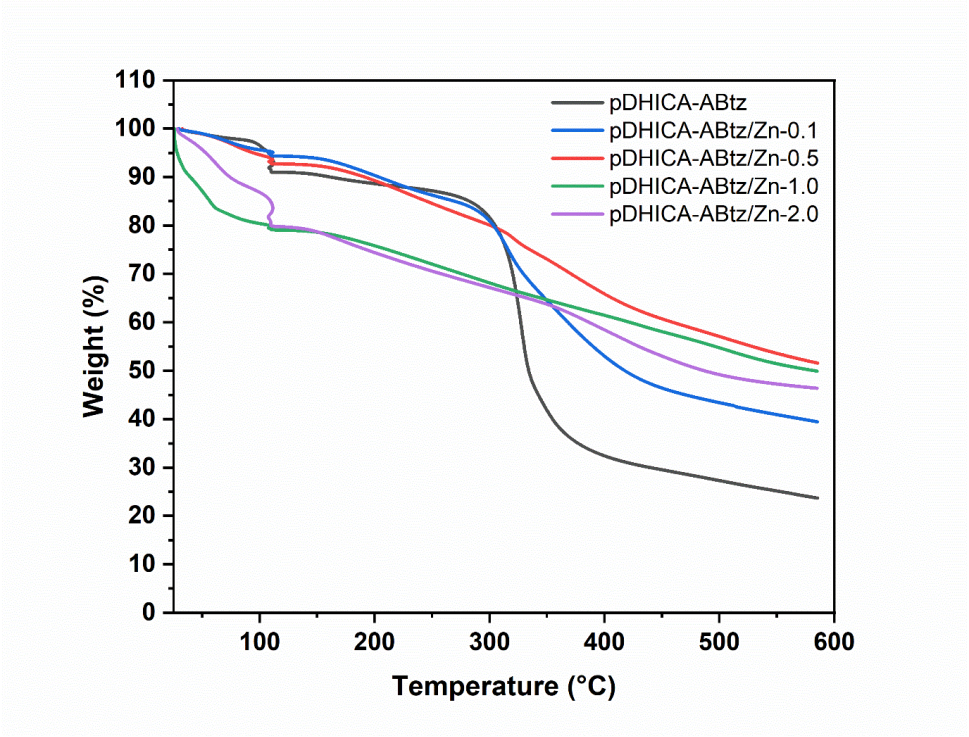

Figure 3.6.11 TG curves of pure DHICA-ABtz-derived polymer and with different contents of $Zn(CH_3COO)_2 * 2H_2O$.

As can be seen from figure 3.6.11, at temperatures below 100 °C approximately two phases of weight loss occurred in all samples. The first weight changes appeared from the start of heating up to 60-75 °C, corresponding to approximately 2% for pDHICA-ABtz, pDHICA-ABtz/Zn-0.1, and pDHICA-ABtz/Zn-0.5, and 17% and 11% for pDHICA-ABtz/Zn-1.0 and pDHICA-ABtz/Zn-2.0. These losses reflected the removal of loosely bound water and ammonia absorbed into the materials during the solid-state polymerization reaction. In the second phase (75–95 °C), in all analyzed samples containing zinc, a further weight loss occurred, particularly significant for pDHICA-ABtz/Zn-2.0, attributed to evaporation of the water contained in the doping salt [109]. Between 95 and 110 °C, notable weight changes were recorded in all samples due to the removal of highly bound water absorbed during the AISSP process [110].

At higher temperatures, between 290 and 375 °C, a dramatic weight loss was observed for the DHICA-ABtz-derived polymer, resulting in a weight reduction of

50%. In this temperature range, literature studies conducted on the thermal stability of synthetic and natural melanins [111, 112] attributed weight loss to the evolution of carbon dioxide.

Notably, the thermal degradation around 300-400 °C observed for the DHICA-ABtz-derived polymer was significantly reduced with increasing zinc salt content. This trend was more appreciable by plotting the derivative thermogravimetric (DTG) curves of the corresponding thermograms of the pure DHICA-ABtz-derived polymer and those containing zinc salt (figure 3.6.12). As the Zn^{2+}: DHICA-ABtz-derived polymer ratio increased, increased resistance to degradation was observed without any appreciable decomposition up to 600 °C. Further addition of zinc decreased the thermal stability to approximately 400 °C, as observed for the DHICA-ABtz/Zn-2 system.

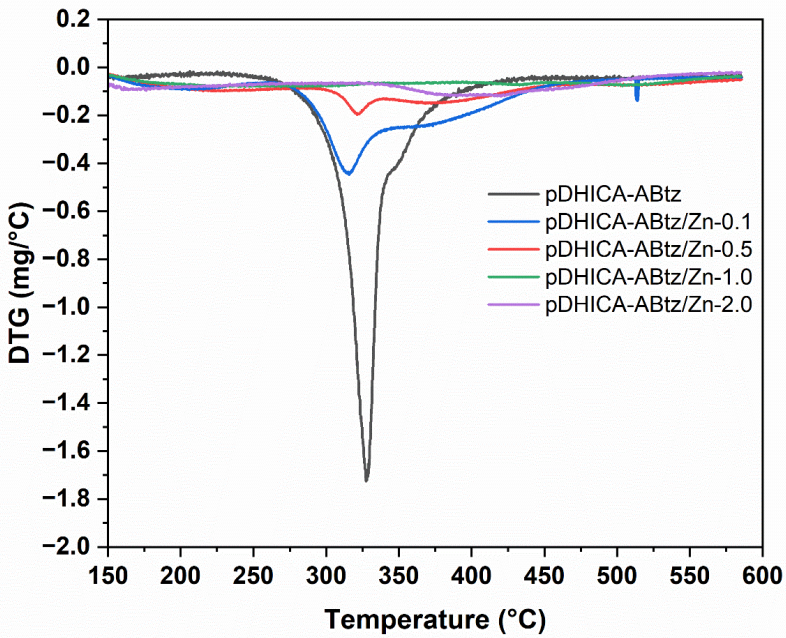

Figure 3.6.12 DTG curves of pure DHICA-ABtz-derived polymer and with different contents of $Zn(CH_3COO)_2 * 2H_2O$.

A structural investigation was performed using X-ray diffraction (XRD) of the films prepared by solution casting to evaluate the impact of the dopant salt on the crystallinity of the eumelanin derivative.

The XRD patterns of DHICA-ABtz-derived polymer, zinc salt, and polymer/Zn^{2+} ions systems at different contents of zinc were showed in figure 3.6.13. DHICA-ABtz-derived polymer revealed narrow peaks at 2θ = 11.7°, 16.7°, and 24.5° and a broad peak at 25.7°. The pristine zinc salt showed several sharp diffraction peaks, with the most intense peak at 12.3°. For the pDHICA-ABtz/$Zn(CH_3COO)_2$ * $2H_2O$ systems, no predominant peaks of the zinc salt were observed, but a single broad wave appeared in the region between 15° and 35°. This feature could be explained by the ability of the eumelanin derivative to chelate zinc ions producing a decrease in the crystallinity of the system. A comparison of pDHICA-ABtz/$Zn(CH_3COO)_2$ * $2H_2O$ systems with increasing content of metal ions led to a reduction in the intensity of the crystalline peaks with a concomitant increase in their width up to a 1:1 molar ratio, in full agreement with the stoichiometry of the binding mode of DHICA-ABtz with Zn^{2+} ions previously found. Increasing the salt content increased the intensity and reduced the width of the wave, as observed for the DHICA-ABtz/Zn-2 system, resulting in a non-uniform distribution.

Evaluating the crystallinity of a polymer electrolyte is crucial to obtain information on the amorphicity of the material, which is essential for achieving high ionic conductivity. Polymer chains are more flexible in the amorphous phase, thus increasing ion mobility and improving ion conduction [113, 114]. Based on these considerations, the pDHICA-ABtz/Zn-1 system is hypothesized to be an optimal composition with high amorphicity that can exhibit high ionic conductivity.

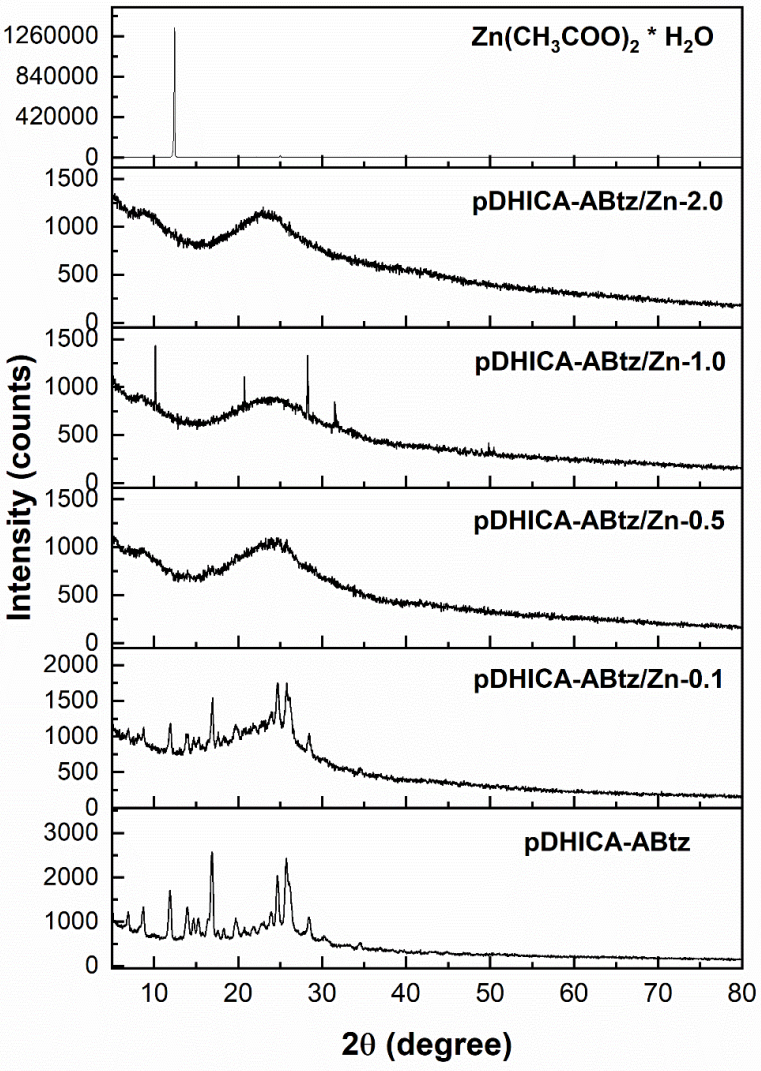

Figure 3.6.13 XRD patterns of pure DHICA-ABtz-derived polymer and with different contents of $Zn(CH_3COO)_2 * 2H_2O$.

3.6.3 Electrochemical characterization

After investigating the thermal stability and crystallinity of the DHICA-ABtz-derived polymer with different contents of zinc ions, an in-depth study on the redox behaviour of the eumelanin-inspired material was carried out involving electrochemical characterization using the cyclic voltammetry (CV) technique.

Cyclic voltammetry experiments were performed in a three-electrode cell consisting of a carbon paper (CP) electrode coated with DHICA-ABtz-derived polymer as the working electrode, a platinum mesh as the counter electrode and Ag/AgCl(aq) as the reference electrode.

Specifically, two solutions were prepared: I) 30 mM DHICA-ABtz in DMSO, II) DHICA-ABtz 30 mM with one molar equivalent of $Zn(CH_3COO)_2 * 2H_2O$ in DMSO: methanol (4:6). 5 µL of each solution was drop-cast onto the surface of carbon paper electrodes. The DHICA-ABtz-derived polymer was synthesized in situ on the carbon paper electrode using the AISSP methodology. After drop casting, the samples were exposed to NH_3(aq) vapor to catalyze the polymerization reaction. The exposure lasted approximately 16 hours.

Furthermore, a DHICA eumelanin sample was also prepared under the same conditions.

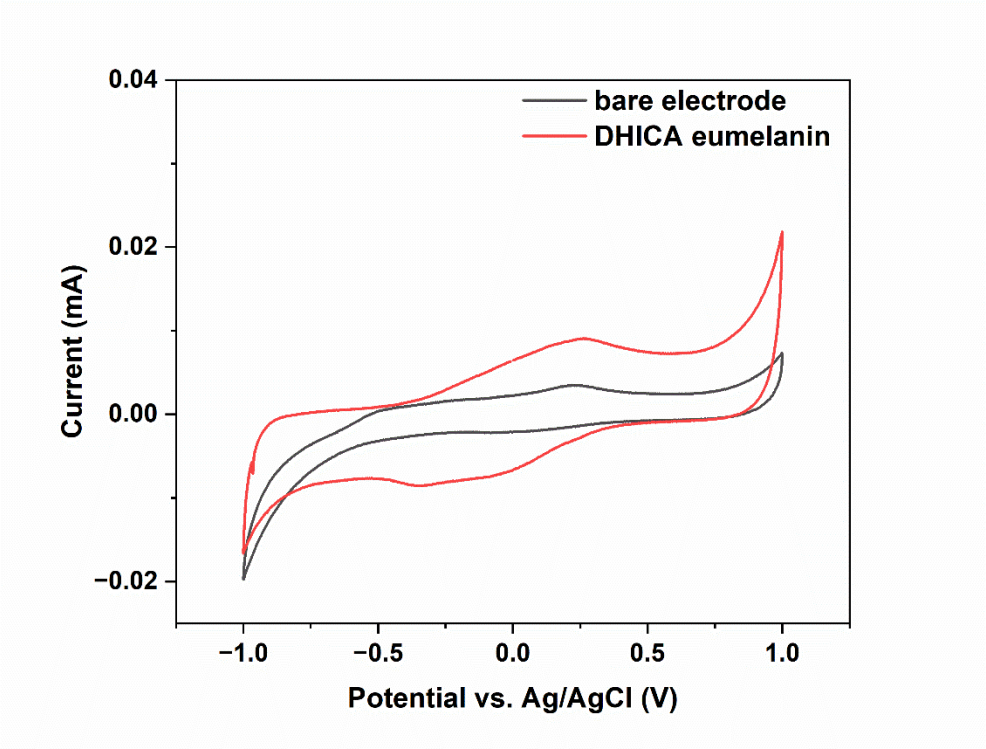

Figure 3.6.14 Cyclic voltammogram of DHICA eumelanin on the CP electrode and the bare CP electrode is reported as blank in $Zn(CH_3COO)_2 * 2H_2O$ (aq) as aqueous electrolyte at pH 5.0. Scan rate: 50 mV s^{-1}.

When explored within the range potential -1.0-1.0V vs. Ag/AgCl, the voltammogram of DHICA eumelanin (figure 3.6.14) showed a broad oxidation peak with a current maximum located around 0.26 V as well as a broad reduction wave was visible within the range -0.4-0.4 V.

The presence of broad and not well-resolved peaks is probably due to the overlap of multiple redox processes that reflect the peculiar chemical disorder of the biopolymer [115]. More specifically, it is reasonable to suppose that the voltammogram of DHICA eumelanin is attributed to the redox disorder of the biopolymer constituted by the coexistence of different oxidation states accessible to the polymer building block [68, 116, 117] and a molecular dimensional disorder determined by the different degrees of polymerization of the oligomers.

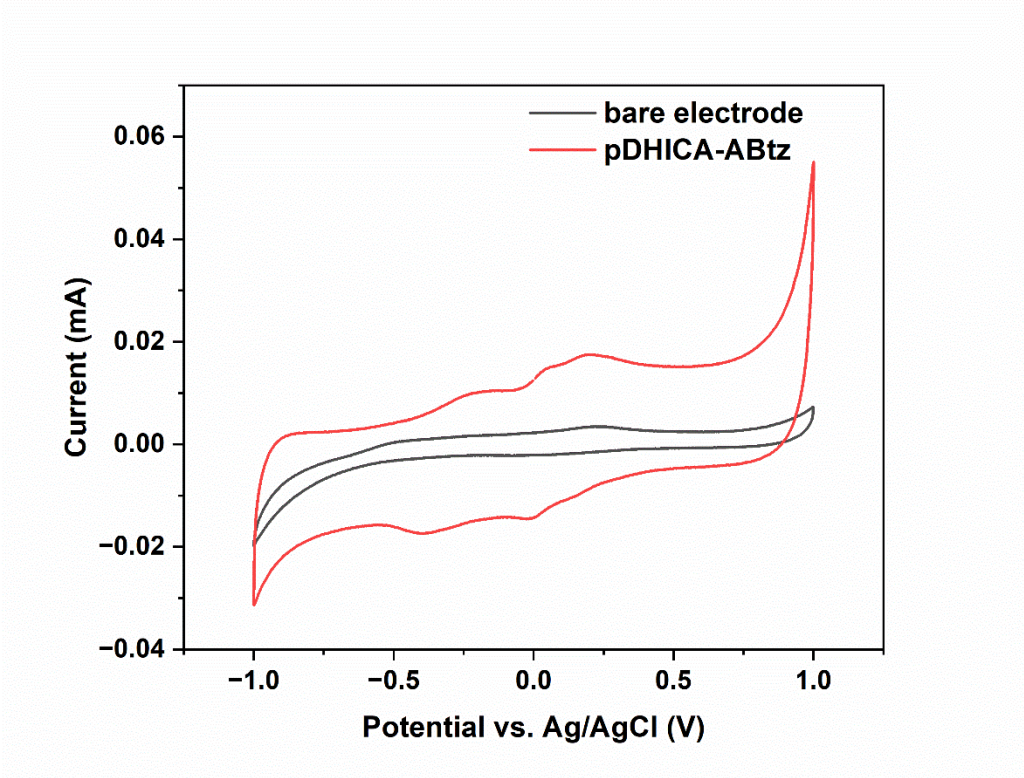

Figure 3.6.15 Cyclic voltammogram of DHICA-ABtz-derived polymer on the CP electrode and the bare CP electrode is reported as blank in $Zn(CH_3COO)_2 * 2H_2O$ (aq) as aqueous electrolyte at pH 5.0. Scan rate: 50 mV s^{-1}.

The voltammogram of the DHICA-ABtz-derived polymer (Figure 3.6.15) had more distinct peaks than those of the DHICA eumelanin in the same potential window. Specifically, the anodic scan revealed a broad peak between 0 V and 0.25 V, with two maxima at 0.05 V and 0.20 V, and a wave centered around -0.20 V, while the cathode scan showed a peak at -0.01 V and a wave in the potential range -0.18 V and -0.55 V.

A higher intensity of the voltammetric current was observed for the voltammogram of the DHICA-ABtz derived polymer than that of the eumelanin DHICA (figure 3.6.16).

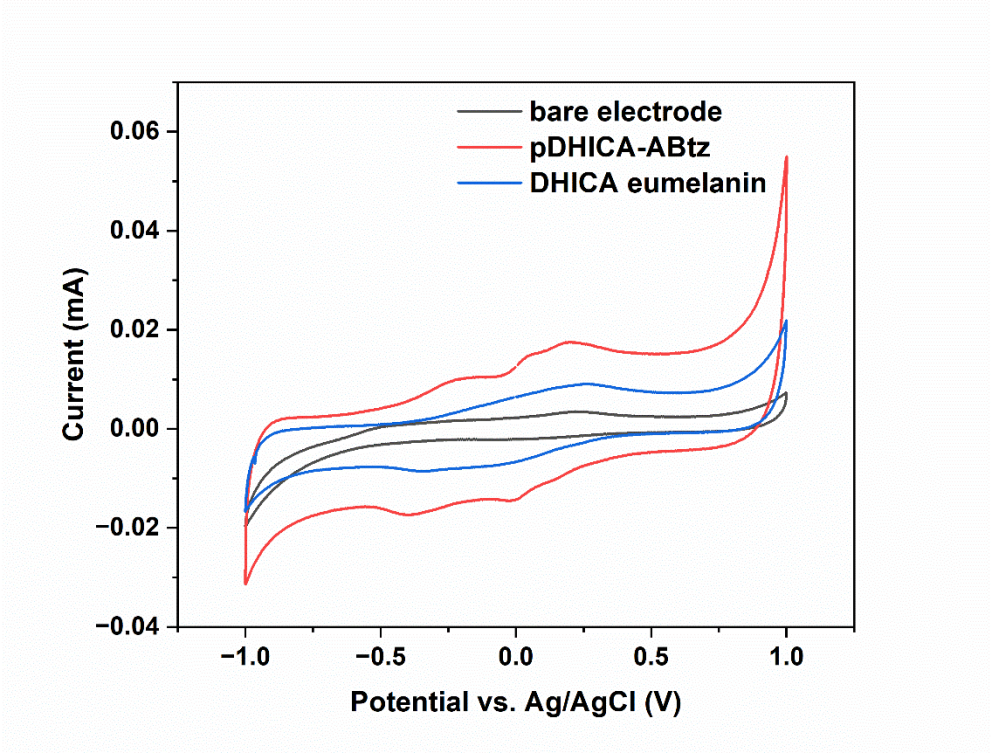

Figure 3.6.16 Cyclic voltammograms of DHICA-ABtz-derived polymer and DHICA eumelanin. The bare CP electrode is reported as white. $Zn(CH_3COO)_2 * 2H_2O$ (aq) as aqueous electrolyte at pH 5.0. Scan rate: 50 mV s-1.

An in-depth electrochemical analysis using specific capacity (Cs) was performed for the working electrodes coated with the two polymers. The specific capacity was calculated from the CV curves using equation 1 [118]:

$$C_s = \frac{\int_{V_1}^{V_2} I\,(V)dV}{2mv} \qquad (1)$$

where Cs is specific capacity of the electrode (C g-1), $\int_{V_1}^{V_2} I\,(V)dV$ is the integrated area of the voltammogram, v is the applied scan rate (V s^{-1}) and m (g) is the deposited mass on CP electrode.

As expected from the voltammograms of the two polymers, the specific capacity of the DHICA-ABtz-derivative polymer (7434 C g^{-1}) was almost twice greater than that of the DHICA eumelanin (4356 C g^{-1}). The values were obtained by subtracting the contribution of the bare CP electrode from both.

The better electrochemical performance of the working electrode coated with the eumelanin-inspired material compared to that coated with the biopolymer could be explained by the chelating properties of the DHICA-ABtz-derived polymer towards the zinc ions present in the electrolyte solution. Specific interactions between the DHICA-ABtz units and the metal ion may have contributed to altering the kinetics of ion exchanges at the polymer/electrolyte interface to which the intensity of the voltammetric current is related [119].

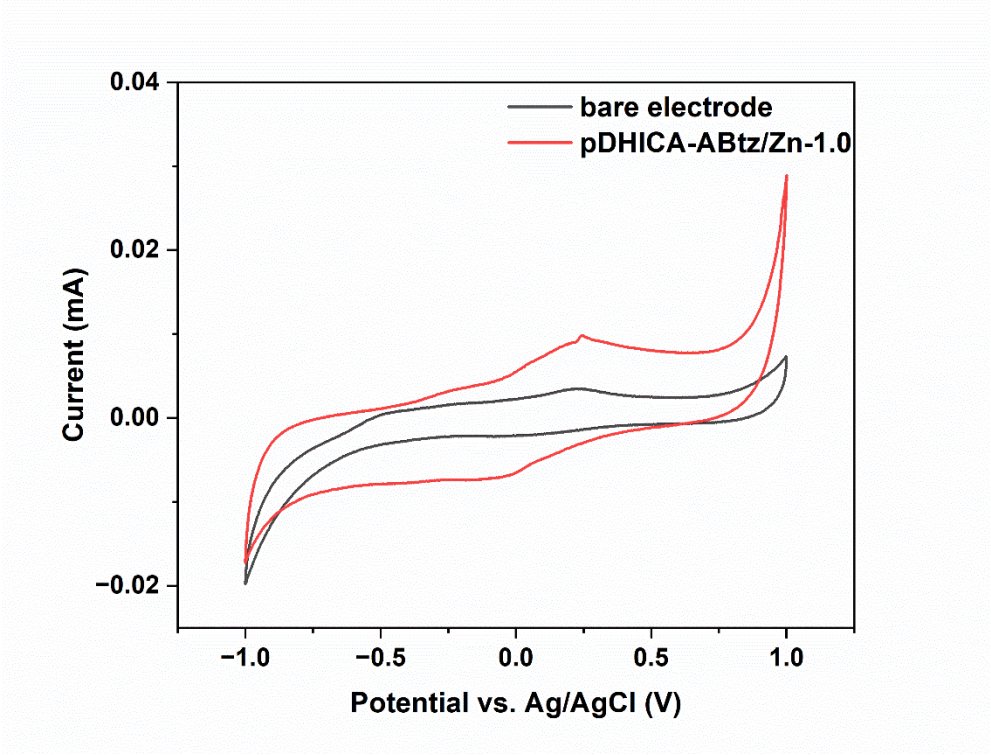

Figure 3.6.17 Cyclic voltammogram of DHICA-ABtz derived polymer with one molar equivalent of $Zn(CH_3COO)_2 * 2H_2O$ on the CP electrode and the bare CP electrode is reported as blank in $Zn(CH_3COO)_2 * 2H_2O$ (aq) as aqueous electrolyte at pH 5.0. Scan rate: 50 mV s^{-1}.

The presence of zinc ions in the DHICA-ABtz-derived polymer significantly changed the intensity of the voltammetric current and signature of the voltammogram (figure 3.6.17). A broad peak with a maximum of 0.24 V, which could result from the convolution of the peaks observed for the DHICA-ABtz-derived polymer, and another signal between 0 V and -0.34 V, were observed. Additionally, a broad reduction wave was located around -0.05 V for pDHICA-ABtz/Zn-1.0.

The specific capacity of the DHICA-ABtz-derived polymer was surprisingly lower than the pure polymer after the addition of $Zn(CH_3COO)_2 * 2H_2O$ (2332 C g^{-1}). The difference in voltammetric current intensities could be partly explained by the formation of a dense film of polymer-zinc ions complex at the electrode/electrolyte interface, which could have hindered ion exchanges [120].

3.7 Fabrication and electrical characterization of DHICA-ABtz-derived polymer thin films with zinc

To exploit the eumelanin-inspired polymer as an active layer in electronic devices, the development of smooth and continuous thin films was a crucial step. For this reason, the next part of the studies focused on the fabrication of thin films of DHICA-ABtz-derived polymers with zinc ions by spin-coating technique.

The DHICA-ABtz-derived polymer/Zn^{2+} blends were prepared starting from $ZnCl_2$ * $2H_2O$/DHICA-ABtz mixtures (molar ratios of 0.1, 0.5, 1.0, 2.0), obtained by two mother solutions of DHICA-ABtz in tetrahydrofuran (THF) at a concentration of 20 mg/mL and the desired amount of $ZnCl_2$ * $2H_2O$ in the same solvent. The solutions were mixed for 5 minutes until completely dissolution. The solutions were filtered through a 0.45 μm nylon membrane, deposited by spin-coating on quartz substrates and then heated to 50 °C for 5 minutes on a hot plate, to evaporate the residual solvent (figure 3.7.1). Films with molar ratios of 0.1:1, 0.5:1, 1:1, and 2:1 ($Zn(CH_3COO)_2$ * $2H_2O$: DHICA-ABtz were denoted as pDHICA-ABtz/Zn-0.1, pDHICA-ABtz/Zn-0.5, pDHICA-ABtz/Zn-1.0, and pDHICA-ABtz/Zn-2.0, respectively. The DHICA-ABtz/Zn^{2+} layers were subjected to the ammonia-induced solid-state polymerization (AISSP) protocol [107, 108] for approximately 16 h to finally obtain the DHICA-ABtz-derived polymer/Zn^{2+} thin films.

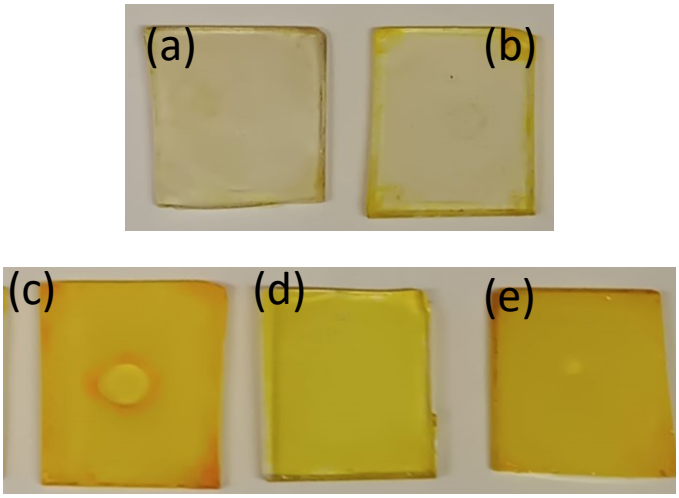

Figure 3.7.1 Films of DHICA-ABtz-derived polymer (a) and with 0.1 (b), 0.5 (c), 1.0 (d) and 2.0 (d) Zn^{2+}/polymer molar ratios.

With Zn^{2+} ions, the absorption profile of DHICA-ABtz in the solid state showed a notable red shift of the absorbance maximum akin the one observed in solution with also a remarkable increase of absorbance (figure 3.7.2).

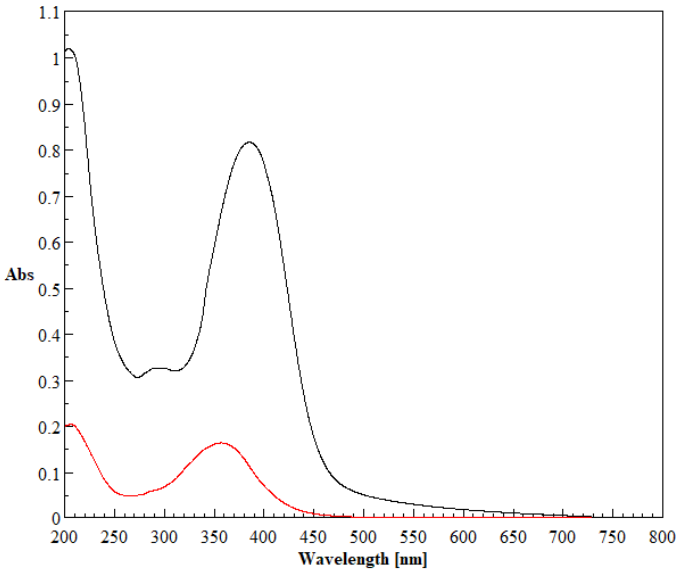

Figure 3.7.2 Uv-vis spectra of the DHICA-ABtz film (red) and the one containing 1:1 $ZnCl_2$ * $2H_2O$/DHICA-ABtz molar ratio (black) normalized with thickness.

Solid-state polymerization of DHICA-ABtz was followed by UV-vis (figure 3.7.3). The spectra recorded at different reaction times, consistently with what was observed from solution studies, showed a progressive broadening of the maximum absorption simultaneously with an increase in absorbance in the visible spectral region.

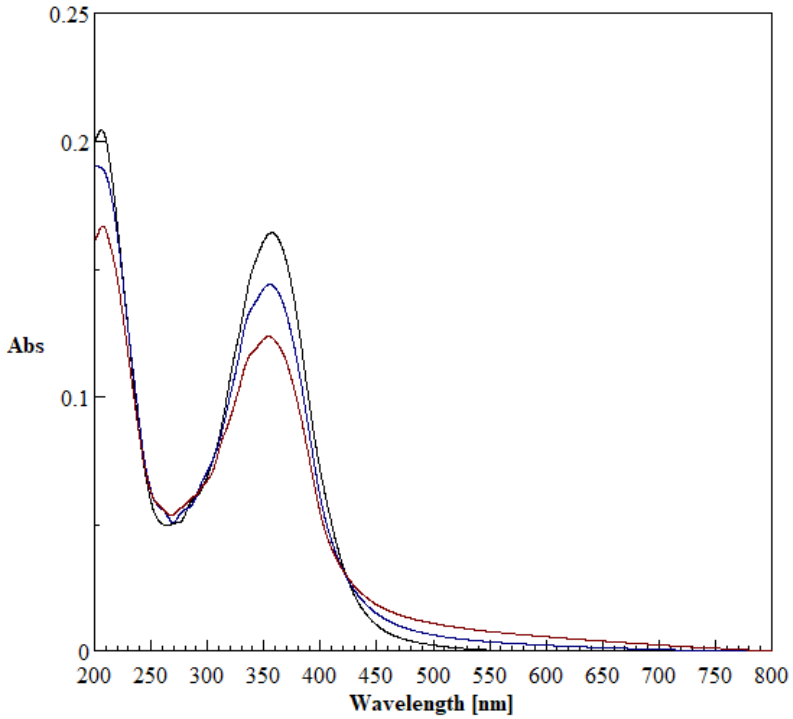

Figure 3.7.3 UV–Vis profiles of DHICA-ABtz film polymerization by AISSP methodology over 16 hours.
t0 (black), 5h (blue), and 16h (dark red).

Surface characterization of DHICA-ABtz-derived polymer and electrolyte films with different zinc contents was carried out by atomic force microscopy (AFM) (Figure 3.6.1). All films ranged in thickness from 24 to 460 nm.
The pure polymer thin film was smooth and continuous, and no porous structure was visible on the surface. With the addition of the zinc salt, the surface morphology was substantially changed, and the porous structure was appreciably visible. Specifically, the pDHICA-ABtz/Zn^{2+} layer exhibited a wrinkled structure with the appearance of

nanopores on the surface. When the salt content increased to the 1:1 molar ratio (sample b), a homogeneous structure enriched with nanopores was formed, indicating a high surface area that could provide increased ion transport pathways promoting ion conduction [121, 122]. By further increasing the 1:2 molar ratio for the DHICA-ABtz-derived polymer: Zn^{2+} ions, the number of pores decreased leading to assume pDHICA-ABtz/Zn-1.0 system as the optimal composition, expecting to show a higher ionic conductivity than to other fabricated films.

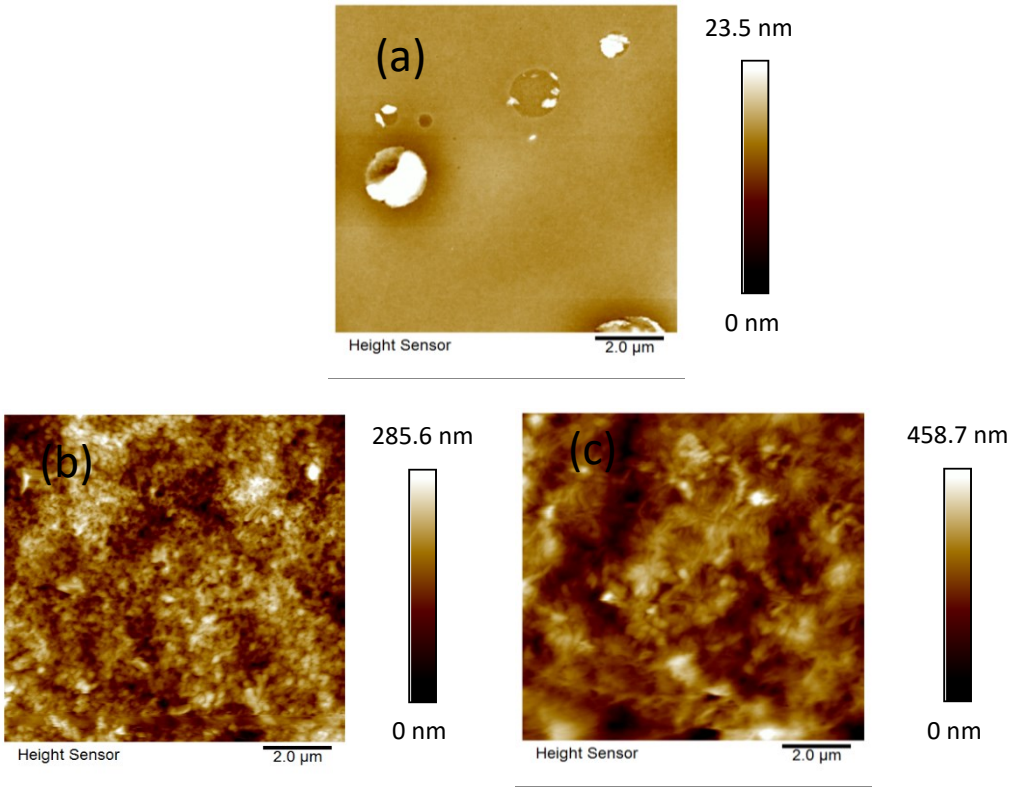

Figure 3.7.4 Atomic force microscopy (AFM) topography of the DHICA-ABtz-derived polymer/Zn^{2+} samples.
The upper panel (a) refers to the pure DHICA-ABtz polymer and the bottom panels, (b) and (c), refer to pDHICA-ABtz/Zn-1.0 and pDHICA-ABtz/Zn-2.0, respectively. The scans are 100 μm^2.

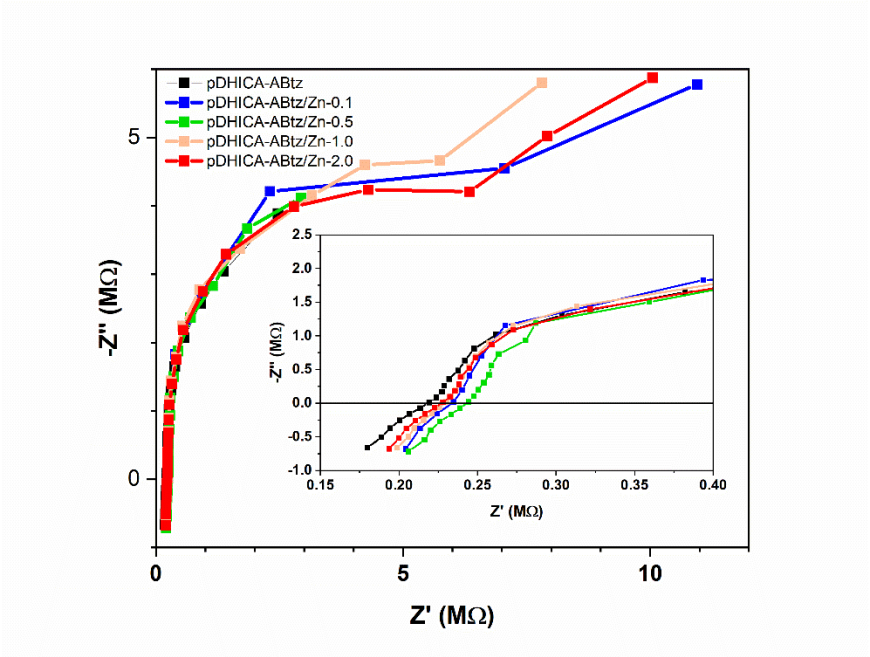

Figure 3.7.5 Room-temperature Nyquist impedance plots of polymer electrolyte films.

Encouraged by these results, the ionic conductivity of DHICA-ABtz-derived polymer/Zn thin films fabricated by spin coating was measured using alternating current (AC) impedance spectroscopy in the frequency range of 10^6 - 10^3 Hz.

In general, Nyquist impedance plots shows a characteristic semicircle shape in the high-frequency region and an inclined line at low frequencies. The high-frequency semicircle is generally associated to the bulk resistance (R_b) effect of the polymer electrolyte, while the low-frequency sloping line is attributed to the blocking effect of the electrodes [123]. The bulk resistance (R_b, Ω) can be determined from the intercept of the semicircle on the real axis (Z'). The ionic conductivity (σ, S cm^{-1}) is given by equation 2 [124]:

$$\sigma = \frac{l}{A\,R_b} \qquad (2)$$

where l is the film thickness (cm) and A is the electrolyte-electrode contact area (cm^2).

The trend of the graphs was quite similar for all the materials in the first measured values while as the frequencies decreased a more apparent semicircular arc was visible as the zinc content increased, unlike a less inclined arc for the pure polymer layer. Although no appreciable differences emerged in the R_b values calculated for the films, the ionic conductivity of the samples (figure 3.7.6) showed a bell-like shape, with a maximum conductivity for the DHICA-ABtz-derived polymer/Zn-1.0 system of 5.3×10^{-11} S cm^{-1}.

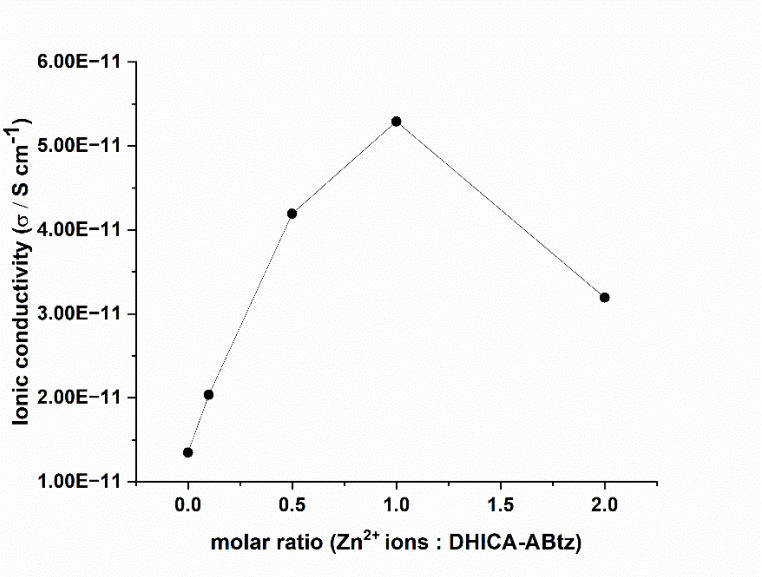

Figure 3.7.6 Dependence of ionic conductivity with the molar ratio of Zn^{2+} ions in DHICA-ABtz-derived polymer.

Further addition of salt reduced the ionic conductivity, probably due to ionic aggregation, as discussed previously in the structural analyses. This can be also explained by equation 3 [125]:

$$\sigma = \sum n_i q_i u_i \qquad (3)$$

where n_i is the density of mobile charge carriers, q_i is the charge of mobile charge carrier and u_i is the mobility of charge carriers. The ionic conductivity of the electrolyte films depends on the number of charge carriers and their mobility [125].

Therefore, increasing n_i and u_i could improve the ionic conductivity of DHICA-ABtz-derived polymer/Zn systems (q_i is the same for all charge carriers).

According to the XRD and AFM analyses, with the addition of zinc salt a large mass of mobile ions was produced by dissociation of the salt, increasing the overall density of charge carriers (n_i) in the system. The intermolecular interactions between the oligomeric scaffolds of the DHICA-ABtz-derived polymer were reduced as the metal ion coordinates the subunits of DHICA-ABtz, thus increasing the free volume space. The formation of nanopores on the surface increased the mobility of charge carriers (u_i) resulting in increased ionic conductivity. When the salt content exceeded the stoichiometric ratio calculated as binding mode between DHICA-ABtz and zinc ions, the free ions aggregated, and their non-uniform dispersion limited the ligand-metal ions interactions by decreasing the density of the mobile charge carriers (n_i). This reduced the mobility of the charge carriers (ui) and thus the overall conductivity decreased.

3.8 Conclusions and future prospects

This PhD thesis focused on the synthesis and study of nature-inspired materials for applications in organic electronics.

The research activities carried out in this context have led to the functionalization of the DHICA eumelanin precursor through the carboxyl group, grafting a benzothiazole system. The optical investigation of the acetylated derivative of the adduct, DAICA-ABtz, revealed specific chelating properties towards zinc ions involving the indole and benzothiazole systems, independently of the catechol moiety.

The straightforward access to the DAICA-ABtz amide and the high isolation yield represented a synthetic approach to obtain eumelanin-inspired materials as well as offering, in a future perspective, the opportunity to improve some drawbacks of this biopolymer such as its insolubility in all solvents.

The optimization of a procedure for deprotection of the catechol group of the adduct led to the obtaining of DHICA-ABtz. Spectroscopic investigation revealed a 1:1 stoichiometry as the binding mode of the deacetylated adduct with Zn^{2+} ions.

The next part of the PhD project focused on the chemistry of the DHICA-ABtz oxidative polymerization with particular interest to the isolation of oligomeric intermediates. The roots of this study lay in the elucidation of the polymerization mechanism to gain insight into the structure of the melanin-inspired material. Isolation and chemical characterization of two DHICA-ABtz dimers concluded that the DHICA derivative polymerized to form oligomers through C–C coupling involving the same positions as the eumelanin precursor under the same conditions, supporting the non-influence of the benzothiazole system on the regioselectivity of polymerization in the early stages of the process.

Optical investigations of the DHICA-ABtz-derived polymer confirmed a change in the absorption profile in the presence of zinc ions even after polymerization, unlike what was observed with DHICA eumelanin.

Encouraged by these outcomes, subsequent research activities addressed the potential application of the DHICA-ABtz-derived polymer as a Zn ion-conducting solid

electrolyte with redox activity, combining the intrinsic redox behaviour of eumelanin with the specific capability of the new eumelanin-inspired material to chelate Zn^{2+} ions.

In this context, the first investigation aimed to find the best composition of DHICA-ABtz/Zn^{2+} as electrolyte system by studying its polymer films with different amounts of zinc. Structural analysis through X-ray diffraction, surface analysis, and thermogravimetric analysis concluded that the best composition of DHICA-ABtz/Zn^{2+} to develop a solid electrolyte (1:1) was equal to the ligand: metal binding ratio found by previous studies in solution.

The next part of the project dealt with revealing the ionic conductivity of the eumelanin-inspired material also as function of different amounts of zinc loaded. The outcomes confirmed 1:1 as the optimal composition for the development of the solid electrolyte. In view of practical exploitation, the ionic conductivity value found for the best investigated polymer/Zn^{2+} system (5.3×10^{-11} S cm^{-1}) was too low compared to the values of current solid electrolytes employed in electrochemical energy storage devices.

Interestingly, the electrochemical characterization of the melanin-inspired polymer immersed in an aqueous electrolyte containing zinc ions highlighted a remarkable specific capacity, almost two times greater than that of the DHICA eumelanin under the same conditions. This finding is vital for the development of an active layer in electrochemical energy storage systems.

In this perspective, the synergy between the intrinsic redox activity of eumelanin and the peculiar ability of the DHICA-ABtz-derived polymer to reversibly chelate zinc ions has strongly oriented the use of this nature-inspired material in pseudocapacitive energy storage systems. Future developments will be aimed at exploiting the electrochemical energy storage performance of the eumelanin-inspired material as a supercapacitor electrode where a potential device design could involve the use of two DHICA-ABtz-derived polymer electrodes in a symmetric supercapacitor configuration immersed in an aqueous electrolyte containing zinc ions, as represented in the following scheme (scheme 3.8.1).

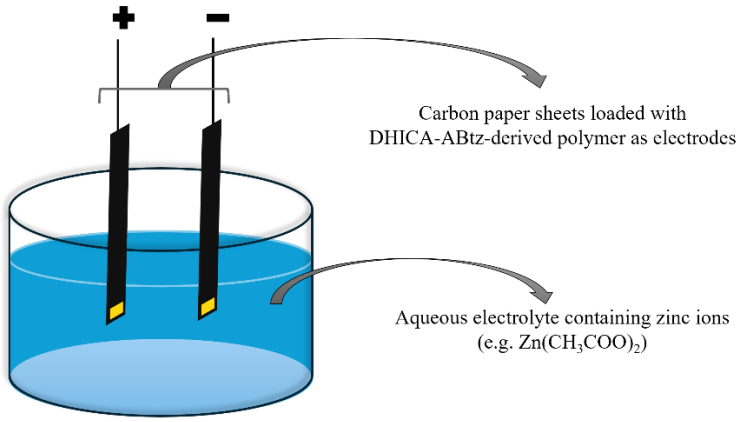

Figure 3.8.1 DHICA-ABtz-derived polymer-based supercapacitor.

3.9 Experimental Part

Materials and Methods. 3,4-dihydroxy-L-phenylalanine (L-DOPA), potassium ferricyanide, sodium bicarbonate, sodium dithionite, acetic anhydride, pyridine, ethyl acetate, tetrahydrofuran (THF), acetonitrile (CAN), methanol, dimethyl sulfoxide (DMSO), *N*-diisopropylethylamine (DIPEA), anhydrous dimethylformamide (DMF), 1-[bis(dimethylamino)methylene]-1*H*-1,2,3-triazolo[4,5-b]pyridinium-3-oxide hexafluorophosphate (HATU), O-(1H-6-Chlorobenzotriazole-1-yl)-1,1,3,3-tetramethyluronium hexafluorophosphate (HCTU), copper acetate, N,N-Diisopropylethylamine (DIPEA), 2-Amino-6-methylbenzothiazole, Butylamine, Ammonia, sodium acetate, zinc acetate dihydrate, zinc chloride dihydrate, magnesium sulphate, chromium (II) chloride, cobalt acetate tetrahydrate, manganese (II) chloride, nickel (II) chloride, calcium chloride were purchased by Sigma-Aldrich. The water (>18 ML) used in this study was obtained from a Super Q water system (Millipore). All solvents were HPLC grade.

Ultraviolet–visible (UV–Vis) and fluorescence spectra were recorded with JASCO spectrometers (JASCO Inc., Mary's Court, Easton, MD, USA).

^{1}H and ^{13}C NMR spectra were recorded at 400 MHz and 100 MHz, respectively, on a 400 Bruker spectrometer, in acetonel-d_6 - DMSO-d_6. In the case of DAICA-ABtz and its dimers, proton and carbon resonance assignments were based on 1D (^{1}H and ^{13}C) and 2D NMR analysis (^{1}H, ^{1}H COSY, ^{1}H,^{13}C HSQC, ^{1}H,^{13}C HMBC, not shown).

HPLC analyses were performed on an Agilent 1100 binary pump instrument equipped with a Shimadzu SPD-10AV VP UV-visible detector using an octadecylsilane-coated column, 250 mm × 4.6 mm, 5 μm particle size (Phenomenex Sphereclone ODS). Detection wavelength was set at 300 nm. 0.1% formic acid – acetonitrile as the eluant at a flow rate of 0.7 mL / min was used; a 0.1% formic acid (solvent A)/acetonitrile (solvent B) gradient elution was performed as follows: from 50 to 80% B, 0 – 40 min.

LC-MS analyses were performed in positive ion mode using an Agilent 1260/6230DA ESI-TOF instrument under the following conditions: 35 psig nebulizer pressure; drying gas (nitrogen) flushed at 5 L/min at a temperature of 325 ° C; capillary voltage 3500 V; fragmentor voltage 175 V. An Eclipse Plus C18 column (150 × 4.6 mm, 5 μm) and 0.1% formic acid - acetonitrile 40:60 v/v as the eluant at a flow rate of 0.4 mL / min was used; a 0.1% formic acid (solvent A)/acetonitrile (solvent B) gradient elution was performed as follows: from 30 to 80% B, 0 – 50 min. Positive Reflectron MALDI spectra were recorded on an AB Sciex TOF/TOF 5800 instrument using 2,5-dihydroxybenzoic acid as the matrix.

AFM in tapping mode (AFM Digital Instruments Dimensions 3100, aluminum-coated silicon cantilever). AFM images were analyzed using NanoScope Analysis software.

X-ray diffraction (XRD) analyses were carried out using a PANalytical diffractometer (Malvern, Worcestershire, United Kingdom) with a nickel filter and CuK α radiation, with a step size of 0.02◦ and a counting time of 80 s/step.

Thermogravimetric analyses (TGA) were carried out with an experimental apparatus composed of a TA instrument simultaneous thermoanalyser SDT Q600 (TA Instrument, New Castle, DE, USA). Samples were dried in an oven to remove moisture and grinded into fine powders. Afterwards, 10 mg of each sample were loaded in platinum pans and submitted to a temperature ramp from 30 to 600°C under air atmosphere, with a heating rate of 10 °C/min.

Cyclic voltammetry was performed using a Biologic VSP 300 multichannel potentiostat, with carbon paper current collectors loaded with polymers acting as the working electrode, Pt mesh as the counter electrode and Ag/AgCl(aq) (3M KCl) as the reference electrode. The electrolyte (5 mL) was composed of 0.25 M $Zn(CH_3COO)*2H_2O$ (≥99%, Sigma Aldrich), buffered with CH_3COOH at pH 5.

The electrical properties of the electrolyte films were studied using an impedance analyzer (PSM 1735, Newton 4th Ltd, UK) over the frequency range of 10^3–10^6 Hz.

Synthesis of DHICA and DAICA. Based on a procedure reported in literature, DHICA was synthesized by ferricyanide oxidation of DOPA [83]. To obtain the corresponding acetylated derivative (DAICA), DHICA (700 mg) was added to a

solution containing acetic anhydride (7 mL) and pyridine (350 µL). After 24 h the resulting mixture was dried using a rotatory evaporator. The hydrolysis of the mixed anhydride with a 1:1 v/v water-methanol mixture at 90° C for 2 h was performed. After removal of the volatile components with the aid of a rotary evaporator, a powder lightly yellow in colour was obtained (98% yield). Purity of the compound was checked by 1H NMR, LC-MS and UV Vis analysis.

Synthesis of DAICA-ABtz. Based on a procedure reported in literature [82], DAICA (50 mg, 0.1804 mmol) was dissolved in 650 mL DMF dry, then coupling agent (0.2708 mmol) were added simultaneously with 47 mL of DIPEA. The reaction is carried out in inert atmosphere. After about 30 minutes, a DMF dry solution of ABtz was added. The progress of the reaction was monitored by TLC. After completion of the reaction, water was added to the solution to promote the precipitation of the DAICA-ABtz; the precipitate was then taken up with ethyl acetate and it was treated with acetic acid. Without the amine, the product precipitated from the organic phase as a white solid and isolated by filtration (52.7 mg, 69% with HATU) (39.7 mg, 52% with HCTU). Mp. 277–279 °C. 1H NMR (acetone-d_6, 400 MHz, δ, ppm): 2.31 (s, 3H), 2.32 (s, 3H), 2.47 (s, 3H), 7.29 (dd, J = 10 Hz, J = 1.5 Hz, 1H), 7.48 (s, 3H), 7.58 (s, 3H), 7.66 (d, J = 10 Hz, 1H), 7.77 (t, J = 1.5 Hz, 1H), 7.78 (dd, J = 2.75, 0.75 Hz, 1H), 11.00 (s, 1H), 11.29 (s, 1H). ^{13}C NMR (acetone-d_6, 100 MHz, δ, ppm), 20.09, 20.15, 20.95, 106.45, 107.01, 116.02, 120.74, 121.46, 125.43, 127.89, 131.25, 132.81, 134.01, 135.48, 138.32, 141.78, 147.26, 157.58, 159.77, 168.58 and 168.85. MS (MALDI) m/z: 446 ($[M +Na]^+$), 462 ($[M + K]^+$). FTIR: n = 1200, 1268, 1380 1460, 1560, 1715, 1759, 3235, 3383.

Synthesis of DAICA butylamide and ABtz acetamide ABtz. (500 mg) was acetylated with acetic anhydride (5 mL) and pyridine (250 µL) for 24 h. After dried a powder light in color was obtained (yield 98%). DAICA (100 mg, 0.3607 mmol) was dissolved in 1.3 mL DMF dry, then HATU (206 mg, 0.5411 mmol) were added simultaneously with 94 µL of DIPEA. The reaction is carried out in argon atmosphere. After about 30 minutes, a DMF dry solution of butylamine was added. The progress of the reaction was monitored by TLC. After completion of the reaction,

water was added to the solution to promote the precipitation of the amide. The product was isolated by filtration as a light brown solid (108 mg, 90%).

Synthesis of DHICA-ABtz. The reaction was carried out in inert atmosphere by dissolving DAICA-ABtz (100 mg) in methanol with a final concentration of 3.6 mM. Then a solution of sodium tert-butoxide (2.3 eq) in methanol was degassed under argon flow and added to the DAICA-ABtz solution. After 7 min the reaction mixture was acidified with HCl 6 M up to pH 2-3 and rapidly dried under vacuo. The solid was then taken up with ethyl acetate and it was treated with water. Finally, the organic phase was dried under vacuo, obtaining a yellow powder (64.9 mg, 81.0% yield).

Synthesis of 4,4'-DHICA-ABtz and 4,7'-DHICA-ABtz dimers. Oxidation of DHICA-ABtz was carried out following a procedure reported in literature with modifications [98]. DHICA-ABtz (100 mg, 3 mM) and 1 molar eq of copper acetate were dissolved in 50 mM carbonate buffer (pH 7.5) and the mixture was stirred for 60 min. The reaction was stopped by acidification to pH 2-3 with 6 M HCl. The mixture was extracted with ethyl acetate and dried under vacuo. The residue (59 mg) was treated with 1.5 mL of acetic anhydride and 75 µL of pyridine overnight. After removal of the solvent, the acetylated mixture was dissolved in methanol and purified by preparative TLC (chloroform: ethyl acetate + 2% v/v methanol as eluent) to give the 4,4'-DHICA-ABtz and 4,7'-DHICA-ABtz in their acetylated forms (12.2 mg, 12.2 % yield for 4,4'-DHICA-ABtz and 9.8 mg, 9.8 % yield for 4,7'-DHICA-ABtz). MS (MALDI) m/z: 867 ($[M+Na]^+$), 883 ($[M+K]^+$).

4,4'-DHICA-ABtz. ^{1}H-NMR (DMSO-d_6): δ (ppm): 2.00 (3H, s), 2.32 (3H, s), 2.39 (3H, s), 7.20 (1H x 2, d), 7.33 (1H x 2, d), 7.47 (1H x 2, s), 7.53 (1H x 2, s), 7.75 (1H x 2, d), 12.23 (1H x 2, s), 12.27 (1H x 2, s). ^{13}C-NMR (DMSO-d_6): δ (ppm): 19.35 (CH3), 19,86 (CH3), 20.46 (CH3), 106.30 (CH), 106.66 (CH), 119.98 (CH), 120.18 (C) 125.2 (C), 127.3 (C), 127.34 (CH), 130.02 (C), 133.42 (C), 135.63 (C), 140.19 (C), 141.77 (C), 146.12 (C), 157.62 (C), 161.34 (C), 167.99 (C), 168.21 (C).

4,7'-DHICA-ABtz. ^{1}H-NMR (DMSO-d_6): δ (ppm): 1.99 (3H, t), 2.01 (3H, s), 2.31 (3H, s), 2.32 (3H, s), 2.38 (3H, s) 2.39 (3H, s), 7.20 (1H, d), 7.20 (1H, s), 7.21 (1H, d), 7.51 (1H, s), 7.53 (1H, d), 7.68 (1H, s), 7.74 (1H, s), 7.75 (1H, s), 7.75 (1H, d), 7.76 (1H, s), 11.25 (1H, s), 12.27 (1H, s), 12.28 (s, 2H).

^{13}C-NMR (DMSO-d_6): δ (ppm): 19.67 (CH3), 19.68 (CH3), 20.48 (CH3), 20.49 (CH3) 20.99 (CH3), 22.06 (CH3), 106.03 (C), 106.09 (C), 106.66 (CH), 106.67 (CH), 119.98 (C), 120.18 (C), 120.19 (C), 120.96 (C), 125.23 (C), 126.75 (CH), 127.33 (C), 127.34 (CH), 129.09 (CH), 130.02 (CH), 130.05 (C),
133.42 (C), 133.43 (C), 133.46 (C), 134.49 (CH), 135.34 (C), 135.63 (C), 135.69 (C), 136.23 (C), 137.91 (CH), 140.19 (CH), 141.71 (C), 141.77 (C), 145.23 (CH), 146.12 (C), 157.62 (C), 161.34 (C), 161.38 (C), 167.92 (C), 167.99 (C), 168.21 (C), 168.22 (C).

Preparation of DHICA eumelanin and DHICA-ABtz-derived polymer. DHICA or DHICA-ABtz (1mM) were taken under stirring at pH 9 in 0.05 M carbonate buffer. After 24 h, the resulting mixture was acidified and bought to pH 3. The precipitate was centrifuged. The solid was washed with HCl 0.01 M and lyophilized. DHICA eumelanin and DHICA-ABtz-derived polymer were obtained in satisfying yields (83 and 74 w/w %, respectively).

Optical measurements. Both absorption and emission spectra were collected on the same solutions, in the same conditions, as described in the following. Stock solutions (2.0 mM) of the metal salts were prepared in methanol and solutions of DAICA-ABtz or DHICA-ABtz (only with $Zn(CH_3COO)_2 * 2H_2O$) (68.5 μM) was prepared in the same solvent. UV-vis of DAICA-ABtz and DHICA-ABtz and fluorescence titrations of DAICA-ABtz against different concentrations of metal ions were executed by adding 17.1 μL aliquots of stock salt solution to 2.0 mL of amide in methanol. After shaking for a few seconds, the spectra were recorded at room temperature. Titration of DAICA-ABtz with metal ions and DHICA-ABtz with zinc ions were performed for several times up to 2.0 equivalents of metal ions.

The solutions prepared for UV-vis titrations of DAICA butylamide and ABtz acetamide in methanol were obtained at the same concentrations under the same conditions as those for DAICA-ABtz.

The continuous variations method [90] was applied for DAICA-ABtz and DHICA-ABtz with $Zn(CH_3COO)_2 * 2H_2O$ in the same conditions,, as described below. The Job's plots [88, 89] were obtained mixing different volumes (from 0.2 to 2.0 mL) of equimolar (68.5 μM) methanol solutions of DAICA-ABtz or DHICA-ABtz and

$Zn(CH_3COO)_2 * 2H_2O$. The molar ratio of metal ion was varied from 0.1 to 0.9, while the total concentration of the ligand and Zn^{2+} remained constant in each solution. After shaking for a few seconds, UV-vis absorption spectra were recorded at room temperature. Similar processes were run for blank test with solution of DAICA-ABtz or DHICA-ABtz only.

The quantum yield of DAICA-ABtz was measured in the absence and in the presence of zinc ions using quantum yield of 0.546 for quinine sulfate dihydrate as standard [126, 127].

Titrations of DHICA eumelanin and DHICA-ABtz-derived polymer were carried out by adding 10 µL of a solution of 0.5 mg/ mL to 2 mL of 0.025 mg / mL DHICA eumelanin or DHICA-ABtz-derived polymer solution up to 50% w/w of metal ions.

Preparation of films for XRD and TGA analyses. The desired amount of $Zn(CH_3COO)_2 * 2H_2O$ was added to a solution of DHICA-ABtz 1 mg / mL in methanol. The mixtures were kept under stirring until complete dissolution. The solutions thus obtained were poured into glass discs and heated at 50°C for 4h. The layers were subjected to AISPP methodology [107, 108]: each sample was exposed for 16 h to an oxidizing atmosphere made of oxygen and ammonia vapors at a controlled temperature (25 °C), produced by the equilibrium of the air with an ammonia solution (28% NH_3 in H_2O) in a sealed chamber at 1 bar pressure.

Preparation of film-coated carbon paper electrodes. Two solutions of 30 mM DHICA-ABtz in dimethyl sulfoxide (DMSO) and DHICA in methanol were prepared. The DHICA-ABtz solution with 1 molar equivalent of zinc salt was obtained by pre-dissolving the salt in methanol. In this case, the final concentration of DHICA-ABtz was 30 mM with a DMSO: methanol ratio = 4:6. 5 µL of each prepared solution was deposited on a carbon paper electrode (0.5 cm^2). Each sample was then subjected for 16 h to AISSP methodology.

Preparation of thin films for AFM analysis and Impedance measurements. The desired amount of $ZnCl_2*2H_2O$ was added to the start solution of DHICA-ABtz 20 mg/mL in tetrahydrofuran. The mixtures were kept under stirring until completely dissolved and then filtered through a 0.2 µm Whatman membrane. Thin films of DHICA-ABtz-derived polymer and DHICA-ABtz-derived polymer /Zn^{2+} blends

were prepared by spin-coating with Laurell WS-650MZ-23NPP/LITE coating on a 2.25 cm^2 quartz substrate the solutions using a 2-phase program: I) 2500 rpm for 30s with an acceleration of 2 rpm/s; II) 800 rpm for 10 s with an acceleration of 1000 rpm/s. 80 µL of solution was deposited for each sample. The thin films were subjected to the AISPP methodology for 16 hours. The resulting film thicknesses were 460 nm - 24 nm, measured using a KLA Tencor P-10 stylus profiler.

References

1. Miller, J.R. and A. Burke, *Electrochemical Capacitors: Challenges and Opportunities for Real-World Applications.* The Electrochemical Society Interface, 2008. **17**(1): p. 53.

2. Miller, J.R. and P. Simon, *Electrochemical Capacitors for Energy Management.* Science, 2008. **321**(5889): p. 651-652.

3. Lukatskaya, M.R., B. Dunn, and Y. Gogotsi, *Multidimensional materials and device architectures for future hybrid energy storage.* Nat Commun, 2016. **7**: p. 12647.

4. Pomerantseva, E. and Y. Gogotsi, *Two-dimensional heterostructures for energy storage.* Nature Energy, 2017. **2**(7): p. 17089.

5. Linden, D. *Handbook of batteries*. in *Fuel and energy abstracts*. 1995.

6. Chen, G.Z., *Supercapacitor and supercapattery as emerging electrochemical energy stores.* International Materials Reviews, 2017. **62**(4): p. 173-202.

7. Mukhopadhyay, A. and B.W. Sheldon, *Deformation and stress in electrode materials for Li-ion batteries.* Progress in Materials Science, 2014. **63**: p. 58-116.

8. Evanko, B., et al., *Redox-Enhanced Electrochemical Capacitors: Status, Opportunity, and Best Practices for Performance Evaluation.* ACS Energy Letters, 2017. **2**(11): p. 2581-2590.

9. Xia, L., et al., *Electrolytes for electrochemical energy storage.* Materials Chemistry Frontiers, 2017. **1**(4): p. 584-618.

10. Liu, Y., et al., *Vanadium nitride for aqueous supercapacitors: a topic review.* Journal of Materials Chemistry A, 2020. **8**(17): p. 8218-8233.

11. Bolognesi, M., M. Prosa, and M. Seri, *9 - Biocompatible and biodegradable organic electronic materials*, in *Sustainable Strategies in Organic Electronics*, A. Marrocchi, Editor. 2022, Woodhead Publishing. p. 297-338.

12. Chen, Y., et al., *High-performance supercapacitors based on a graphene–activated carbon composite prepared by chemical activation.* RSC Advances, 2012. **2**(20): p. 7747-7753.

13. Shi, K. and I. Zhitomirsky, *Fabrication of Polypyrrole-Coated Carbon Nanotubes Using Oxidant–Surfactant Nanocrystals for Supercapacitor Electrodes with High Mass Loading and Enhanced Performance.* ACS Applied Materials & Interfaces, 2013. **5**(24): p. 13161-13170.

14. Zou, Q., et al., *Supercritical ethanol deposition of $Ni(OH)_2$ nanosheets on carbon cloth for flexible solid-state asymmetric supercapacitor electrode.* The Journal of Supercritical Fluids, 2020. **159**: p. 104774.

15. Lin, Z., et al., *A high capacity small molecule quinone cathode for rechargeable aqueous zinc-organic batteries.* Nature Communications, 2021. **12**(1): p. 4424.

16. Holze, R. and Y. Wu, *Intrinsically conducting polymers in electrochemical energy technology: Trends and progress.* Electrochimica Acta, 2014. **122**: p. 93-107.

17. Enderby, J.E. and G.W. Neilson, *The structure of electrolyte solutions.* Reports on Progress in Physics, 1981. **44**(6): p. 593.

18. Petrovic, S., *Battery technology crash course : a concise introduction*. 2021, Springer Cham, Switzerland: Cham, Switzerland.

19. Collins, J., G. Gourdin, and D. Qu, *Chapter 3.23 - Modern Applications of Green Chemistry: Renewable Energy*, in *Green Chemistry*, B. Török and T. Dransfield, Editors. 2018, Elsevier. p. 771-860.

20. Karim, J., et al., *Influence of Electron beam radiation on the properties of Surface-Modified Titania-Filled gel polymer electrolytes using vinyltriethoxysilane (VTES) for lithium battery application.* Results in Chemistry, 2022. **4**: p. 100383.

21. Chen, R., et al., *A Comparative Review of Electrolytes for Organic-Material-Based Energy-Storage Devices Employing Solid Electrodes and Redox Fluids.* ChemSusChem, 2020. **13**(9): p. 2205-2219.

22. Muench, S., et al., *Polymer-Based Organic Batteries.* Chem Rev, 2016. **116**(16): p. 9438-84.

23. Choudhury, N.A., S. Sampath, and A.K. Shukla, *Hydrogel-polymer electrolytes for electrochemical capacitors: an overview.* Energy & Environmental Science, 2009. **2**(1): p. 55-67.

24. Zheng, H., et al., *TiO_2@C core–shell nanowires for high-performance and flexible solid-state supercapacitors.* Journal of Materials Chemistry C, 2013. **1**(2): p. 225-229.

25. Jónsson, E., *Ionic liquids as electrolytes for energy storage applications – A modelling perspective.* Energy Storage Materials, 2020. **25**: p. 827-835.

26. Singh, P., A. Sachdeva, and C. Bhargava, *Polymer Electrolyte a Novel Material for Electrochemical Devices: A Review.* Journal of Physics: Conference Series, 2022. **2327**(1): p. 012021.

27. Mauger, A., et al., *Building Better Batteries in the Solid State: A Review.* Materials, 2019. **12**(23): p. 3892.

28. Li, A., et al., *A Review on Lithium-Ion Battery Separators towards Enhanced Safety Performances and Modelling Approaches.* Molecules, 2021. **26**(2): p. 478.

29. Ngai, K.S., et al., *A review of polymer electrolytes: fundamental, approaches and applications.* Ionics, 2016. **22**: p. 1259-1279.

30. Fenton, D.E., J.M. Parker, and P.V. Wright, *Complexes of alkali metal ions with poly(ethylene oxide).* Polymer, 1973. **14**(11): p. 589.

31. Vashishta, P. and J.N. Mundy, *Fast ion transport in solids: electrodes and electrolytes*. 1979, United States: Elsevier North Holland, Inc.

32. Gray, F.M., *Polymer electrolytes*, ed. J.A. Connor. Vol. RSC Materials Monographs. 1997: Royal Society of Chemistry.

33. Owen, J.R., *Lithium Batteries — new materials, developments and perspectives : G. Pistoia (Ed.), Elsevier Science, Amsterdam, 1994, ISBN 0-444-89957-X, X + 493 pp., Dfl 425.* Journal of Electroanalytical Chemistry, 1994. **374**: p. 283-284.

34. Song, J.Y., Y.Y. Wang, and C.C. Wan, *Review of gel-type polymer electrolytes for lithium-ion batteries.* Journal of Power Sources, 1999. **77**(2): p. 183-197.

35. Osada, I., et al., *Ionic-Liquid-Based Polymer Electrolytes for Battery Applications.* Angew Chem Int Ed Engl, 2016. **55**(2): p. 500-13.

36. Park, M.J., et al., *Polymer electrolytes integrated with ionic liquids for future electrochemical devices.* Journal of Applied Polymer Science, 2013. **129**(5): p. 2363-2376.

37. Arya, A. and A. Sharma, *Polymer electrolytes for lithium ion batteries: a critical study.* Ionics, 2017. **23**: p. 497-540.

38. Mallaiah, Y., et al., *Impact of polymer blending on ionic conduction mechanism and dielectric properties of sodium based PEO-PVdF solid polymer electrolyte systems.* Journal of Physics and Chemistry of Solids, 2021. **155**: p. 110096.

39. Yazie, N., et al., *Development of polymer blend electrolytes for battery systems: recent progress, challenges, and future outlook.* Materials for Renewable and Sustainable Energy, 2023. **12**(2): p. 73-94.

40. Rodrigues, L.C., et al., *Electrochemical and thermal properties of polymer electrolytes based on poly(epichlorohydrin-co-ethylene oxide-co-ally glycidyl ether).* Electrochimica Acta, 2007. **53**(4): p. 1427-1431.

41. Akinwolemiwa, B., C. Peng, and G.Z. Chen, *Redox Electrolytes in Supercapacitors.* Journal of The Electrochemical Society, 2015. **162**(5): p. A5054.

42. Nguyen, T. and M.F. Montemor, *Redox active materials for metal compound based hybrid electrochemical energy storage: a perspective view.* Applied Surface Science, 2017. **422**: p. 492-497.

43. Senthilkumar, S.T., R.K. Selvan, and J.S. Melo, *Redox additive/active electrolytes: a novel approach to enhance the performance of supercapacitors.* Journal of Materials Chemistry A, 2013. **1**(40): p. 12386-12394.

44. Frackowiak, E., et al., *Redox-active electrolyte for supercapacitor application.* Faraday Discussions, 2014. **172**(0): p. 179-198.

45. Lota, G. and E. Frackowiak, *Striking capacitance of carbon/iodide interface.* Electrochemistry Communications, 2009. **11**(1): p. 87-90.

46. Lota, G., K. Fic, and E. Frackowiak, *Alkali metal iodide/carbon interface as a source of pseudocapacitance.* Electrochemistry Communications, 2011. **13**(1): p. 38-41.

47. Yu, H., et al., *Application of a novel redox-active electrolyte in MnO2-based supercapacitors.* Science China Chemistry, 2012. **55**(7): p. 1319-1324.

48. Roldán, S., et al., *Mechanisms of Energy Storage in Carbon-Based Supercapacitors Modified with a Quinoid Redox-Active Electrolyte.* The Journal of Physical Chemistry C, 2011. **115**(35): p. 17606-17611.

49. Zhou, Y., et al., *Polyanthraquinone-based nanostructured electrode material capable of high-performance pseudocapacitive energy storage in aprotic electrolyte.* Nano Energy, 2015. **15**.

50. Song, Z., et al., *A quinone-based oligomeric lithium salt for superior Li–organic batteries.* Energy & Environmental Science, 2014. **7**(12): p. 4077-4086.

51. Kim, Y.J., et al., *Biologically derived melanin electrodes in aqueous sodium-ion energy storage devices.* Proceedings of the National Academy of Sciences, 2013. **110**(52): p. 20912-20917.

52. Liang, Y., Z. Tao, and J. Chen, *Organic Electrodes: Organic Electrode Materials for Rechargeable Lithium Batteries (Adv. Energy Mater. 7/2012).* Advanced Energy Materials, 2012. **2**.

53. Wang, C., et al., *High-Performance Alkaline Organic Redox Flow Batteries Based on 2-Hydroxy-3-carboxy-1,4-naphthoquinone.* ACS Energy Letters, 2018. **3**(10): p. 2404-2409.

54. Lin, K., et al., *Alkaline quinone flow battery.* Science, 2015. **349**(6255): p. 1529-1532.

55. Liang, Y., et al., *Universal quinone electrodes for long cycle life aqueous rechargeable batteries.* Nat Mater, 2017. **16**(8): p. 841-848.

56. Janoschka, T., et al., *An aqueous, polymer-based redox-flow battery using non-corrosive, safe, and low-cost materials.* Nature, 2015. **527**(7576): p. 78-81.

57. Huskinson, B., et al., *A metal-free organic-inorganic aqueous flow battery.* Nature, 2014. **505**(7482): p. 195-8.

58. Holze, R., *Overoxidation of Intrinsically Conducting Polymers.* Polymers (Basel), 2022. **14**(8).

59. Song, Z. and H. Zhou, *Towards sustainable and versatile energy storage devices: an overview of organic electrode materials.* Energy & Environmental Science, 2013. **6**(8): p. 2280-2301.

60. Mukhopadhyay, A., et al., *Heavy Metal-Free Tannin from Bark for Sustainable Energy Storage.* Nano Lett, 2017. **17**(12): p. 7897-7907.

61. Marrikar, F.S., et al., *Modification of indium-tin oxide electrodes with thiophene copolymer thin films: optimizing electron transfer to solution probe molecules.* Langmuir, 2007. **23**(3): p. 1530-42.

62. Wei, B., et al., *Significant enhancement of PEDOT thin film adhesion to inorganic solid substrates with EDOT-acid.* ACS Appl Mater Interfaces, 2015. **7**(28): p. 15388-94.

63. Zhang, S., et al., *Water stability and orthogonal patterning of flexible micro-electrochemical transistors on plastic.* Journal of Materials Chemistry C, 2016. **4**(7): p. 1382-1385.

64. Jorfi, M., et al., *Progress towards biocompatible intracortical microelectrodes for neural interfacing applications.* J Neural Eng, 2015. **12**(1): p. 011001.

65. Yoon, D.H., et al., *PEDOT:PSS as multi-functional composite material for enhanced Li-air-battery air electrodes.* Scientific Reports, 2016. **6**(1): p. 19962.

66. Irimia-Vladu, M., N.S. Sariciftci, and S. Bauer, *Exotic materials for bio-organic electronics.* Journal of Materials Chemistry, 2011. **21**(5): p. 1350-1361.

67. Kim, Y.J., et al., *Catechol-Mediated Reversible Binding of Multivalent Cations in Eumelanin Half-Cells.* Advanced Materials, 2014. **26**(38): p. 6572-6579.

68. Kumar, P., et al., *Melanin-based flexible supercapacitors.* Journal of Materials Chemistry C, 2016. **4**(40): p. 9516-9525.

69. Cheng, F., et al., *Squid inks-derived nanocarbons with unique "shell@pearls" structure for high performance supercapacitors.* Journal of Power Sources, 2017. **354**: p. 116-123.

70. Xu, R., et al., *Melanin: A Greener Route To Enhance Energy Storage under Solar Light.* ACS Omega, 2019. **4**(7): p. 12244-12251.

71. Ajjan, F.N., D. Mecerreyes, and O. Inganäs, *Enhancing Energy Storage Devices with Biomacromolecules in Hybrid Electrodes.* Biotechnology Journal, 2019. **14**(12): p. 1900062.

72. Yang, L., et al., *Synthetic Biopigment Supercapacitors.* ACS Applied Materials & Interfaces, 2019. **11**(33): p. 30360-30367.

73. Yang, L., et al., *Emergence of melanin-inspired supercapacitors.* Nano Today, 2021. **37**: p. 101075.

74. Caruso, U., et al., *Two aminobenzothiazole derivatives for Pd(II) and Zn(II) coordination: Synthesis, characterization and solid state fluorescence.* Inorganic Chemistry Communications, 2011. **14**(1): p. 46-48.

75. Diana, R. and B. Panunzi, *The Role of Zinc(II) Ion in Fluorescence Tuning of Tridentate Pincers: A Review.* Molecules, 2020. **25**(21).

76. Joseph, J., G. Janaki, and J. Dharmaraja, *Metal complexes of 2-aminobenzothiazole derivatives as a versatile system tuning up their structural and biological properties.* 2016. **8**: p. 133-152.

77. Naoki Shimidzu, T.U., *Studies on Benzothiazole Derivatives as Chelating Agents. I. Syntheses of Benzothiazole Derivatives and Their Reactions with Metal Ions.* Chem. Pharm. Bull., 1973. **21**(1): p. 184-190.

78. Das, S., et al., *Benzothiazole based fluorescent probes for the detection of biomolecules, physiological conditions, and ions responsible for diseases.* Dyes and Pigments, 2022. **199**: p. 110074.

79. Huang, Y., et al., *Metal-Chelating Benzothiazole Multifunctional Compounds for the Modulation and 64 Cu PET Imaging of Aβ Aggregation.* Chemical Science, 2020. **11**.

80. Shimidzu, N. and T. Uno, *Studies on Benzothiazole Derivatives as Chelating Agents. IV. Coordination to Divalent Metal Ions.* Chemical & Pharmaceutical Bulletin, 1978. **26**: p. 127-134.

81. Jiang, L.-Y., et al., *Identification of 2-subsituted benzothiazole derivatives as triple-functional agents with potential for AD therapy.* RSC Advances, 2016. **6**: p. 17318-17327.

82. Mocerino, F., A. Pezzella, and U. Caruso, *Eumelanin pigment precursor 2-carboxy-5,6-dihydroxyindole and 2-amino-6-methylbenzothiazole chromophore integration towards melanin inspired chemoresponsive materials: the case of the Zn^{2+} ion.* RSC Adv, 2022. **12**(33): p. 21050-21055.

83. Sugumaran, M., et al., *Nonenzymatic Spontaneous Oxidative Transformation of 5,6-Dihydroxyindole.* Int J Mol Sci, 2020. **21**(19).

84. Alewood, P., et al., *Rapid in situ neutralization protocols for Boc and Fmoc solid-phase chemistries.* Methods Enzymol, 1997. **289**: p. 14-29.

85. Carpino, L.A., *1-Hydroxy-7-azabenzotriazole. An efficient peptide coupling additive.* Journal of the American Chemical Society, 1993. **115**(10): p. 4397-4398.

86. Marder, O., Y. Shvo, and F. Albericio, *HCTU and TCTU: New Coupling Reagents — Development and Industrial Aspects.* ChemInform, 2003. **34**(32).

87. Carpino, L.A., et al., *Comparison of the Effects of 5- and 6-HOAt on Model Peptide Coupling Reactions Relative to the Cases for the 4- and 7-Isomers.* Organic Letters, 2000. **2**(15): p. 2253-2256.

88. Huang, C.Y., *Determination of binding stoichiometry by the continuous variation method: the Job plot.* Methods Enzymol, 1982. **87**: p. 509-25.

89. Renny, J.S., et al., *Method of continuous variations: applications of job plots to the study of molecular associations in organometallic chemistry.* Angew Chem Int Ed Engl, 2013. **52**(46): p. 11998-2013.

90. Benesi, H.A. and J.H. Hildebrand, *A Spectrophotometric Investigation of the Interaction of Iodine with Aromatic Hydrocarbons.* Journal of the American Chemical Society, 1949. **71**(8): p. 2703-2707.

91. Alam, R., et al., *A rhodamine based fluorescent trivalent sensor (Fe^{3+}, Al^{3+}, Cr^{3+}) with potential applications for live cell imaging and combinational logic circuits and memory devices.* New Journal of Chemistry, 2017. **41**(16): p. 8359-8369.

92. Aragoni, M.C., et al., *Zn^{2+}/Cd^{2+} optical discrimination by fluorescent chemosensors based on 8-hydroxyquinoline derivatives and sulfur-containing macrocyclic units.* Dalton Transactions, 2013. **42**(40): p. 14516-14530.

93. Lee, J.J., et al., *A highly selective CHEF-type chemosensor for monitoring Zn^{2+} in aqueous solution and living cells.* RSC Advances, 2015. **5**(52): p. 41905-41913.

94. Lee, H., et al., *Mechanism of "turn-on" fluorescent sensors for mercury(II) in solution and its implications for ligand design.* Inorg Chem, 2012. **51**(20): p. 10904-15.

95. Moradi, S.E., et al., *Benzo[d]imidazo[2,1-b]thiazole-based fluorescent sensor for Zn^{2+} ion detection.* Journal of Photochemistry and Photobiology A: Chemistry, 2020. **389**: p. 112184.

96. Lee, H., R.D. Hancock, and H.S. Lee, *Role of fluorophore-metal interaction in photoinduced electron transfer (PET) sensors: time-dependent density functional theory (TDDFT) study.* J Phys Chem A, 2013. **117**(50): p. 13345-55.

97. Goswami, S., et al., *A new visible-light-excitable ICT-CHEF-mediated fluorescence 'turn-on' probe for the selective detection of Cd^{2+} in a mixed aqueous system with live-cell imaging.* Dalton Transactions, 2015. **44**(12): p. 5763-5770.

98. Palumbo, P., et al., *Isolation of a new intermediate in the oxidative conversion of 5,6-dihydroxyindole-2-carboxylic acid to melanin.* Tetrahedron Letters, 1987. **28**(4): p. 467-470.

99. Pezzella, A., et al., *Short-Lived Quinonoid Species from 5,6-Dihydroxyindole Dimers en Route to Eumelanin Polymers: Integrated Chemical, Pulse Radiolytic, and Quantum Mechanical Investigation.* Journal of the American Chemical Society, 2006. **128**(48): p. 15490-15498.

100. Argenziano, R., et al., *A Model Eumelanin from 5,6-Dihydroxyindole-2-Carboxybutanamide Combining Remarkable Antioxidant and Photoprotective Properties with a Favourable Solubility Profile for Dermo-Cosmetic Applications.* International Journal of Molecular Sciences, 2023. **24**(4): p. 4241.

101. Micillo, R., et al., *Unexpected impact of esterification on the antioxidant activity and (photo)stability of a eumelanin from 5,6-dihydroxyindole-2-carboxylic acid.* Pigment Cell & Melanoma Research, 2018. **31**(4): p. 475-483.

102. Murphy, B.P. and T.M. Schultz, *Synthesis and physical properties of 5 6 dihydroxyindole.* Journal of Organic Chemistry, 1985. **50**(15): p. 2790-2791.

103. Tran, M.L., B.J. Powell, and P. Meredith, *Chemical and structural disorder in eumelanins: a possible explanation for broadband absorbance.* Biophys J, 2006. **90**(3): p. 743-52.

104. Napolitano, A., M.G. Corradini, and G. Prota, *A reinvestigation of the structure of melanochrome.* Tetrahedron Letters, 1985. **26**(23): p. 2805-2808.

105. Beer, R.J.S., T. Broadhurst, and A. Robertson, *The chemistry of the melanins. Part V. The autoxidation of 5 : 6-dihydroxyindoles.* Journal of the Chemical Society (Resumed), 1954(0): p. 1947-1953.

106. Grieco, C., et al., *Probing the heterogeneous structure of eumelanin using ultrafast vibrational fingerprinting.* Nat Commun, 2020. **11**(1): p. 4569.

107. Migliaccio, L., et al., *Eumelanin Precursor 2-Carboxy-5,6-Dihydroxyindole (DHICA) as Doping Factor in Ternary (PEDOT:PSS/Eumelanin) Thin Films for Conductivity Enhancement.* Materials, 2020. **13**(9): p. 2108.

108. Migliaccio, L., et al., *Impact of Eumelanin–PEDOT Blending: Increased PEDOT Crystalline Order and Packing–Conductivity Relationship in Ternary PEDOT:PSS:Eumelanin Thin Films.* Advanced Electronic Materials, 2019. **5**(3): p. 1800585.

109. Horzum, N., M. Elhousseini Hilal, and T. Isık, *Enhanced Bactericidal and Photocatalytic Activities of ZnO Nanostructures Changing the Cooling Route.* New Journal of Chemistry, 2018. **42**.

110. Pralea, I., et al., *From Extraction to Advanced Analytical Methods: The Challenges of Melanin Analysis.* International Journal of Molecular Sciences, 2019. **20**: p. 3943.

111. Piattelli, M. and R.A. Nicolaus, *The structure of melanins and melanogenesis—I: The structure of melanin in Sepia.* Tetrahedron, 1961. **15**(1): p. 66-75.

112. Ito, S., *Reexamination of the structure of eumelanin.* Biochimica et Biophysica Acta (BBA) - General Subjects, 1986. **883**(1): p. 155-161.

113. Karan, S., et al., *Characterization of ion transport property in hot-press cast solid polymer electrolyte (SPE) films: [PEO: $Zn(CF_3SO_3)_2$].* Ionics, 2017. **23**.

114. Long, L., et al., *Polymer electrolytes for lithium polymer batteries.* Journal of Materials Chemistry A, 2016. **4**(26): p. 10038-10069.

115. d'Ischia, M., et al., *Melanin Biopolymers: Tailoring Chemical Complexity for Materials Design.* Angewandte Chemie International Edition, 2020. **59**(28): p. 11196-11205.

116. Gidanian, S. and P.J. Farmer, *Redox behavior of melanins: direct electrochemistry of dihydroxyindole-melanin and its Cu and Zn adducts.* J Inorg Biochem, 2002. **89**(1-2): p. 54-60.

117. Micillo, R., et al., *Eumelanin broadband absorption develops from aggregation-modulated chromophore interactions under structural and redox control.* Sci Rep, 2017. **7**: p. 41532.

118. Reddy Inta, H., et al., *Ni3Se4 Nanostructure as a Battery-type Positive Electrode for Hybrid Capacitors.* ChemElectroChem, 2023. **10**(2): e202201041.

119. Xu, R., et al., *An electrochemical study of natural and chemically controlled eumelanin.* APL Materials, 2017. **5**(12).

120. Subianto, S., *Electrochemical Synthesis of Melanin-Like Polyindolequinone*, in *School of Physical and Chemical Sciences*. 2006, The Queensland University of Technology. p. 197.

121. Song, S., et al., *Preparation, properties, and Li-ion battery application of EC + PC-modified PVdF-HFP gel polymer electrolyte films.* Ionics, 2017. **23**.

122. Ramesh, S. and S.-C. Lu, *A simple P(VdF-HFP)–LiTf system yielding highly ionic conducting and thermally stable solid polymer electrolytes.* Journal of Molecular Liquids, 2013. **177**: p. 73-77.

123. Fan, L., et al., *Thermal, electrical and mechanical properties of plasticized polymer electrolytes based on PEO/P(VDF-HFP) blends.* Electrochimica Acta, 2002. **48**(2): p. 205-209.

124. Yang, C., et al., *A Novel Flexible Supercapacitor Based on Cross-Linked PVDF-HFP Porous Organogel Electrolyte and Carbon Nanotube Paper@π-Conjugated Polymer Film Electrodes.* ACS Sustainable Chemistry & Engineering, 2015. **3**(9): p. 2067-2076.

125. Ravi, M., et al., *Ionic liquid incorporated biodegradable gel polymer electrolyte for lithium ion battery applications.* Journal of Materials Science: Materials in Electronics, 2016. **27**: p. 1370-1377.

126. Melhuish, W.H., *Quantum efficiencies of fluorescence of organic substances: effect of solvent and concentration of the fluorescent solute.* The Journal of Physical Chemistry, 1961. **65**(2): p. 229-235.

127. Williams, A.T.R., S.A. Winfield, and J.N. Miller, *Relative fluorescence quantum yields using a computer-controlled luminescence spectrometer.* Analyst, 1983. **108**(1290): p. 1067-1071.